2016-01-01

Influence of the Stress Path, Moisture, and Fine Content on Permanent Deformation of Geomaterials

Uriel Brian Arteaga
University of Texas at El Paso, uarte01@gmail.com

INFLUNCE OF THE STRESS PATH, MOISTURE, AND FINE CONTENT ON PERMANENT DEFORMATION OF GEOMATERIALS.

URIEL BRIAN ARTEAGA

Master's Program in Civil Engineering

APPROVED:

Reza S. Ashtiani, Ph.D.

Diane Doser, Ph.D.

Soheil Nazarian, Ph.D.

Charles Ambler, Ph.D.
Dean of the Graduate School

Dedication

I dedicate this thesis to my father, Juan, I am grateful for your wisdom and your knowledge. Thank you for showing me that the most important things in the world, are not those which one can purchase, but rather those which one cannot. To my mother, Jacqueline, thank you for always believing in me, for your support, and for your care. Thank you for showing me the power of education and the reason as to why education should always be a priority in my life. To my loving grandmother, Pilar, thank you for being a second mother to me, for your constant prayers, and for your unconditional love. I am grateful for all of the joy that you brought into my life, and for the blessings that you left within me. To the special woman the lord created for me, Yareli, thank you for motivating me to become a better person and for always supporting me in every way. To my sister, Katy, thank you for always reminding me that there is joy in everything. To my younger brother, David, thank you for your tolerance towards me and for the fun days of our adolescence.

INFLUNCE OF THE STRESS PATH, MOISTURE, AND FINE CONTENT ON PERMANENT DEFORMATION OF GEOMATERIALS.

by

URIEL BRIAN ARTEAGA

THESIS

Presented to the Faculty of the Graduate School of

The University of Texas at El Paso

in Partial Fulfillment

of the Requirements

for the Degree of

MASTER OF SCIENCE

Department of Civil Engineering

THE UNIVERSITY OF TEXAS AT EL PASO

December 2016

Acknowledgements

I would like to acknowledge Dr. Ashtiani, for his expert guidance, encouragement, and support. Thank you, Southern Plains Transportation Center, for funding of the research.

Abstract

Permanent deformation within the unbound granular is a predominant feature that results in the degradation and loss of serviceability to the pavement structure as the passage of traffic wheel loads accumulate. Proper characterization of the multi-layer structures is necessary to improve the rutting performance by mechanistically identifying the factors that contribute to the progression of plastic deformations. A consequence of ignoring these features results in the underestimation of the rutting potential, which amounts to premature failure. Current rutting models fail to incorporate factors such as moisture state, gradation, and stress-paths which are paramount to proper characterization of base and sub-base layers. Analysis of the deformation induced by dynamic loads under a controlled laboratory environment can provide valuable information regarding the pavement responses to variations in permanent deformation factors. Therefore, the studies focus in the development of a framework, which successfully acknowledges the permanent deformation components in a synergistic manner. A comprehensive laboratory experiment consisting of a limestone source incorporating three different gradations, three different moisture states, and three different stress paths were considered in this study. The material was then molded into cylindrical samples, which were in turn subjected to various constant confining pressure stress path test to analyze how the parameters affect the rutting potential of laboratory specimen. Valuable understandings were obtained from the analysis regarding the rutting sensitivity and dissipated strain energy of the unbound granular layers subjected to variations in the stress, amount of fines content, and moisture content in the repeated dynamic loading tests.

Table of Contents

List of Tables

List of Figures

Chapter 1: Introduction

Problem Statement

Permanent deformation in Unbound Granular Layers (UGL) is a direct consequence of repetitive wheel load applications. As the accumulation of plastic strains increases with each vehicle passage, the rut depth becomes substantial in the serviceability of the pavement. If no proper attention is paid to the permanent deformation rate; the strain accumulation can result in failure or decline of pavement integrity. Proper characterization of the deformation behavior of geomaterials in the laboratory is vital in the decrease of future maintenance costs and prolongation of road serviceability. The problem encountered in current permanent deformation prediction models, is that the models focus in stress variations and number of loading applications with limited incorporation of the influences of moisture and fines content. Failing to incorporate these important features can potentially induce a systematic error that results in the underestimation of the rutting performance of geomaterials in pavement foundations. The optimization of current rutting models can be achieved by understanding the responses of the geomaterials under repeated loading to variations in the moisture, fines content, and stress path.

Objective and Scope of Study

The main motivation for this study is to understand how permanent deformation is affected by variations in the moisture state, fines content, and stress path sensitivity in a combined manner. The study will utilize dynamic loading triaxial tests to simulate the accumulation of traffic load applications that a pavement section experiences. To achieve this objective an experimental testing program was developed which consisted in permutations of three Constant Confining Pressure (CCP) stress paths, three different measures of moisture, and three different gradations of El Paso limestone material with adjustments of the fines content.

OUTLINE

The contents of the thesis are divided into four sections. The first section establishes the literature review portion of the study which focuses on the compilation of previous research related to permanent deformation under repeated cyclic tests. The second section focuses on the detailed description of the preparation of the specimens and description of the utilized loading protocols. The third section corresponds to the presentation and discussion of the results obtained. The fourth section emphasizes in the conclusion made after the analysis of the test results and provides recommendations for future research.

BACKGROUND

In pavements, permanent deformation is described as rutting, which is the repeated load-induced displacement of pavement material that creates channels along the wheel path. Pavements should provide a reasonably smooth riding surface, adequate tire friction, and protection to the unbound granular layers from moisture intrusion and erosion (Adlinge, 2013). It is vital that the base and subbase layers do not intake significant strain levels which affect the serviceability of the pavement. Therefore, permanent deformation models are important in the prolongation of pavement life as well as the reduction of premature pavement failure costs. Factors such as moisture, fines content, gradation, stress path, confinement, and aggregate degradation contribute to the rate of accumulation of permanent deformation (Seyhan, 2002).

PERMANENT DEFORMATION CHARACTERISTICS

The deformation that results after a cyclic load magnitude is applied to a pavement section can be characterized by an elastic and a plastic portion. The elastic portion, also known as the resilient deformation, is the recoverable segment of the deformation that is unable to perform work in the UGLs. The plastic section is the non-recoverable deformation that results in the

rearrangement and compaction of the aggregate particles in the soil. Each load application induces a different amount of permanent deformation depending on the soil characteristic, and the magnitude of the loading conditions. As the loading is applied cyclically the permanent deformation begins to accumulate as the number of load applications increase. The accumulated permanent strains can be expressed as a function of load applications, where the accumulated strain is equal to the summation of the permanent strains progressively produced after the N^{th} loading cycle as seen in Equation 1.1.

$$\varepsilon(N) = \sum_{N=1}^{n} \varepsilon_{p(N)} \tag{1.1}$$

Where:

ε_p = strain after a particular load cycle

Figure 1.1 shows the combination of the resilient and the permanent strain which accumulate as the progression of loading applications increases.

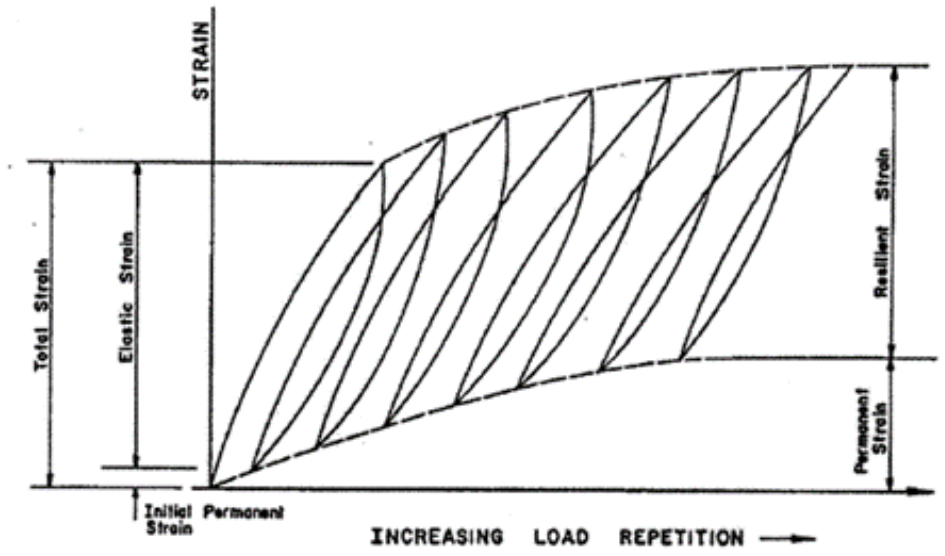

Figure 1.1: Deformation response of a pavement element under dynamic loading (Kim, 2005a).

Further, the shakedown theory characterizes the mechanical behavior of granular specimen subjected to cyclic loading into three distinct regions which are: plastic shakedown, plastic creep, and incremental collapse as seen in Figure 1.2.

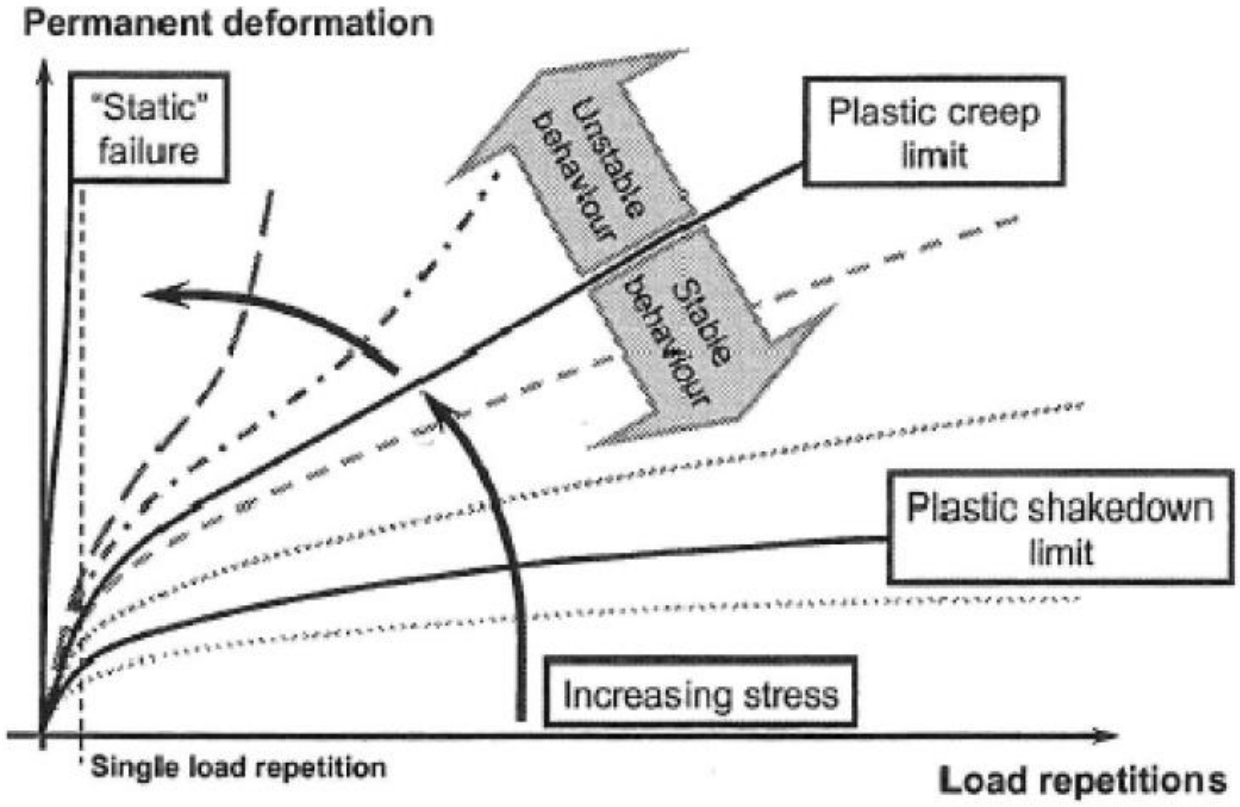

Figure 1.2: Different types of permanent deformation behavior found under repeated loading (Theyse et al, 2007).

During plastic shakedown, the permanent deformation rate generated by the application of the stresses decreases rapidly as the number of loading cycles increase. Hence the permanent deformation at the $(N-1)^{th}$ load application is greater in magnitude than that of the N^{th} and $(N+1)^{th}$

load cycles. For this reason, plastic shakedown behavior results in an asymptotic curve that is identified as the hardening behavior. In plastic creep, the soil initially experiences some hardening behavior, however after a certain number of load cycles the $(N-1)^{th}$ load application will be approximately equal to the N^{th}, and to the $(N+1)^{th}$ load application. Therefore, plastic creep occurs when the gradient of the permanent deformation stabilizes and reaches a constant value resembling resilient behavior. Incremental collapse occurs when the permanent deformation rate increases exponentially eventually resulting in shear banding of the geomaterials (Arnold, 2004). During incremental collapse the permanent deformation slope gradually increases as the loading cycle transitions from the N^{th} to the $(N+1)^{th}$ load application.

DISSIPATED STRAIN ENERGY

Permanent deformation can similarly be expressed as cyclic energy storage in the base layers induced by mechanical energy inputs of traffic. Additionally, parameters such as temperature, relative humidity, freeze-thaw potential, and the soil suction properties associated with wetting and drying curves contribute to the energy storage in geomaterials (Pasten and Santamarian, 2010). Therefore, analysis of the load-induced plastic strains when superimposed by the environmental cycles provide valuable information on the rutting performance of granular layers in the field. The mechanism that governs load transfer in base layers mainly corresponds to particle interactions by means of frictional forces. Frictional forces are non-conservative forces that dampen kinetic energy resulting in various forms of energy transformations. These energy transformations account for the shifting and readjustment of the aggregate particles in the unbound matrix which in turn influences the energy storage in the aggregate systems (Ashtiani, 2009). Conversely, the portion of the energy that is not stored in the system allows the material to retake

a fragment of its original shape resembling an elasto-plastic response. Making usage of the cylindrical specimen and triaxial equipment in the laboratory allows for the generation of a controlled environment that prevents loss of soil material and moisture. Hence, changes of the initial dimensions of the specimen can be recorded, providing strain and stress readings which allow for the calculation of the dissipated strain energy.

Hysteresis Loops Formed Under Cyclic Loading

When analyzing the hysteresis loops generated by cyclic loading in the lab, two regions can be found within a hysteresis loop. The plastic region is the non-recoverable permanent deformation that results in the densification of the soil strata by means of stored energy. The elastic region also recognized as resilient strain is the non-plastic strain energy that is not capable of performing work in the material. Both the plastic and elastic strain can be observed within the generation of the hysteresis loop as seen in Figure 1.3.

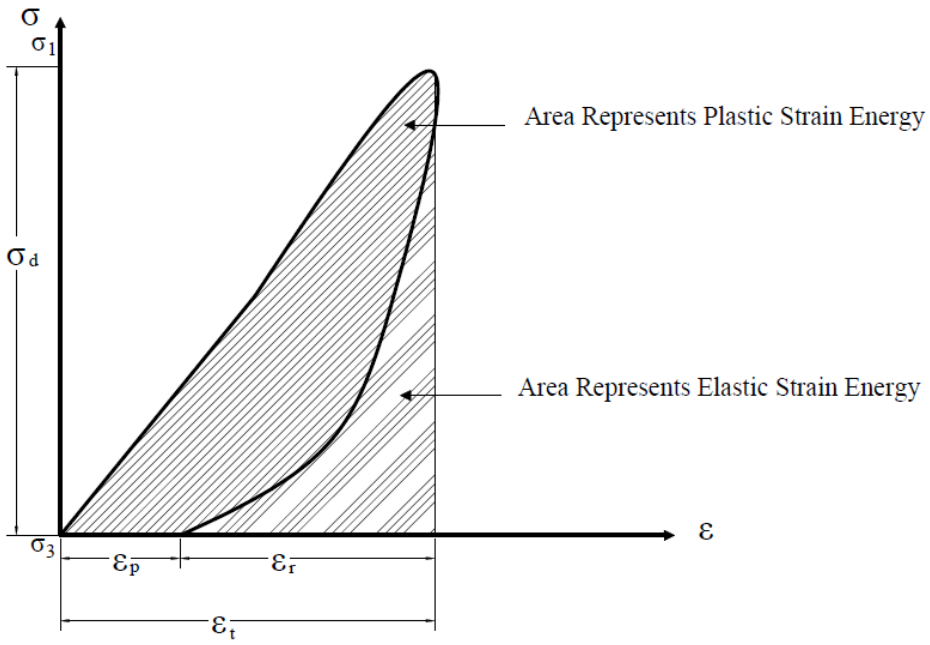

Figure 1.3: Energy associated with the areas produced by a hysteresis loop under cyclic loading.

Conceptually the area constrained by the hysteresis loop represents the dissipated strain energy, and the area formed by the peak strain and the elastic strain represents the elastic energy. Analysis of the hysteresis loop provides valuable information with regards to the loading scheme and the ways in which the soils respond to the applied stresses. The size of the hysteresis loops provides information regarding the magnitude of the stored energy imparted by the stress states on geomaterials. The inclination of the hysteresis loop demonstrates the rate of progression of the deformation and the damage imparted into the material. Sharper slopes of the orientation angle with increasing load cycles are an indication of the hardening behavior of the materials under repeated loading. Conversely, flattening of the slope of the inclination angle of the hysteresis loops is an indication of the softening and damage of the specimen as seen in Figure 1.4.

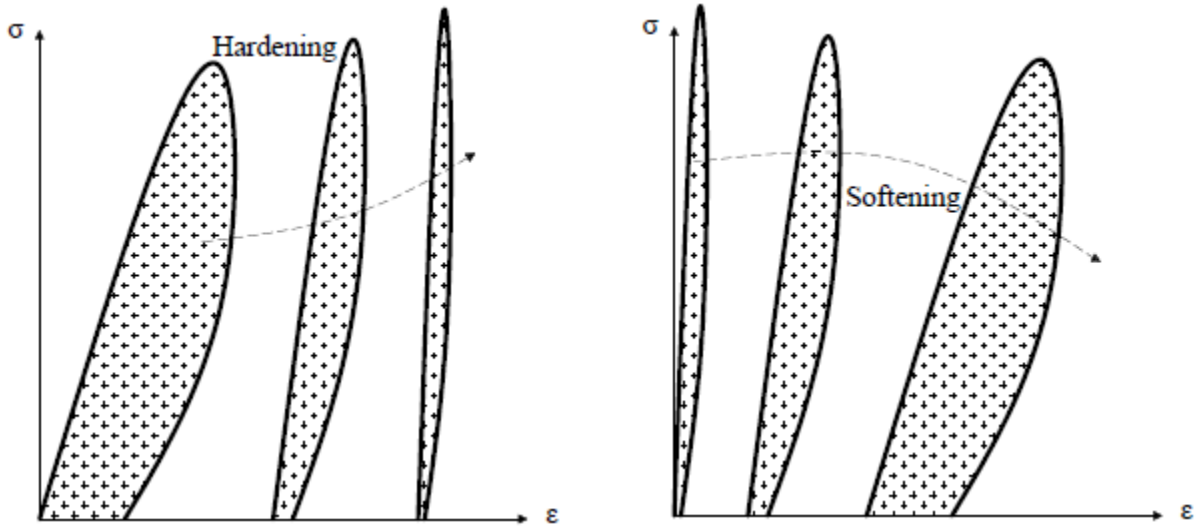

Figure 1.4: Orientation and size of the hysteresis loop with the (a) hardening behavior, and (b) softening behavior.

The behavior of the hysteresis loops with the progression of loading applications can likewise be described by the three distinct regions of plastic shakedown, plastic creep, and incremental collapse. When the material exhibits plastic shakedown, the dissipated energy reduces with increasing number of load applications because the material begins to stabilize within the system. Therefore, during plastic shakedown the inclination and size of the hysteresis loops will tend to decrease as the number of loading applications increases. Similarly, when the material experiences plastic creep the size of the hysteresis loops remains constant because no increase in strain energy intake is registered. Upon incremental collapse, the hysteresis loops grow rapidly and the inclination of the loops will tend to align with the horizontal axis. Based on laboratory observations, conventional laboratory specimens of well graded aggregates molded at optimum moisture content often show plastic shakedown behavior. Conversely unbound specimens with high amount of fines compacted at elevated saturation levels exhibit either plastic creep or incremental collapse behavior. Since plastic shakedown behavior is the desired mode for pavement design purposes, it is important to understand both the hardening and softening behavior and the factors that trigger such mechanical behavior.

Calculation of the Area Inside the Hysteresis Loops.

A polynomial approximation can be utilized to calculate the area constrained by the hysteresis loop in dynamic loading of geomaterials in the laboratory. The hysteresis loop can be approximated by two polynomials; one forming the top portion of the loop, and the other shaping the bottom portion of the loop ultimately meeting in the point of maximum stress and strain. Equation 1.2 presents the relationship used to calculate the dissipated strain energy as the constrained area of the hysteresis loop.

$$E_s = [\int_{\varepsilon_{\min}}^{\varepsilon_{\max}} \sigma_t(\varepsilon)d\varepsilon - \int_{\varepsilon_p}^{\varepsilon_{\max}} \sigma_b(\varepsilon)d\varepsilon]V_s \quad (1.2)$$

Where:

E_s =Stored energy

$\sigma_t(\varepsilon)$ = top polynomial approximation

$\sigma_b(\varepsilon)$ = bottom polynomial approximation

$\varepsilon_{\min}, \varepsilon_{\max}$, and ε_p = Critical strain points

V_s = Volume of specimen

Using polynomials to approximate the area of the hysteresis loops allows for the utilization of the collected data points to predict the top and bottom curves of the hysteresis loop. It can be inferred that having more data points within the hysteresis loop conveniently allows for the use of higher order of polynomial degrees suitably increasing the accuracy. Furthermore, making use of both the area inside of the hysteresis loop and the area formed by the peak stain and the elastic strain provides a measurement of the total energy within the load application. Equation 1.3, provides valuable information of the degree of plastic behavior of the system. A P value of 0 corresponds to perfectly elastic material with no stored energy and a P value of 1 refers to a perfectly plastic material where all the energy is stored.

$$P = \frac{E_s}{E_t} \quad (1.3)$$

Where:

P = Degree of plastic behavior

E_s = Stored energy

E_t = Total energy

Making use of the polynomial approximation, the derivative of the equation as seen in Equation 1.4, can be used for the determination of the modulus of elasticity.

$$E = \frac{d(\sigma_t(\varepsilon))}{d\varepsilon} \tag{1.4}$$

Where:

E =Modulus of elasticity

$\sigma_t(\varepsilon)$ = top polynomial approximation

Another important parameter found within the hysteresis loop is the angle of orientation of the hysteresis loop (θ) as seen in Equation 1.5.

$$\theta = \arctan[\frac{\sigma_{\max} - \sigma_{\min}}{(\varepsilon_{\max} - \varepsilon_{\min})a'}] \tag{1.5}$$

Where:

$\sigma_{\min}, \sigma_{\max}$ = Critical stress points

$\varepsilon_{\min}, \varepsilon_{\max}$ = Critical strain points

a' = Constant amplifying factor

The amplifying factor present in the equation is used because cyclic loading strains usually range from 10^{-4} to 10^{-3} strain units (Atkinson, 2000). If a' = 1 then the angle of orientation of the

hysteresis loop will approximately equal 90 degrees. Therefore, to get a good representation of the angle of orientation it is important to maintain this amplifying factor as a constant.

STRESS PATH CHARACTERIZATION

In order to characterize traffic stresses in the laboratory, the equipment needs to replicate the natural resting stresses of the soil, the traffic loading conditions, and the path of the stresses from one point to another. For this reason, testing equipment that utilizes a CCP triaxial cell can be used to replicate the stresses a pavement experiences during dynamic loading. Figure 1.5 shows a common cylindrical specimen used in the laboratory placed inside a triaxial confining cell.

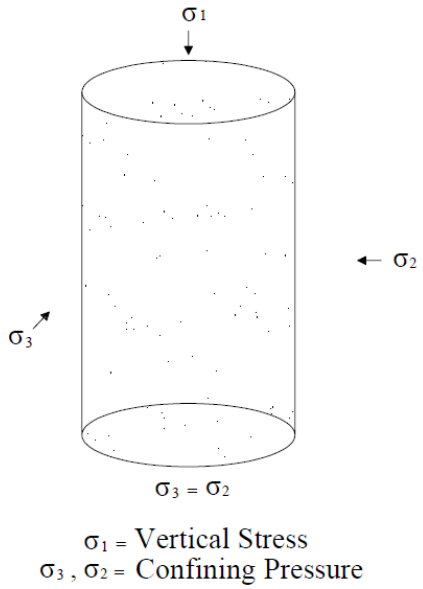

Figure 1.5: Stresses in the vertical, axial, and transvers directions in a laboratory specimen.

In triaxial testing, the applied vertical stresses selected to replicate vehicle loading in the field are denoted as σ_1. The horizontal stresses which correspond to the natural pavement confinement are

represented as σ_3, since ($\sigma_3 = \sigma_2$) due to all around confinement. A way to combine these two parameters into measurable quantities is by the analysis of the stress path length and the stress path slope. Traditionally, the stress path plots are developed in the deviatoric stress space; where the average of the principal stresses as seen in Equation 1.6, is plotted on the abscissa and the deviatoric stress as seen in Equation 1.7, is plotted on the ordinate.

$$p = \frac{\sigma_1 + 2\sigma_3}{3} \tag{1.6}$$

$$q = \sigma_1 - \sigma_3 \tag{1.7}$$

Additionally, a stress path in cyclic loading consists of two different sets of stresses; the seating stresses (σ_{1i}, σ_{3i}) which are the stresses at a resting state, and the maximum stresses (σ_{1f}, σ_{3f}) which are the stresses experienced when the moving wheel is directly on top of the pavement section. Both stress measurements alternate during the loading period creating a change in the deviatoric stress $(\Delta q = q_f - q_i)$, and change in the mean stress $(\Delta p = p_f - p_i)$, which ultimately shape the stress path. The length of the stress path as seen in Equation 1.8 captures the magnitude of the stresses imposed by the trajectory moving wheel. Figure 1.6 depicts the length of the stress path as a measurement of the stress magnitude induced by the movement of the wheel.

$$\mathrm{L} = \sqrt{(\Delta q)^2 + (\Delta p)^2} \tag{1.8}$$

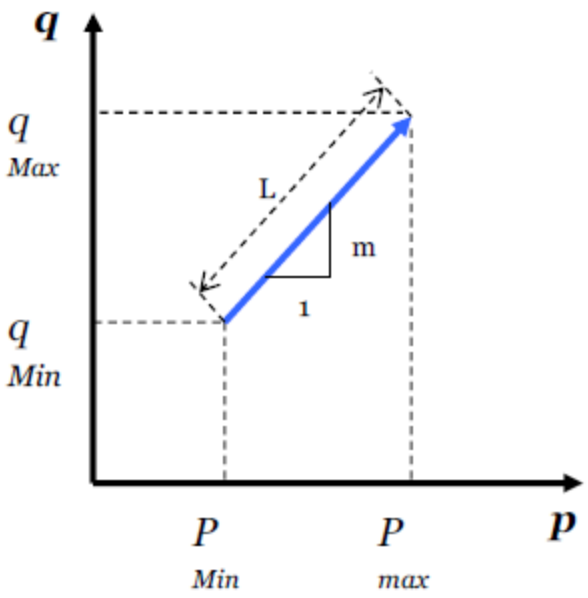

Figure 1.6: Stress path length characterization (Ashtiani, 2009).

The slope of the stress path as expressed in Equation 1.9, is related to the stress regime acting on geomaterials expressing either extension or compression of the stress path. A stress path slope of (m = 0) represents an isotropic stress condition at which ($\sigma_3 = \sigma_1$), a stress path slope greater than zero represents compressive stress conditions, and a stress path less than zero represents extension conditions (Ashtiani, 2009). Figure 1.7 presents multiple stress path slopes that can be observed in cyclic loading.

$$m = \frac{\Delta q}{\Delta p} \tag{1.9}$$

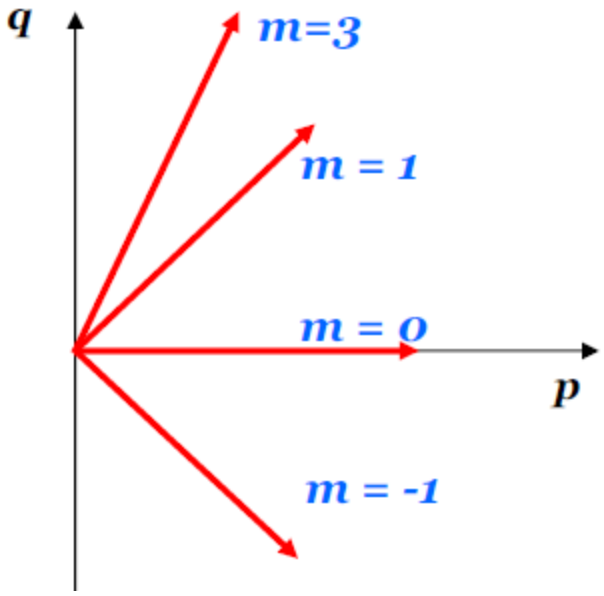

Figure 1.7: Stress path slope characterization (Ashtiani, 2009).

Field Versus Laboratory Stress Paths

An issue encountered in stress paths generated under CCP in the laboratory is that the stress path is limited to only one slope (m = 3). This indicates that a loading scenario under CCP portrays a setting in which the wheel of the vehicle is directly on top of the pavement, therefore failing to incorporate the arrival and departure of the wheel. The significance of the arrival and departure of the moving wheel correspond to the orientation of the principle stress plane. As seen in Figure 1.8, the rapid change from positive to negative shear results in the rotation of the principal stress plane which suggests that the most critical loading conditions may not occur when the wheel is directly on top of the pavement section but also at the extremities (Kim, 2005b).

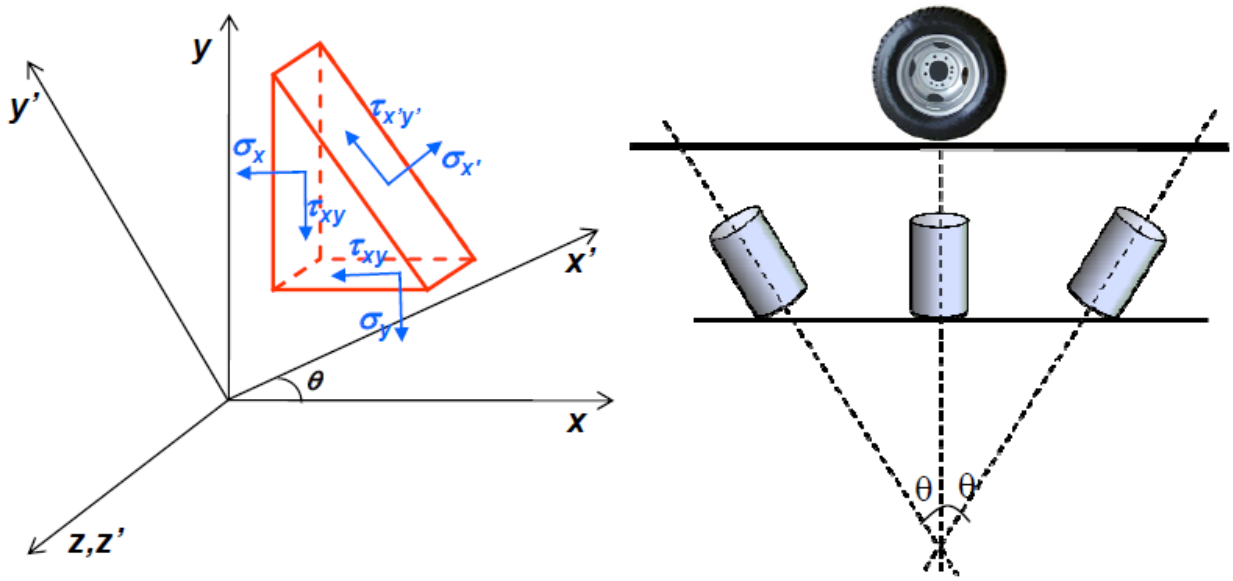

Figure 1.8: Rotation of the orientation of the principle stress plane under the moving wheel load (Ashtiani, 2009).

Analyzing the constraints associated with CCP, traditional equipment allows a window of potential stress path combinations that can be summarized into a parallelogram region as seen in Figure 1.9a. A noteworthy observation from Figure 1.9a is that the extension and compression regions are associated with the extension and compression behavior of the moving wheel seen in Figure 1.9b. Examining Figure 1.9b shows how the stress regimes change from extension to compression as the wheel moves a distance (d).

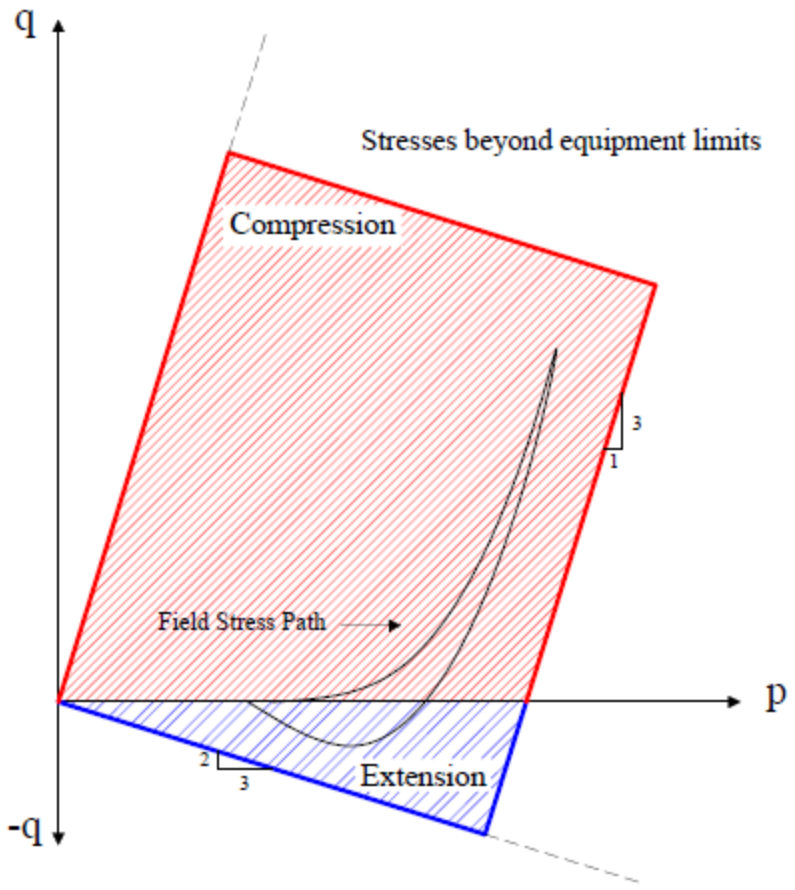

(a)

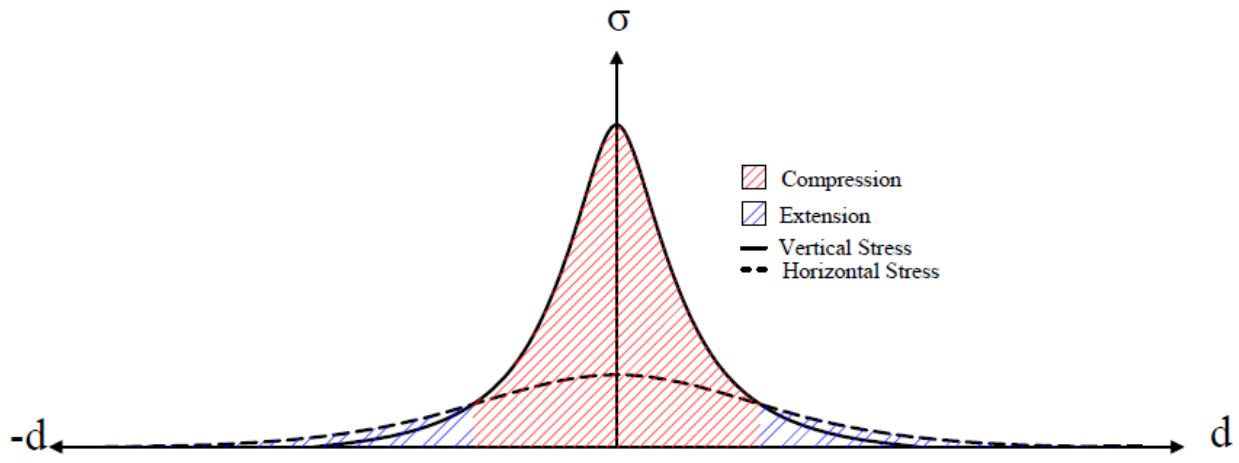

(b)

Figure 1.9: (a) Stress path limits imposed by traditional triaxial testing equipment. (b) Extension and compression behavior associated with the arrival of the wheel.

As indicated in this plot, only the stress paths that are constrained within the parallelogram can be replicated in the laboratory. Conceptually, the upper bound limits of confining pressure and vertical stresses do not exist for field-measured responses; however, laboratory equipment will inevitably always have a maximum stress limit. It can also be noted that the stress path parallelogram has two significant regions divided by the mean stress axis which ultimately play an important role for the proper selection of the stress path protocol. The upper region separated by the mean stress axis is the compression region, where the vertical stress is greater than the horizontal stress ($\sigma_1 > \sigma_3$). Conversely, the section located under the mean stress axis, is the extension region where the vertical stress is less than the horizontal stress ($\sigma_1 < \sigma_3$). Considering that soils can only sustain and carry compressive loads through particle contacts, the extension behavior represented in the figures appears counterintuitive. However, field measurement of responses showed that realistic stress paths induced by the movement of the wheel are not always positive, but alternate from negative to positive throughout the trajectory of the wheel as seen in Figure 1.10 (Kim, 2005b).

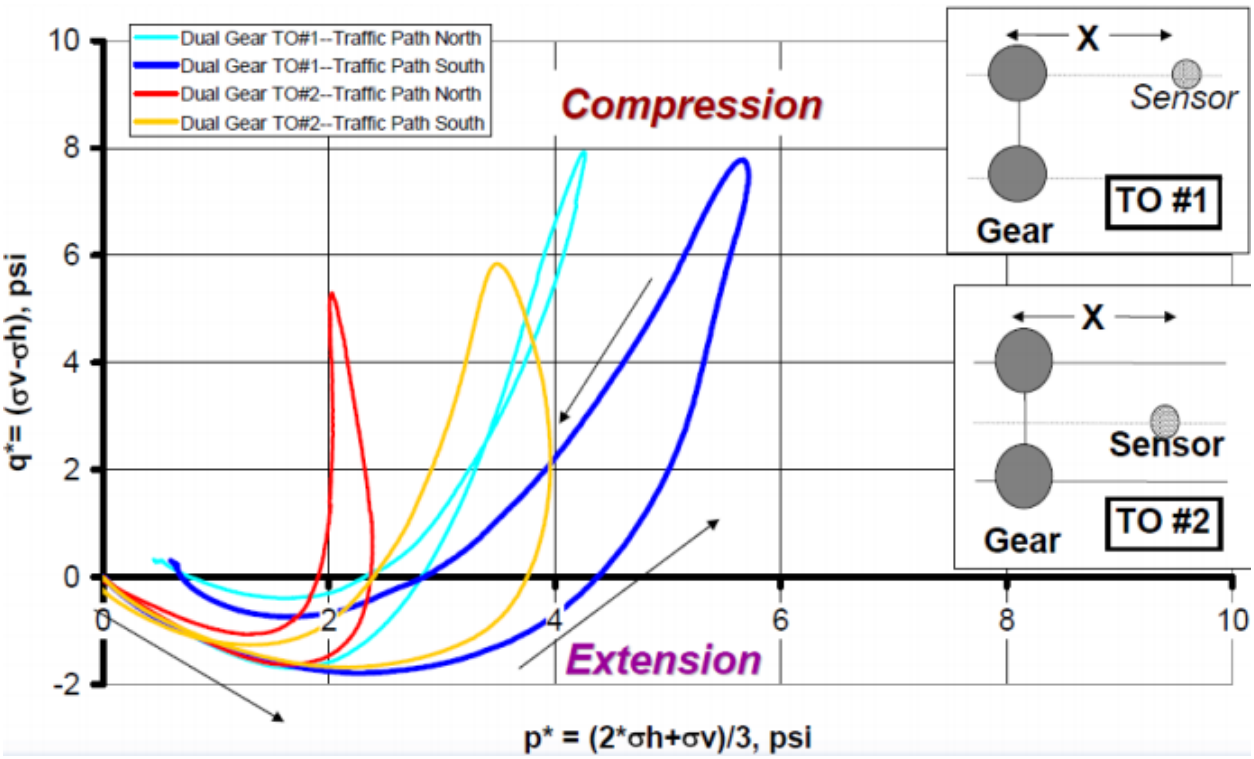

Figure 1.10: Field measurements of the arrival and departure of the moving wheel. (Kim, 2005b).

A more suitable method of replicating the movement of the wheel in the laboratory is by the generation of multiple stress paths to initially create an extension stress path followed by a compression stress path. Figure 1.11 shows a single constant confining pressure stress path compared to a multi-stress path which advantageously incorporates both extension and compression.

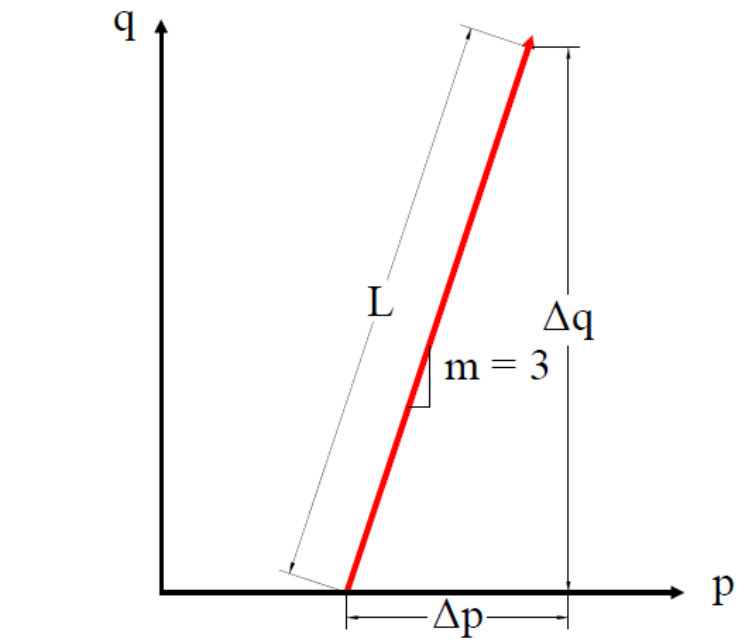

(a)

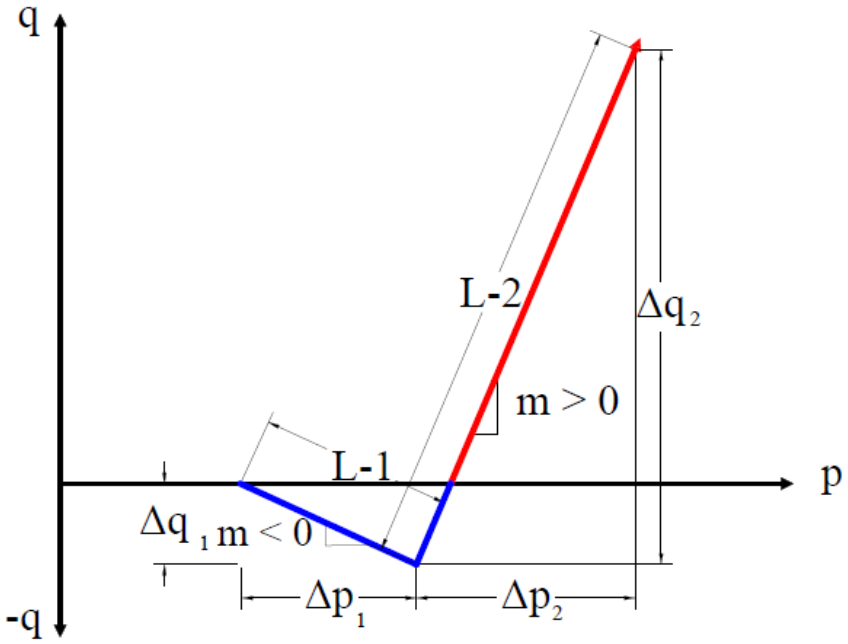

(b)

Figure 1.11: Stress paths corresponding to (a) single CCP stress path, (b) multi stress path.

Although a multi stress path incorporating extension and compression would be ideal, the generation of cyclic confinement is restrained by the difficulty associated with the increase and

decrease in confinement in a synchronized timed manner. In order for this to happen the equipment would have to increase and decrease the confinement in a tenth of a second to coordinate the vertical and horizontal load application similar to those seen in the movement of the wheel.

FACTORS THAT INFLUENCE PERMANENT DEFORMATION

It is well established in the literature that UGLs are nonlinear, stress sensitive and anisotropic materials (Ashtiani, 2008). Therefore, the ability to predict soil behavior is naturally complicated and requires proper understanding and reasoning to adequately predict desirable outcomes. Further, the complex nature of such nonhomogeneous materials requires a multi-scale analysis of the factors that contribute most to the deformation characteristics of geomaterials.

Traffic

An important factor influencing pavement performance, exclusively permanent deformation potential, is the loading produced by traffic. Traffic loads are important because different traffic sections can induce various types of loads that differ greatly depending on the types of vehicles utilizing the sections (Wang, 2011). Traffic also establishes the frequency of vehicle arrivals, and the specific loading scenario the pavement section will bare (Enright and Obrien, 2012). Some examples of loading scenarios would be: an intersection where the pavement experiences rapid deceleration, the lift off of aircraft on an airfield runway, a roadway which is subjected to bidirectional traffic, and an unexpected complete stop of traffic in a highway section due to an automobile accident. Since a roadway can be subjected to a combination of the presented scenarios, it is important to successfully replicate the demanding traffic stresses during laboratory testing. Because traditional equipment has difficulty imposing stresses in such irregular means,

replication of traffic stresses in the laboratory can critically affect the permanent deformation prediction. Therefore, in order to understand and successfully model the rutting potential of pavements it is important to initially understand the stress invariants and stress paths a moving wheel imposes on the road (Parry, 2004).

Dynamic Wheel Loading

When examining traffic loading, it also important to analyze the manner in which the vehicles project stresses onto the pavement. As a vehicle travels along the road path, the moving wheel induces different stresses onto the pavement, which vary significantly in the vertical and horizontal directions due random distribution of stresses through particulate material (Wang and Imad, 2009). Studies found that the lateral and transverse stresses change significantly as the wheel loading transitions from static to dynamic loading (Wang, 2011). The major issue generated when different load magnitudes occurs in the vertical and horizontal direction is that the material experiences stress induced anisotropy. Anisotropy is defined as the difference in the directional dependency of the material properties in unbound granular layers, where the vertical modulus is not equal to the horizontal modulus (Ashtiani, 2009; Tutumluer and Seyhan, 1999). Since the moving wheel induces a different vertical and horizontal stress while in motion, a proper laboratory loading protocol should account for these abnormalities. However traditional cyclic loading methods used today such as the CCP triaxial test, incorporate a loading scheme, which on the contrary, follows an isotropic model (Seyhan et al, 2005). This scenario disregards the horizontal stresses involved in the arrival and departure of a moving wheel. As seen in Figure 1.12, when the vehicle's wheel approaches the pavement section, the pavement undergoes extension where the horizontal stress is greater than the vertical stress. The pavement then moves into a state of

compression where the vertical stress becomes greater than the horizontal stress. Finally, as the wheel departs, the pavement once more moves into a stage of extension where again the horizontal stress becomes greater than the vertical stress.

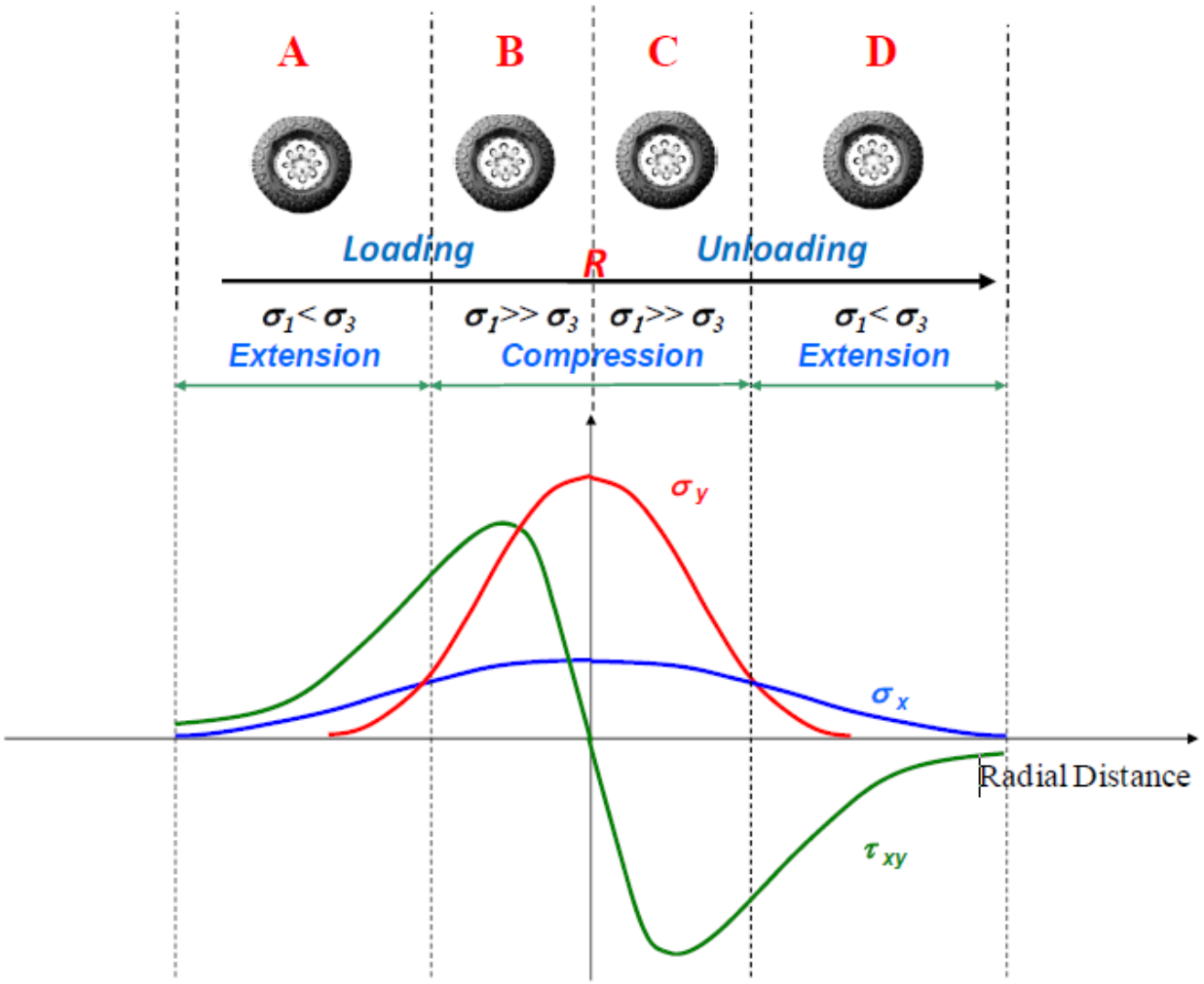

Figure 1.12: Horizontal and vertical stresses induced by wheel trajectory (Ashtiani, 2009).

This erratic behavior cannot be simulated with traditional equipment mainly because inducing pressure variations within a short time frame are both costly and unreliable.

Speed of Moving Wheel

The speed of the moving wheel plays a critical role in the shaping of the stress path characteristics which are crucial to the proper recreation of pavement loading conditions in the laboratory (Ghanizadeh et al, 2013). The speed at which a vehicle passes is significant because it indicates the loading and resting periods that should be utilized in the laboratory. The combination of the loading period and the stress magnitude are important input parameters, which indicate how the vehicle's load will be transferred onto the pavement section and the frequency at which load will pass over the pavement section (Fakhri et al, 2013). Loading rates can vary depending on the traffic scenario, for example an eighteen-wheeler traveling at 65 miles per hour on a highway will induce a high cyclic stress onto a pavement section in a small amount of time. However, if the same vehicle utilizes a congested road, stress will remain the same but the amount of time in which the vehicle load passes over the pavement section will be prolonged. The loading period can also be expressed as a function of depth since it takes time for the stresses to transfer from the surface layer to the base and subgrade layers (Benedetto et al, 2003). The resting period is the amount of time available for the pavement to recover before the arrival of another vehicle. Research conducted in cyclic loading tests with different resting periods found that as the resting period was increased the material had more time to recover therefore, experienced less permanent deformation (Elliot, 2007). As seen in Figure 1.13, soils in the laboratory are modeled by a haversine function which expresses the loading and resting periods.

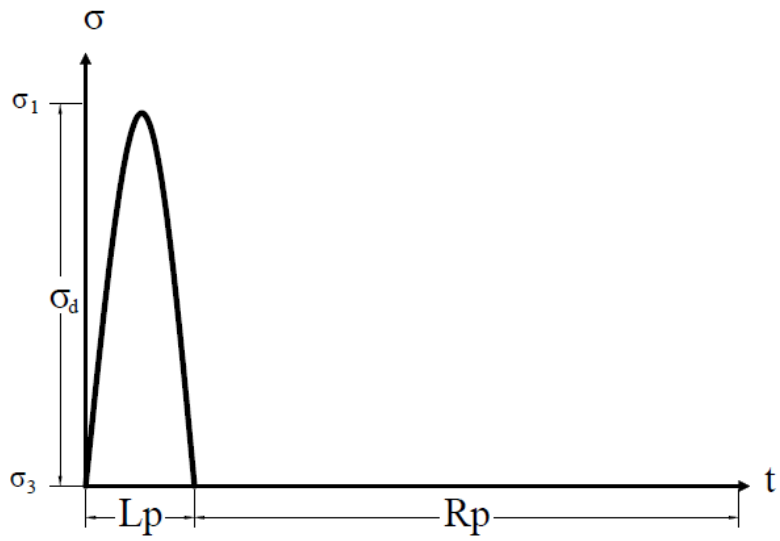

Figure 1.13: Loading and resting period experiences by a pavement section under one loading cycle.

Confinement

A unique aspect of geomaterials is the manner in which the strength of the soil increases nonlinearly as the horizontal confinement increases (Parry, 2004). Confinement naturally increases with depth, generating higher confinements that restrain volumetric displacement of the material. Studies involving different confining stresses demonstrated that as the level of confinement increases the axial permanent deformation reduces (Kim, 2005a; Uzan, 2004; Sweere, 1990). Correspondingly, maintaining the confinement constant and increasing the vertical stress had an opposite effect where the permanent deformation increased. Figure 1.14 shows the deviatoric stress increase with the increase in permanent strain. As observed in the figure, the slope of axial strain decreases as the confinement increases.

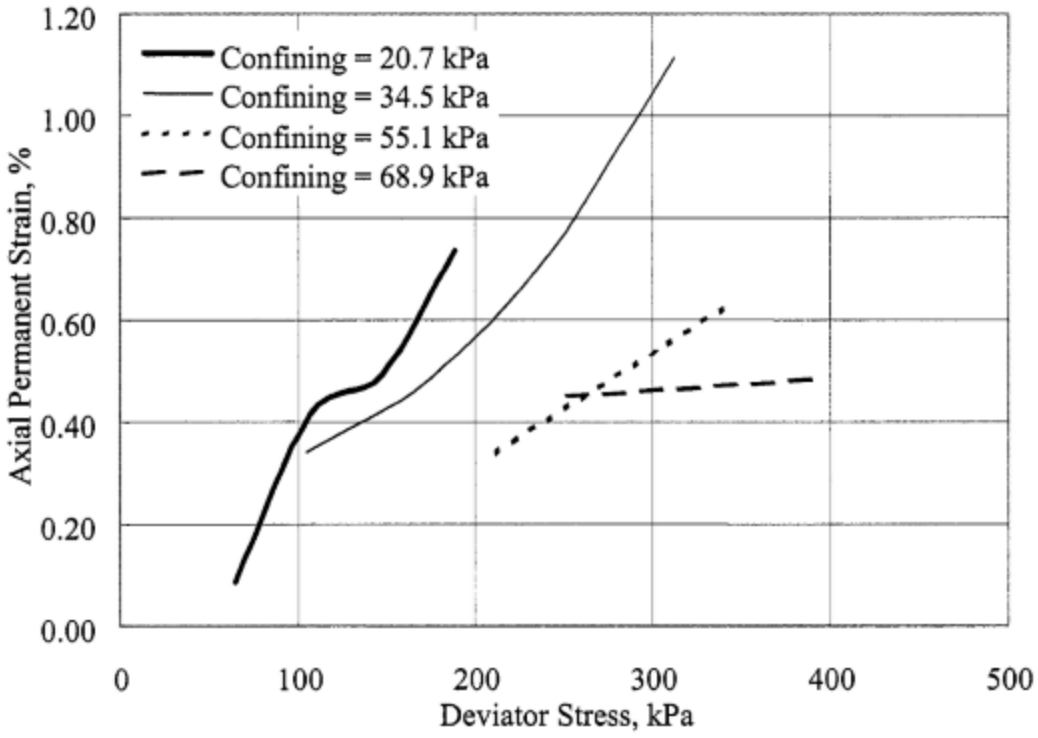

Figure 1.14: Effect of Confining pressure on the NAPTF P209 Permanent Deformation Development (Kim, 2005a).

Ideally geotechnical engineering structures should only be exposed to static loading conditions where the confinement and vertical loads remain constant throughout the life of the structure. However, since pavements experience dynamic loading conditions it is important to note that confinement undergoes changes with the arrival and departure of the moving wheel (Kim, 2005a). Therefore, future studies should include a dynamic confinement protocol to approach a more realistic loading simulation.

Particle Size Distribution

The most common manner of classifying geomaterials and identifying the associated engineering application involved with the soils is by looking at the particle size distribution (Bittelli et al, 1999; Holtz et al, 1981). A well graded soil is characterized by having a good representation of all particle sizes, often associated with high density and good stiffness properties.

On the other hand, a uniformly graded soil has high concentration of particle sizes in a narrow range, resulting in a totally different behavior. Therefore, load bearing capacity, and density of the material can unfavorably change due to minor alterations in the gradation (Pan et al, 2006; Tutumluer and Pan, 2008). It is therefore important to prescribe and maintain the most suitable gradation to reduce potential permanent deformation. However, maintaining the prescribed gradation can be difficult in the field as well as in the laboratory because many external factors can result in the crushing, degradation, and erosion of the aggregates (Karan et al, 2014). Further, particle geometry which includes particle shape, particle angularity, and particle macro texture combined with particle size distribution, can completely change the load bearing capacity of the soil. For example, two mixes having the same gradation with one utilizing semi rounded rock with slight jagged edges, and the other using angular equidimensional crushed aggregate will perform completely different. This is due to the distinct aggregate interlock both particles have which affects the frictional forces contributing to the load bearing capacity (Petersen et al, 2002).

Aggregate Degradation

One of the issues encountered in maintaining the initial gradations is that the methods of compaction employed in the laboratory and in the field, can result in the crushing of the aggregate. The most common compaction protocol in the laboratory is the Proctor Test which compacts the material by the means of impact energy (Tex-113-E, 2011; Tex-114-E, 2011). The proctor test consists of dropping a weight from a specific height onto the material densifying the soil into a compacted layer. Another compaction method used in the asphalt industry is the Superpave Gyratory Compactor which compacts the material by rotating the cylindrical specimen at an angle until achieving desired density (Tex -241-F, 2015). It is important to note that both of the

compaction methods used in the lab are very different from the compaction methods used in the field. In the field compaction is accomplished by means of roller compaction and vibratory compaction. Further, utilizing an impact force as the means compaction in the lab can result in some cracking and crushing of the aggregates resulting in undesired shifts in the gradation. A laboratory protocol utilized to simulate aggregate crushing under compaction is the L.A. Abrasion test (Tex-410-A, 1999). The test makes use of the collision force induced by solid steel spheres and soil particles inside a rotating cylinder to simulate aggregate crushing. Studies performed in aggregate degradation made usage of the L.A. Abrasion test to determine the change in permanent deformation potential before and after the aggregate degradation. As seen in Figure 1.15, the selected gradation underwent a high increase in the generation of fines.

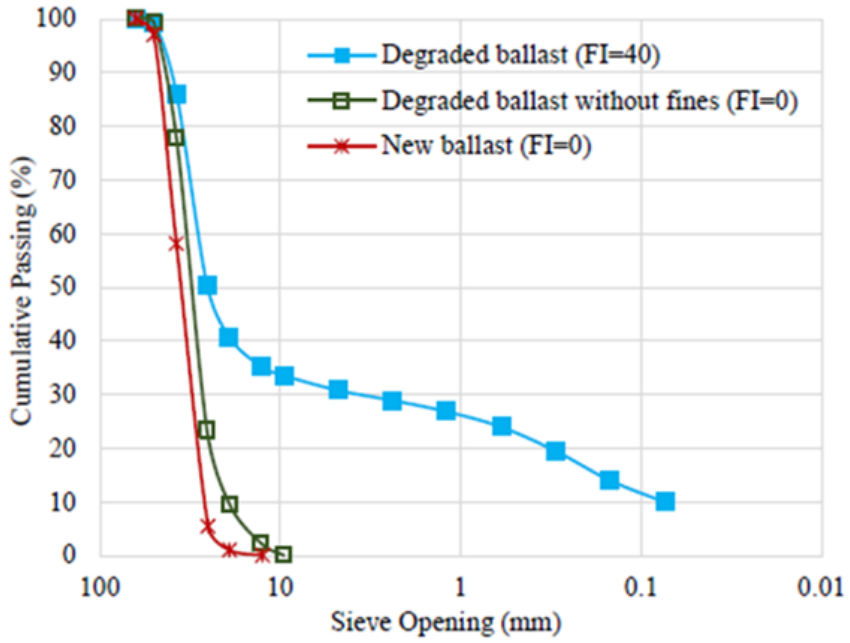

Figure 1.15: Limestone uniform gradation before and after degradation via L.A. Abrasion test (Qian et al, 2014).

Similarly, after the prepared specimens were subjected to 10,000 loading applications as seen in Figure 1.16, the gradation containing the degraded material had higher permanent deformation (Qian et al, 2014).

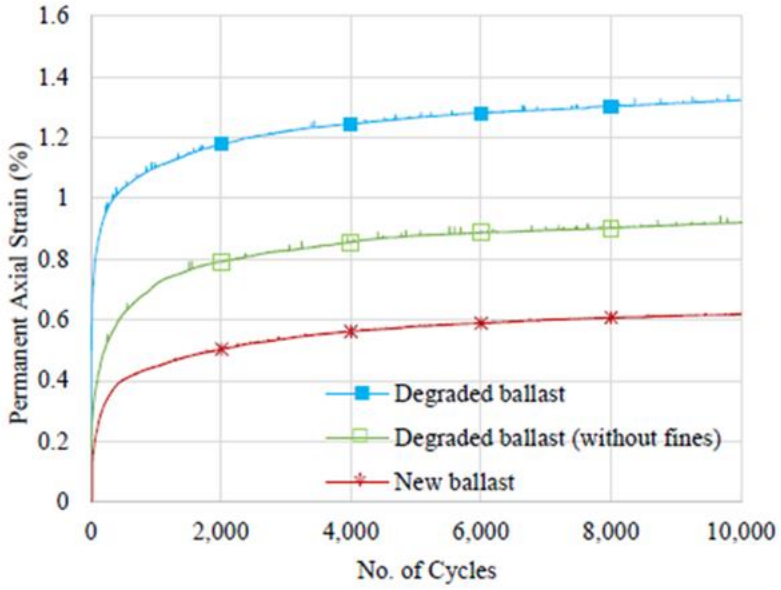

Figure 1.16: Axial strain versus number of load applications for new material, degraded material under initial gradation, and degraded material under shifted gradation (Qian et al, 2014).

From this research, it can be summarized that the degradation of the UGLs will result in an increase of the rutting potential. This can be caused by the reduction of particle angularity, and reduction of particle size. Although it is difficult to perceive aggregate degradation in the field, it is important to prescribe the appropriate compaction, maintain the initial gradation, and avoid any shifts in gradation due to aggregate crushing. The degree of compaction can also influence the permanent deformation potential since a higher void ratio indicates higher compressibility potential (Rahman

et al, 2008). Research performed using variations in the degree of compaction showed that higher compaction efforts decreased the permanent deformation as seen in Figure 1.17 (Kim 2005a).

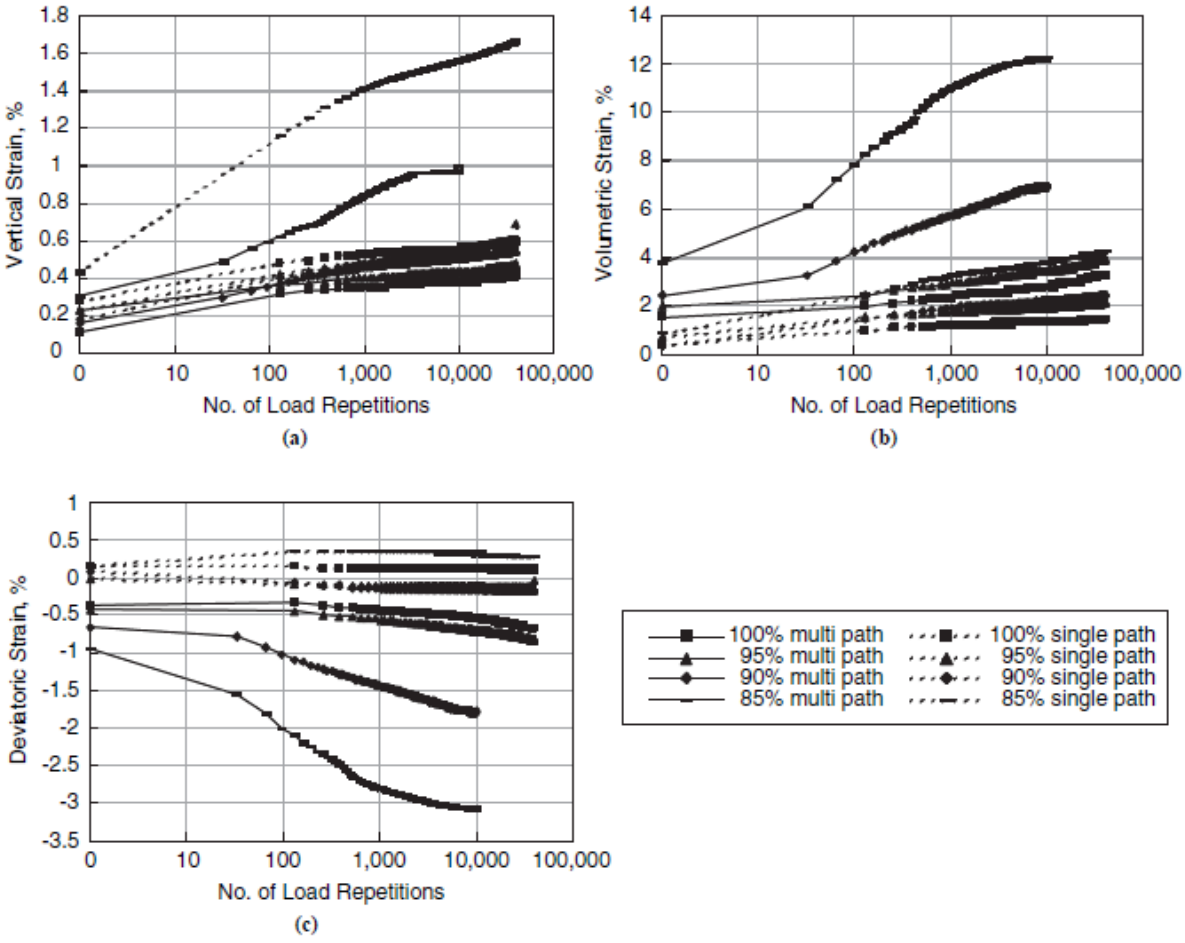

Figure 1.17: Aggregate permanent strains obtained from single and multiple stress path tests at various compaction levels: (a) permanent axial strain accumulation, (b) permanent volumetric strain accumulation, and (c) permanent deviatoric strain accumulation (Kim, 2005a).

The figure above shows that the material subjected to lower levels of compaction displayed a higher strain level compared to the material which had higher degrees of compaction. This peculiarity is caused because the material's degree of compaction is related to the air trapped in the aggregate matrix which affects density. Another factor that can cause aggregate degradation is

the propagation of micro-cracks found in the aggregates due to fatigue. Studies show that as the progression of loading applications increase, the ability of the material to sustain loading decreases as seen in Figure 1.18 (Pasten and Santamiran, 2010).

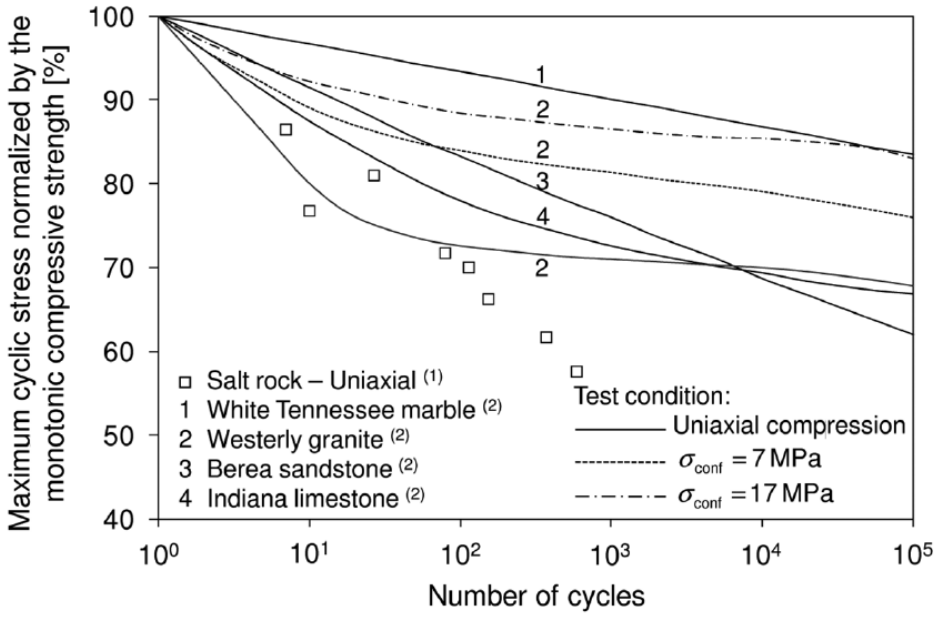

Figure 1.18: Fatigue strength of various types of rocks subjected to cyclic loading (Pasten and Santamarina, 2010).

Fine Particles

The load bearing capacity in the base layers consists mainly of inter-particle friction provided by coarse grained aggregates. As the particle size of the aggregate decreases, the contribution to the load bearing capacity via friction also decreases (Li, 2013). Fine particles contribute to an increase in the dry density of the material by filling in the gaps generated by larger aggregates. However, having too many fine particles in the mix can result in the replacement of higher sized aggregate rather than only filling in the gaps (Deb et al, 2010). Further, soils that

contain high amounts of fine particles are highly susceptible to moisture, making any excess amount of moisture highly unfavorable for the pavement's integrity. One of the reasons why fine particles tend be hydrophilic in nature is that they encompass a vast surface area relative to coarse particles (Santamarina et al, 2002). To get a better understanding of how the surface area of fine particles is greater than the surface area of coarse particles, an idealized cubical sample with length (L) can be assumed. If the surface area of a cubical sample with length (L) is assumed to be (S_A) as seen in Equation 1.10, and the cube is cut in half along every axis an n^{th} number of times as seen in Figure 1.19, the new surface area will become $S_{A(n)}$ as seen in Equation 1.11. From Equation 1.12, which represents the ratio between new surface area generated by slicing the cube divided by the initial surface area, it can be seen that the surface area of the cubical samples increases exponentially by a factor of two for every slicing of the cube.

$$S_A = 6L^2 \tag{1.10}$$

Where:

S_A = Initial surface area

L= Original length of cube

$$S_{A(n)} = 2^n 6L^2 \tag{1.11}$$

Where:

$S_{A(n)}$ = Surface area after the n^{th} slicing

L= Original length of cube

n = Number of slicing's

$$\frac{S_{A(n)}}{S_A} = 2^n \tag{1.12}$$

Where:

$S_{A(n)}$ = Surface area after the n^{th} slicing

S_A = Initial surface area

n = Number of slicing's

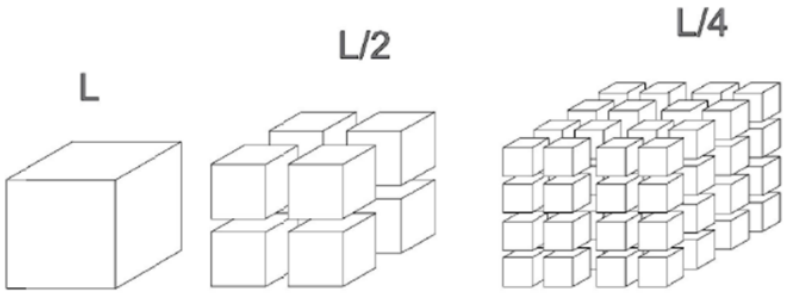

Figure 1.19: Cubical sample with length (L) cut in half along each axis.

Similar to the idealized cubical scenario mentioned above, the surface area of fine particles increases greatly as the particles become smaller. This allows more area for water molecules to interact with soil particles increasing the moisture susceptibility. Studies demonstrate that as the percent of fines content increased in the soil material, the permanent deformation potential also increases, especially for high plasticity fines (Ohiduzzaman et al, 2012).

Moisture Content

Moisture is one of the permanent deformation factors that is difficult to control and maintain at a constant level due to its ability to randomly appear in any location at any given time. Naturally, water travels from a higher concentration to a lower concentration seeking equilibrium and exploiting any gaps available. For example, if a pavement undergoes shrinking and swelling, which leads to the development of cracks in the pavement structure, water molecules will take advantage of these pathways to infiltrate the UGLs, resulting in higher moisture contents in the permeated areas. Therefore, it is important to acknowledge that a pavement section will inevitably be exposed to higher moisture contents than those initially anticipated. It is also important to monitor the position of the water table because some material may be exposed to capillary rise in the subgrade. Therefore, when analyzing the permanent deformation potential of UGLs it is important to include different moisture levels to understand the effect of moisture at different concentrations. Studies utilizing repeated loading applications demonstrated that moisture is a primary contributor to the permanent deformation potential (Ahmad, 2014).

Synergistic effect of moisture and fines content

Since soils will always contain a combination of moisture and the percent of fines content, it is important to consider both parameters synergistically. Research performed using variations in the moisture and amount of fines content utilized the dynamic loading tests to determine how permanent deformation changes with alteration in the parameters (Soliman and Shalaby, 2015). For the studies, a limestone and a gravel material were tested under three different gradations, which varied in the percent of fines resulting in six different combinations. Figures 1.20 and 1.21 demonstrate how the permanent deformation increased with an increase in the moisture content and an increase in the fines content.

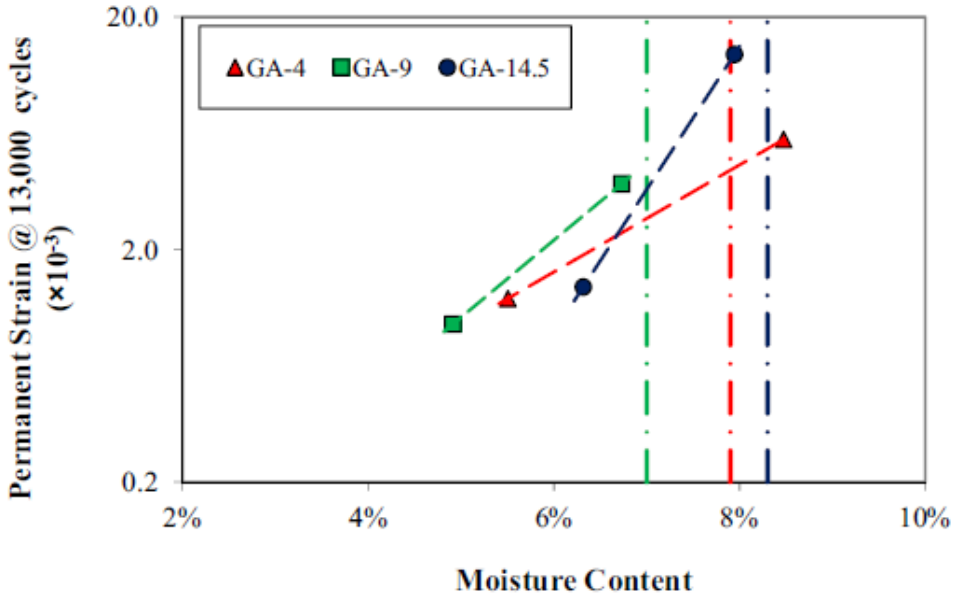

Figure 1.20: Permanent strain versus moisture content for gravel material with varying fines content (Soliman and Shalaby, 2015).

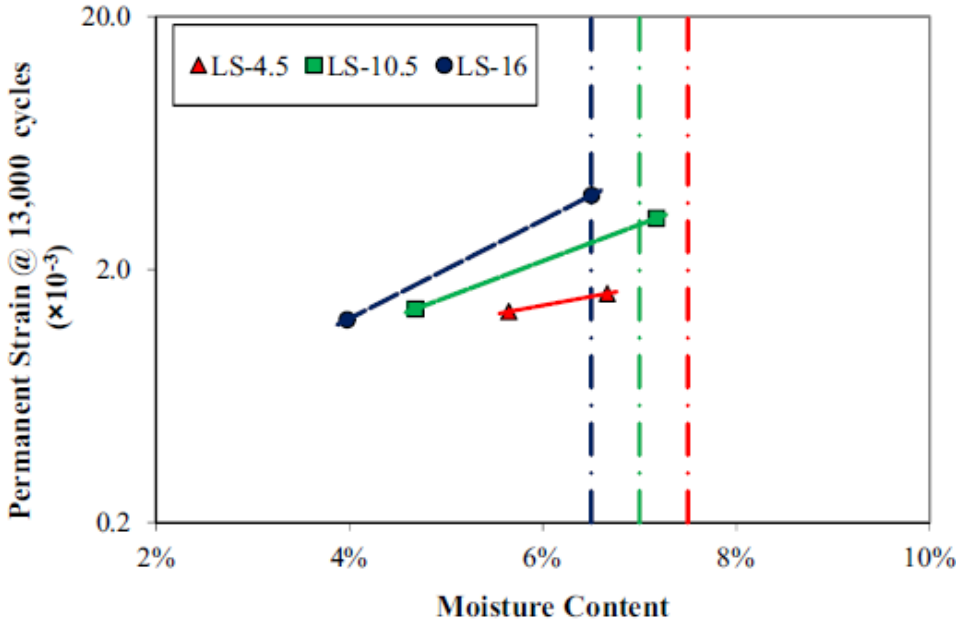

Figure 1.21: Permanent strain versus moisture content for the limestone material with varying fines content (Soliman and Shalaby, 2015).

As shown in Figures 1.20 and 1.21, permanent deformation increased as the moisture content was elevated. Further the slope of the permanent deformation also increases as the percent of fines content in the mix increased; demonstrating the effect of the fines in the deformation potential.

MODELING OF PERMANENT DEFORMATION

The genesis of permanent deformation prediction models begins with the Barksdale logarithmic model (Barksdale, 1972), and the Monismith's power model (Monismith et al, 1975) as seen in Equations 1.13 and 1.14. Both models utilize the number of load repetitions accompanied by regression parameters to estimate the permanent deformation. These early models assume that permanent deformation of geomaterials follow an asymptotic behavior as earlier stated in the plastic shakedown theory. Later Verveka proposed the incorporation of the resilient strain within the model as seen in Equation 1.15, which accounted for the resilient properties of the material (Verveka, 1979). However, the model parameters are not capable of expressing the influence of moisture state, gradation, and the stress states in the laboratory testing protocol. Therefore, a more suitable model needed to be developed to include more permanent deformation factors in the regression parameters. Tseng and Lytton developed a three-parameter model that is capable of capturing all three shakedown modes as seen in Equation 1.16. For their model the regression parameters correlated to the moisture state and resilient properties of the specimen in the laboratory (Tseng and Lytton, 1989). The current Mechanistic Empirical Pavement Design Guide as seen in Equation 1.17, adopted the same model shape function for the estimation of the rut depth during the service life of flexible pavements. This implementation managed to incorporate stresses into the regression parameters making permanent prediction more receptive to the loading effects (NCHRP, 2004). A more precise approach to successfully incorporate

stresses in the field should be made via the length and the slope of the stress path which will ultimately incorporate all the factors involved in the dynamic movement of the wheel load. Table 1.1 summarizes all of the mentioned models.

Table 1.1: Permanent Deformation Models

Evolution of Permanent Deformation Models		
Model	Model source	Variables
(1.13) $\varepsilon_p = a + b\log(N)$ (1.14) $\varepsilon_p = aN^b$ (1.15) $\varepsilon_p = a\varepsilon_r N^b$ (1.16) $\varepsilon_p = \varepsilon_0 e^{-(\frac{\rho}{N})^\beta}$ (1.17) $\delta_a(N) = \beta_1(\frac{\varepsilon_0}{\varepsilon_r})e^{-(\frac{\rho}{N})^\beta}\varepsilon_v h$	(1.13) (Barksdale, 1972) (1.14) (Monismith et al, 1975) (1.15) (Verveka, 1979) (1.16) (Tseng and Lytton, 1989) (1.17) (NCHRP, 2004)	$a, b, \varepsilon_0, \beta, \rho$ - Model parameters β_1 - Calibration factor of UGL $\delta_a(N)$ - Permanent Deformation ε_r - Resilient strain ε_p - Permanent strain ε_v - Average vertical resilient strain h - Thickness of layer/sub-layer N - Number of load applications

Chapter 2: Methods and Testing

MATERIAL

The material used in the study consisted of a limestone sourced from El Paso. The fines in the mix gave a liquid limit and plasticity index of 23% and 9%, respectively. The material was then adjusted into three different gradations with variations in the amount of fines content. The gradations were selected on the basis of TxDOT item 247 specifications which identifies the tolerances for base and subbase layers. Each gradation varies and is adjusted according to the amount of material passing sieve #200, denoted as fine grained materials. In this effort, the gradation with 5% fines grained material is referenced as the coarse gradation, the gradation with 10% passing sieve #200 material is referenced as the intermediate gradation, and finally the gradation with 15% particles smaller than 75 μm is denoted as the fine gradation as seen in Figure 2.1.

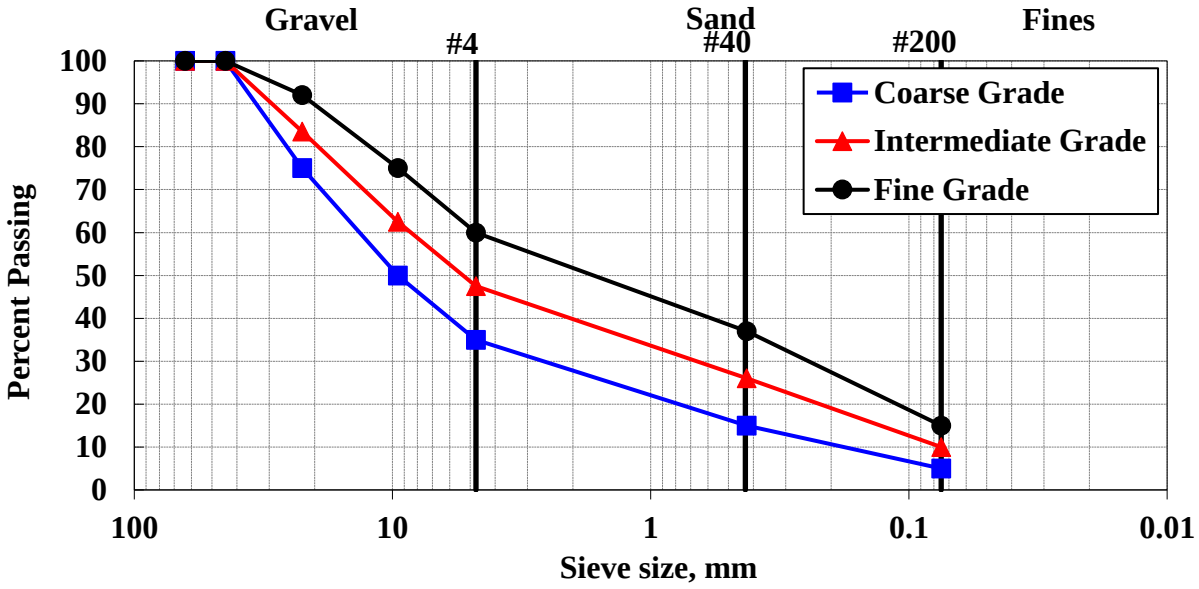

Figure 2.1: Gradation Curves for the Limestone Materials with Different fine contents.

SELECTION OF MOISTURE CONTENTS

In order to properly capture the deleterious effect of moisture ingress in geomaterials each gradation was tested at three different moisture states. The usage of multiple moisture states with increasing saturation levels, provided a better representation of both the softening and hardening behavior of laboratory specimen. The maximum dry density and optimum moisture content of each gradation were obtained with the use of the modified proctor test to determine how each gradation responded to different levels of moisture. Figure 2.2 demonstrates the maximum dry density and optimum moisture content of each gradation. For the calculation of the degrees of saturation a specific gravity of 2.67 was assumed (Holtz et al, 1981) and Equation 2.1 was used. Table 2.1, demonstrates the moisture values utilized to approximate 40%, 60%, and 80% degree of saturation.

$$S_r = \frac{\omega G_s}{\frac{G_s \gamma_w}{\gamma_d} - 1} \tag{2.1}$$

Where:

S_r = Degree of saturation

ω = Moisture content

G_s = Specific gravity of soil ≈ 2.67

γ_w = Unit weight of water $\approx 62.4 \ \frac{lbs}{ft^3}$

γ_d = Dry unit weight of soil

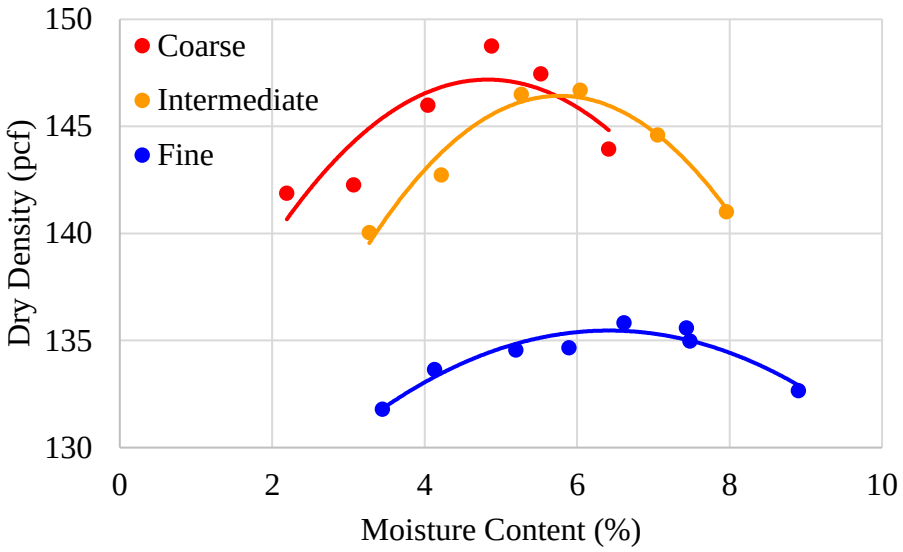

Figure 2.2: Dry density curves for the coarse, intermediate, and fine gradations.

Table 2.1: Moisture Contents that Correspond to the 40%, 60% and 80% Degree of Saturation for Each Gradation

Gradation	Degree of Saturation	Moisture Content (%)
Coarse	40%	2.3
	60%	3.1
	80%	4
Intermediate	40%	2.8
	60%	3.8
	80%	4.7
Fine	40%	4
	60%	5
	80%	6

The 40% degree of saturation trials were used to target the effects of low pore water pressures and understand how increasing the fines content affected permanent deformation at low moisture levels. The 80% degree of saturation samples were used to simulate saturation levels close to the optimum moisture state, while the 60% degree of saturation levels were used to resemble the

transition between saturation degrees. Specimen molded at saturation levels higher than 80% became un-testable due to reduced stiffness properties which are more pronounced for high fines content systems; therefore, such permutations were eliminated from the experiment design.

EQUIPMENT

The equipment utilized to generate the soil specimen in the laboratory consisted of a steel mold with a 12-inch height and a 6-inch dimeter as seen in Figure 2.3. Compaction of the specimen was performed by a compaction machine as seen in Figure 2.4, to eliminate compaction discrepancies made by human error.

Figure 2.3: Shows the cylindrical mold utilized for the specimen generation.

Figure 2.4: Shows the compaction machine during compaction of a cylindrical specimen.

The compaction machine followed the compaction protocol of the modified Procter test (Tex-114-E, 2011). For the application of stresses, the Universal Testing Machine (UTM–25) as seen in Figure 2.5, was selected for the execution of the repeated load permanent deformation tests of geomaterials in the laboratory.

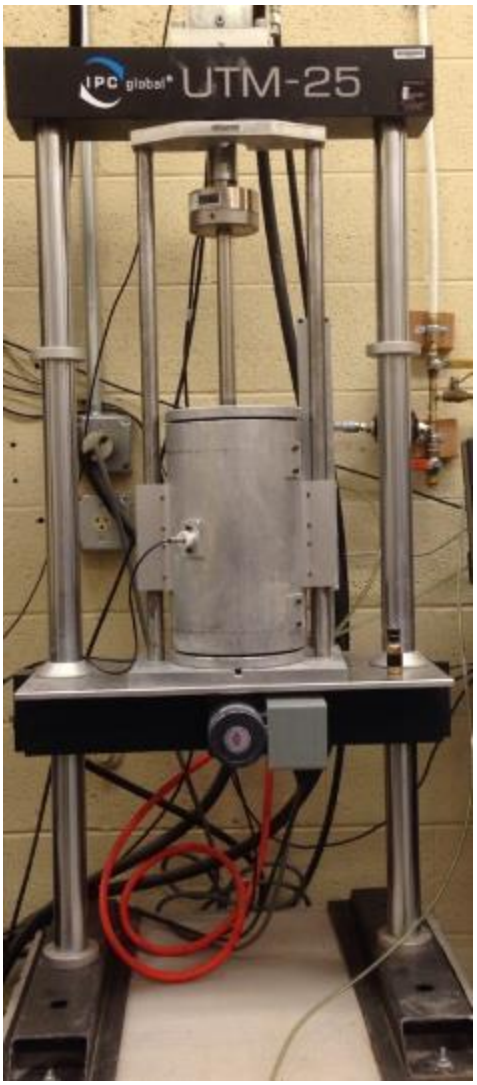

Figure 2.5: UTM-25 utilized for the application of various stress paths on laboratory specimen.

For the application of the confinement a rigid triaxial cell with a multi-channel data acquisition systems capable of applying constant confinement via a pressure membrane was utilized for testing the specimens as seen in Figure 2.6.

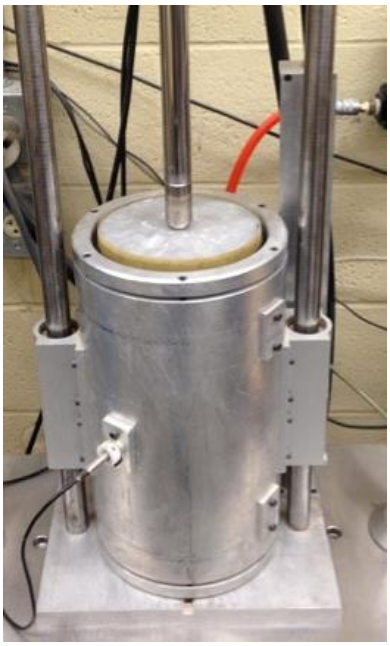

Figure 2.6: Rigid triaxial cell used to apply confinement to the laboratory specimen.

DEVELOPMENT OF SOIL SPECIMEN

The soil specimens utilized for the test were constructed in four different phases of: mixing, moisturizing, compacting, and sealing. Every specimen created was made under the same rigid steel mold, with the same compaction machine, mixed, and compacted by the same individual to insure no variations occurred during the construction phases. The mixing of the specimens were done manually inside a plastic container as seen in Figure 2.7, for the coarse, intermediate, and fine gradation.

(a)

(b)

(c)

Figure 2.7: Shows the (a) coarse, (b) intermediate, and (c) fine gradation in containers before the addition of moisture.

Second, moisture was slowly added and mixed thoroughly until the water distribution was uniform through the material as seen in figure 2.8

(a)

(b)

(c)

Figure 2.8: Material after the addition and mixing of water for the (a) coarse, (b) intermediate, and (c) fine gradation.

After the material had been mixed uniformly the soil was then slowly added in layers into the cylindrical mold for compaction as seen in Figure 2.9

(a)

(b)

(c)

(d)

Figure 2.9: Shows the process of compaction of (a) loose material in the first layer, (b) compacted first layer, (c) loose material in the middle layer, (d) compacted final layer.

After the compaction, the specimens were removed from the cylindrical mold via a bottle jack as seen in Figure 2.10.

(a) (b) (c)

Figure 2.10: Specimen removed from mold for the (a) coarse gradation, (b) intermediate gradation, (c) fine gradation.

Once the material had been successfully removed from the cylindrical mold, a rubber membrane was placed around the specimen to prevent moisture loss as seen in Figure 2.11.

Figure 2.11: Cylindrical specimen ready for testing.

The membrane extremities were sealed with a tight band to prevent moisture intrusion in the top and bottom areas of the specimen. After sealing from moisture intrusion, the specimens were placed inside the confinement triaxial cell ready for the test sequence to begin.

TESTING

The testing scheme consisted of subjecting the specimen to a repeated loading test with varying fines content, different moisture states, and multiple stress paths to determine the synergistic effect these factors have over permanent deformation. For the calculation of the stress paths, Equation 1.8 was used where a CCP of 5 psi was used for (σ_{3i}) and (σ_{3f}), and an isotropic loading of 5 psi was used (σ_{1i}). The first stress path used a max vertical stress of 20 psi, the second stress path used a max vertical stress of 25 psi, and the third stress path used a max vertical stress of 35 psi. Table 2.2 shows the experimental matrix for the testing scheme of the research.

Table 2.2: Experimental Matrix Consisting of Stress Path Length, Degree of Saturation, and Fine Content

	Fines Content (%)	40% Degree of Saturation		60% Degree of Saturation		80% Degree of Saturation	
		Sample A	Sample B	Sample A	Sample B	Sample A	Sample B
Stress Path 1	5%	1	2	3	4	5	6
	10%	7	8	9	10	11	12
	15%	13	14	15	16	17	18
Stress Path 2	5%	19	20	21	22	23	24
	10%	25	26	27	28	29	30
	15%	31	32	33	34	35	36
Stress Path 3	5%	37	38	39	40	41	42
	10%	43	44	45	46	47	48
	15%	49	50	51	52	53	54

Each permutation was duplicated to obtain the average deformation of the two specimens, resulting in a total of 54 specimens.

Load applications

For the cyclic loading tests, each test consisted of 10,000 load cycles, where each cycle had a 0.1 second loading phase followed by a 0.9 second resting period. The permanent strain was measured with the actuator LVDT capturing 40 points per loading cycle. The collected data points served for the calculation of the area of the hysteresis loop and the determination of the maximum permanent deformation per cycle.

Chapter 3: Analysis and Results

PERMANENT DEFORMATION

A comprehensive experimental matrix consisting of 54 specimens tested at different moisture states, fines content, and stress paths was undertaken in this research effort. The average strain at the 10,000th loading cycle was obtained to approximate the deformation potential under varying conditions. Data for the third stress path with 80% degree of saturation for the intermediate and fine gradations is limited to only a few hundred loading cycles due to failure of materials during testing. In such cases when the equipment registers a rapid increase in the deformation gradient, the program automatically stops testing as a precaution to prevent equipment damage. Therefore, data for these specimens is limited to a few hundred cycles. Figure 3.1 demonstrates the increase in permanent deformation with an increment in the degree of saturation and amount of fines content.

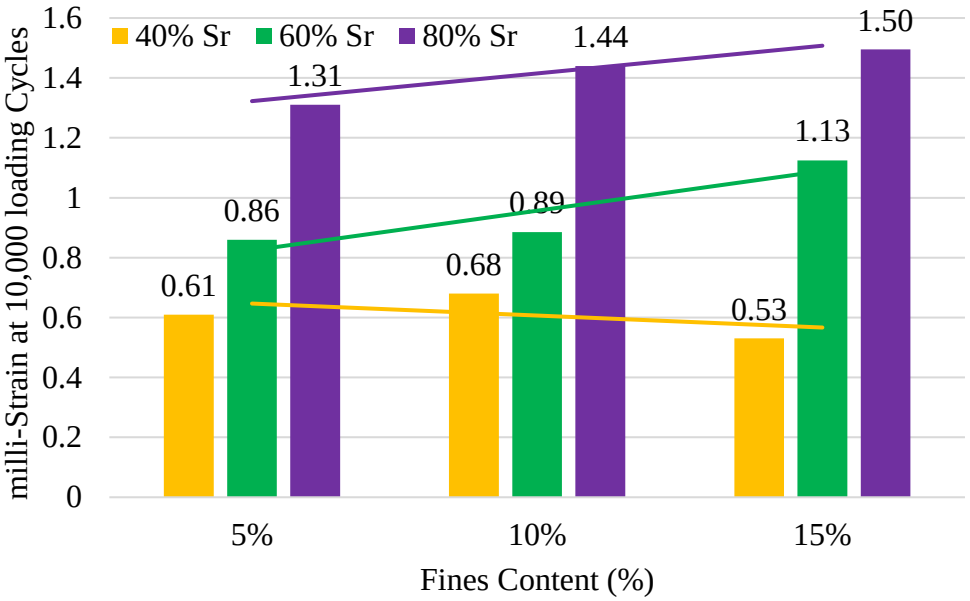

(a)

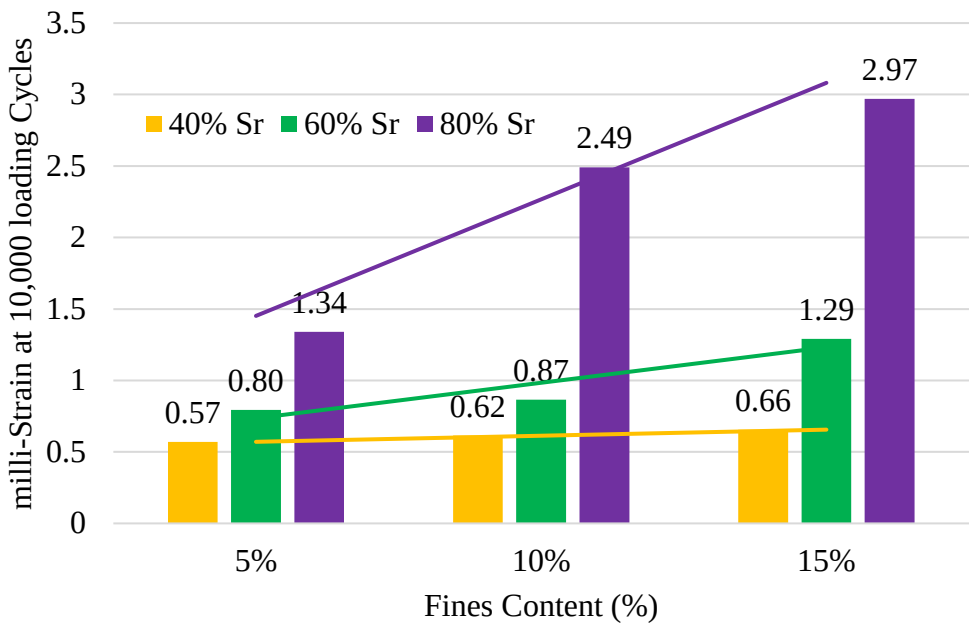

(b)

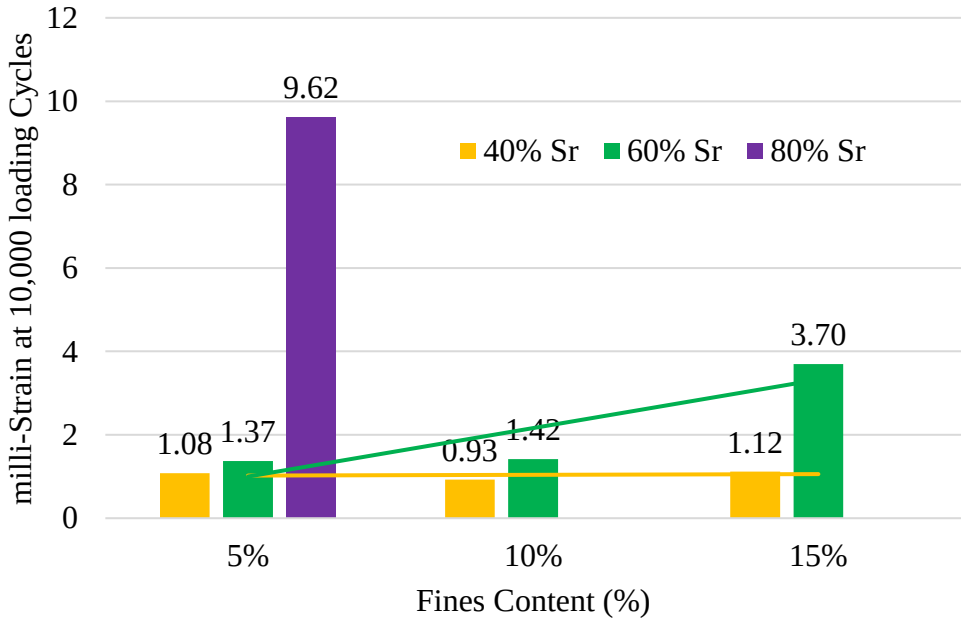

(c)

Figure 3.1: Strain at the 10000th loading cycle for (a) stress path 1, (b) stress path 2, and (c) stress path 3.

As observed in the previous figures, permanent deformation increases with the increase of moisture, increase of fines, and increase of the stress path length. A noteworthy observation is that the registered growth in permanent deformation with moisture increase is independent of the percent of fines content and the stress path. This means that permanent deformation is highly responsive to fluctuations in the moisture. It can also be noted that intensifying the stresses increases the permanent deformation at an exponential rate exclusively for high fines and high saturation values. Further, the slope of the fitted lines demonstrates the influence of the fines content increase. For 60% and 80% degrees of saturation the increase in permanent deformation was highly influenced by the percent of fines content. However, for a 40% degree of saturation the permanent deformation did not experience a significant increase. This anomaly might be caused by suction values that are more produced in soils with low saturation values and interaction of the fines in the specimen.

HYSTERESIS LOOPS

Figure 3.2, shows a more detailed representation of the permanent deformation increase with the progression of load applications for the 1^{st}, 100^{th}, and $10{,}000^{th}$ load cycles. Since specimens molded at high amounts of moisture, high fines content, and high stresses did not reach 10,000 loading applications, the data for these specimen is only presented for the 1^{st}, 10^{th}, and 100^{th} load cycle.

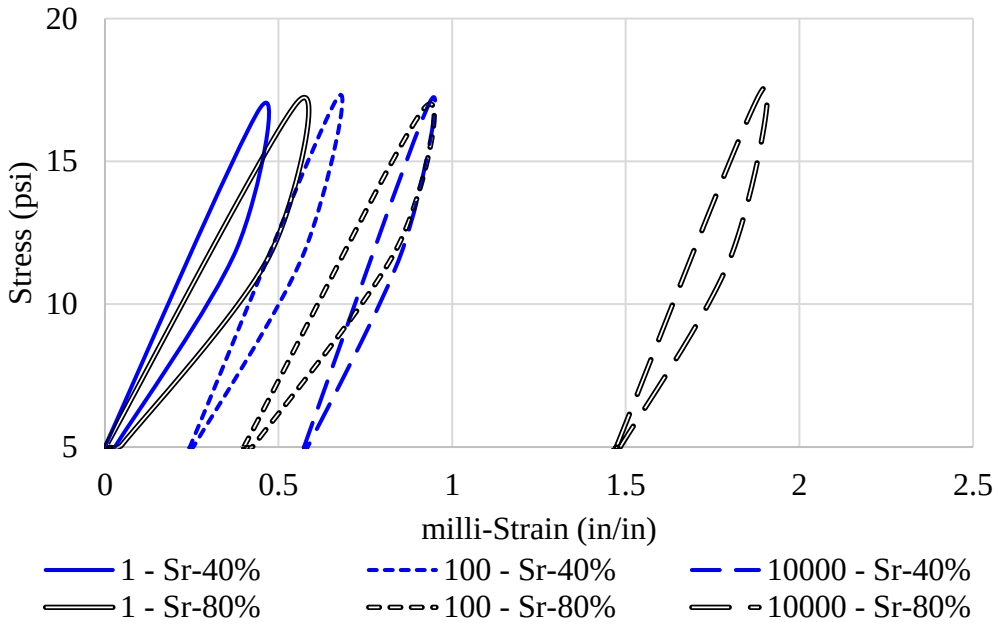
20
15
10
5
Stress (psi)
0
0.5
1
1.5
2
2.5
milli-Strain (in/in)
1 - Sr-40%
100 - Sr-40%
10000 - Sr-40%
1 - Sr-80%
100 - Sr-80%
10000 - Sr-80%

(a)

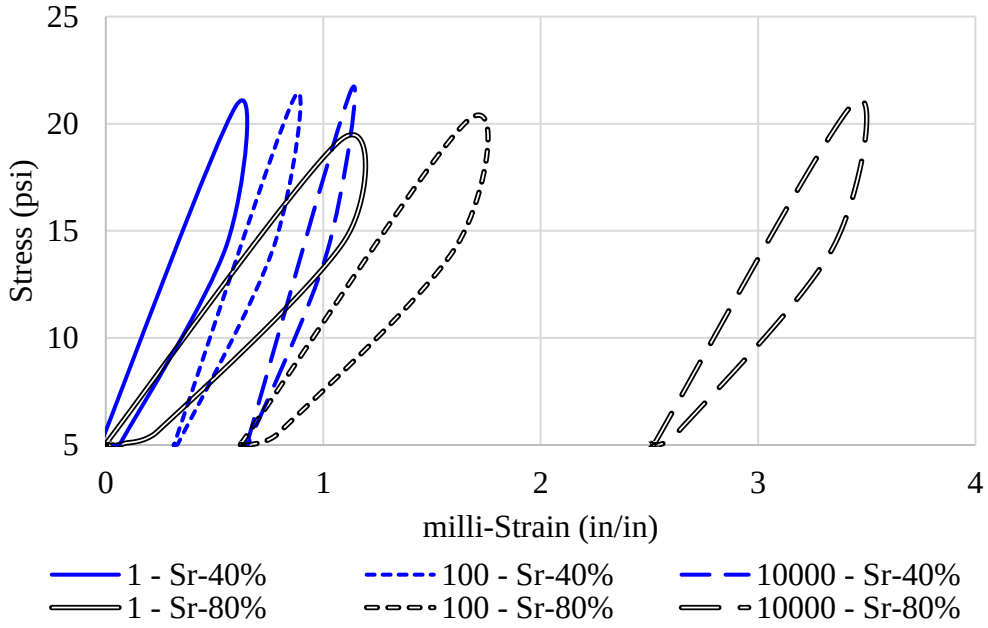
25
20
15
10
5
Stress (psi)
0
1
2
3
4
milli-Strain (in/in)
1 - Sr-40%
100 - Sr-40%
10000 - Sr-40%
1 - Sr-80%
100 - Sr-80%
10000 - Sr-80%

(b)

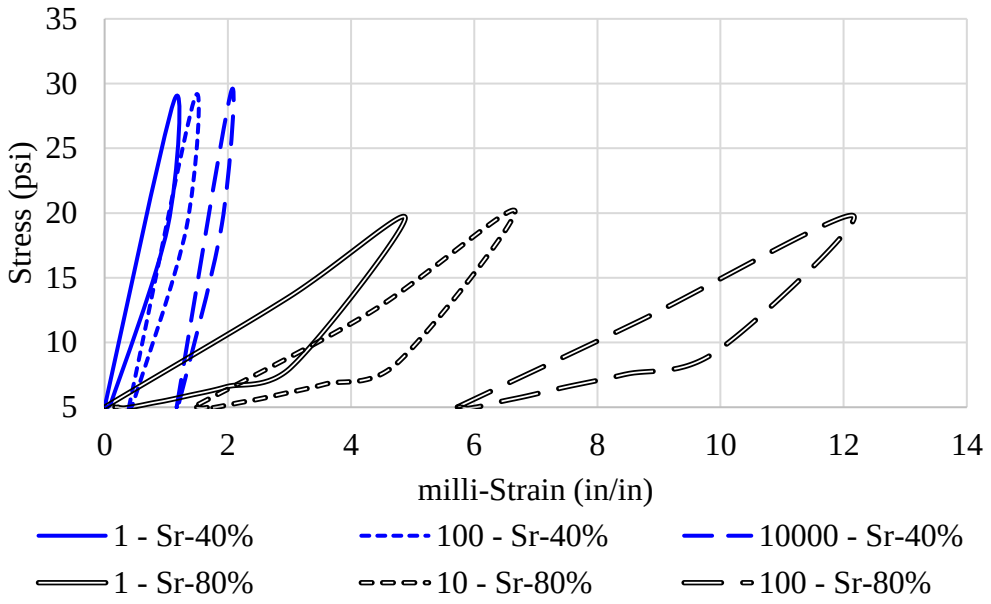

(c)

Figure 3.2: Permanent deformation of (a) the first stress path under the coarse gradation, (b) second stress path under the intermediate gradation, (c) third stress path under the fine gradation.

Analysis presented in the figure above demonstrates how the specimen subjected to the first and second stress path underwent hardening behavior where the orientation of the hysteresis loop increased as the progression of load applications increased. This behavior is due to stiffening of the material where the loading applications act as an extra means of compaction for the specimen. Figure 3.2c demonstrates how the specimen with 80% degree of saturation underwent a softening behavior where the orientation of the hysteresis loops decreases as the number of loading applications increased. It can also be noted that the size of the hysteresis loops increased as the moisture was elevated from 40% to 80% degree of saturation.

DISSIPATED STRAIN ENERGY

In a different approach, analysis of the dissipated strain energy can provide valuable insights of the specimen responses to variations in moisture, fines content, and stress path. Figure 3.3 provides a summary of the strain energy calculations for the 40% and 80% degree of saturation, 5% and 15% fines content, and first and third stress path permutations of the experiment design. Specimen of the 60% degree of saturation, 10% fines content, and second stress path are not presented to avoid crowding of the figure.

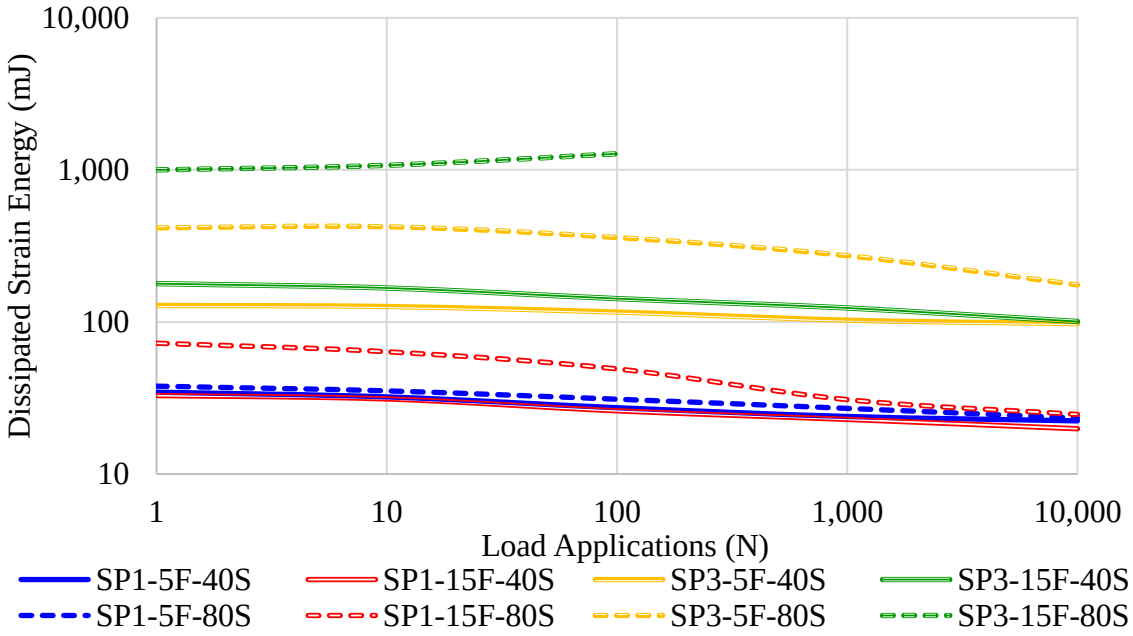

Figure 3.3: Variation of the dissipated energy with the increase in the number of load cycles

As shown in this plot, aggregate systems with high fines content compacted at elevated moisture states had significantly higher dissipated strain energies compared to low fines, low moisture counterparts. Low dissipated energy levels in low fines content permutations confirms the recent efforts to minimize the P-200 portion of the mix to improve the rutting potential and stability of

granular layers in the field. This is particularly important in cold climates where the depth of the freeze zone stretches several feet down in the ground. Additionally, specimens subjected to higher stress states exhibited higher dissipated strain energies compared to the specimens tested at lower stress levels. Figure 3.4 provides the results for the degree of plasticity of the tested variants in the experiment design. The plastic values are essentially the ratio of stored energy divided by total energy as presented in Equation 1.4. The results provide valuable insight on the synergistic influence of the moisture content, fines content, and stress states on the rutting potential of granular layers.

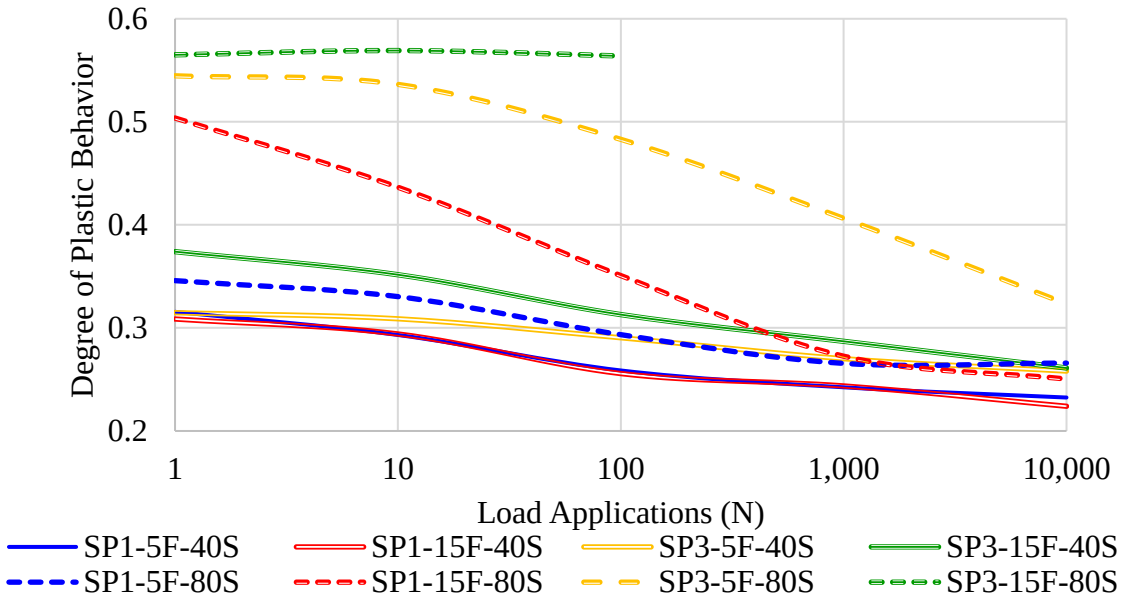

Figure 3.4: Degree of plastic behavior versus load applications.

The descending nature of the curves in Figure 3.4 indicates that the level of plasticity of the materials reduces with increasing number of load cycles. A plausible explanation for this behavior could be attributed to the initial shifting and readjustment of the aggregate particles in the first few loading cycles due to compaction and handling of specimen to the test set up. However, it can be

noted that the degree of plastic behavior is high in those specimens with higher levels of moisture, and fines content. This is a direct consequence of softening behavior of aggregate systems with high fines molded at high moisture content. The sharp descending slope in the first few cycles is an indication of the readjustment and stiffening of the materials under cyclic loading. This stiffening behavior under repeated loading is also evident in the analysis of the modulus of elasticity of the materials presented in Figure 3.5.

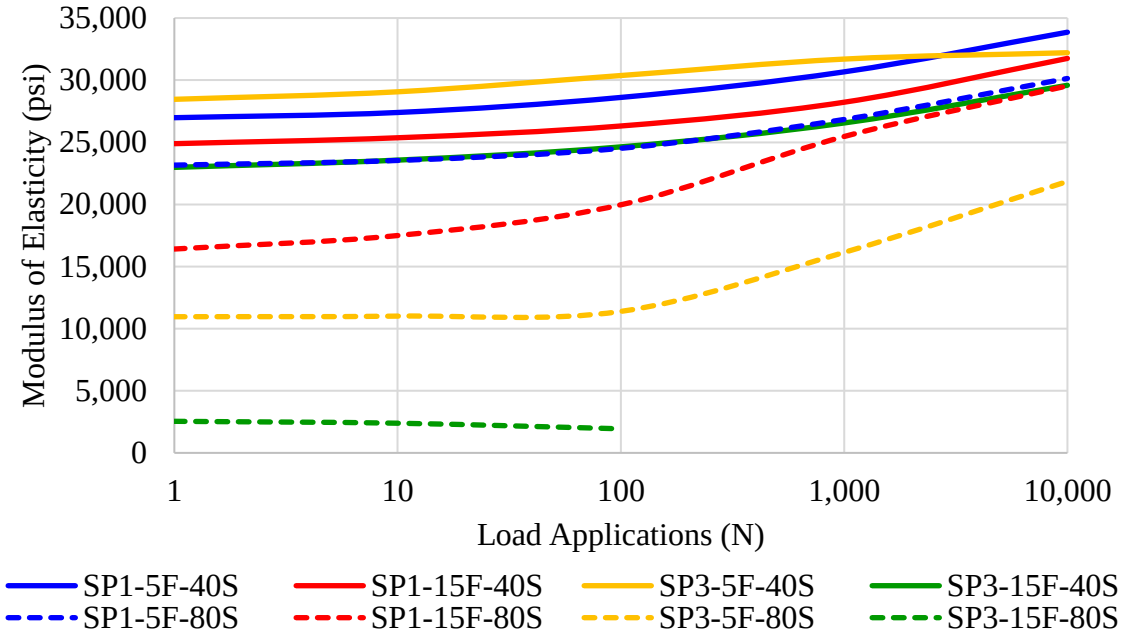

Figure 3.5: Changes in modulus of elasticity with progression of load applications.

The ascending nature of the modulus curves with load cycles is associated with the reduction of the air void content and better particle interlocking effect which is manifested in higher modulus values. A noteworthy observation is that the modulus registers a high drop when an increase in the degree of saturation occurs. This effect may be caused by the increase in the pore water pressure which in turn reduces the effective stresses of the soil.

CORRELATIONS

A side-by-side comparison of Figure 3.4 and 3.5 can provide noteworthy information on the inverse relationship between the degree of plasticity and the calculated modulus values. Figure 3.6 provides such comparisons between the modulus values and the degree of plastic behavior of the permutations tested in this study.

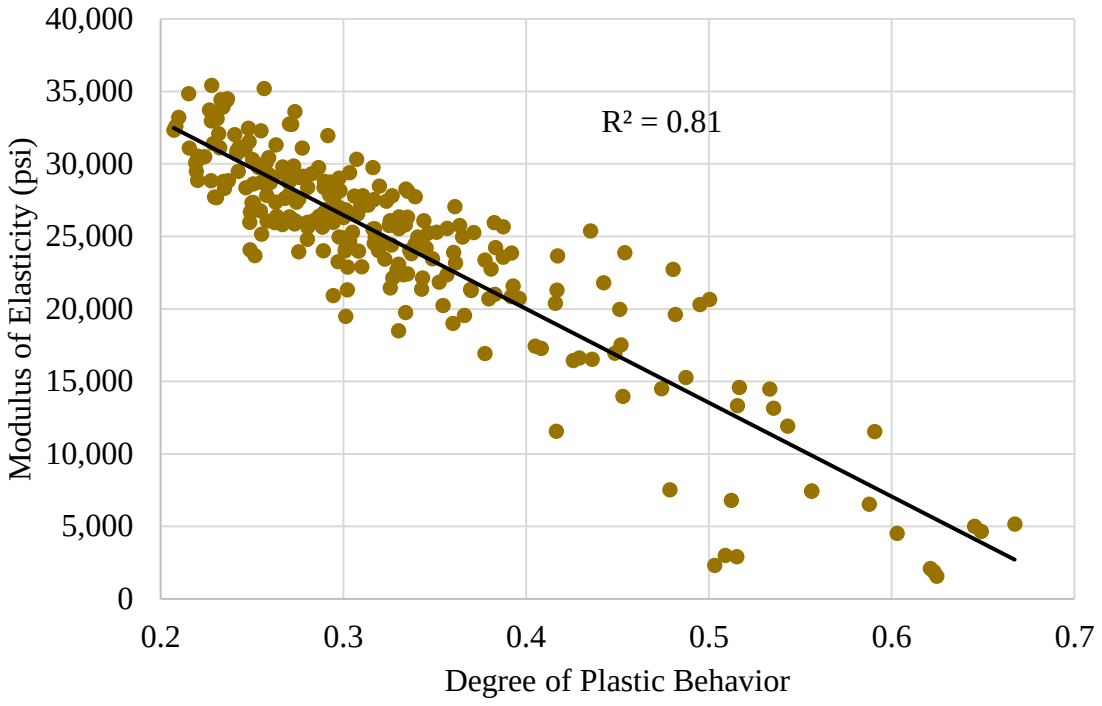

Figure 3.6: Correlation between the modulus of elasticity and the degree of plastic behavior

Essentially, the trendline indicates that a material with a low degree of plastic behavior exhibits a higher modulus of elasticity in the repeated load permanent deformation tests in the laboratory. Similarly, the angle of inclination of the hysteresis loops can be plotted against the modulus values. It is worth noting that smaller values of orientation angles correspond to flatter loops upon

experiencing damage in the system. Figure 3.7 shows the direct relationship between the inclination angle and the calculated modulus values of the aggregate systems.

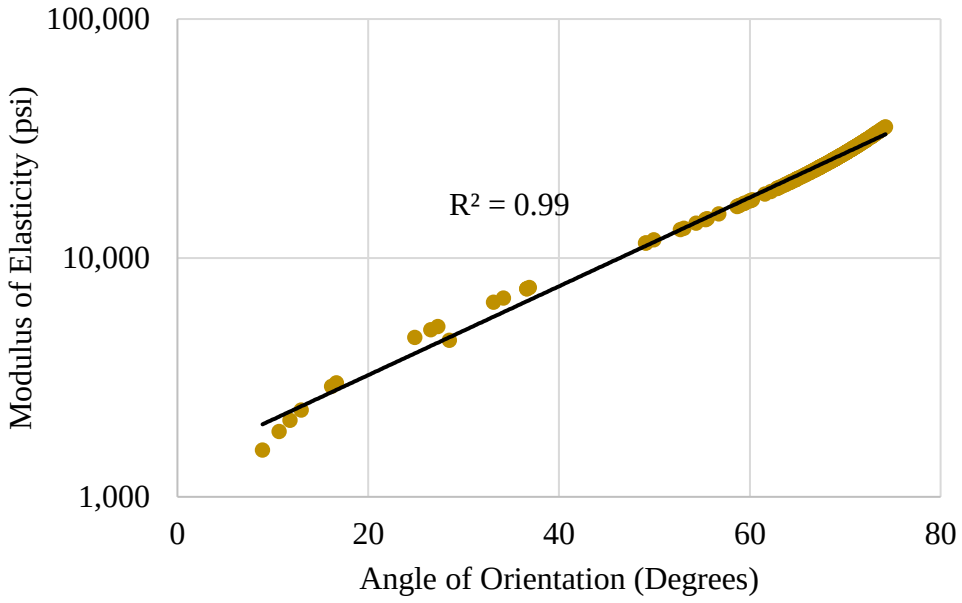

Figure 3.7: Correlation between the angle of orientation and the modulus of elasticity.

As shown in this plot, aggregate specimens with higher modulus values exhibited less inclination in the hysteresis loops when subjected to the cyclic loading. This behavior demonstrates that the reduction of the orientation angle is caused by the reduction of the load bearing capacity due to softening. Figure 3.8 demonstrates the correlation between the total permanent deformation at 10,000 load cycles and the degree of plastic behavior.

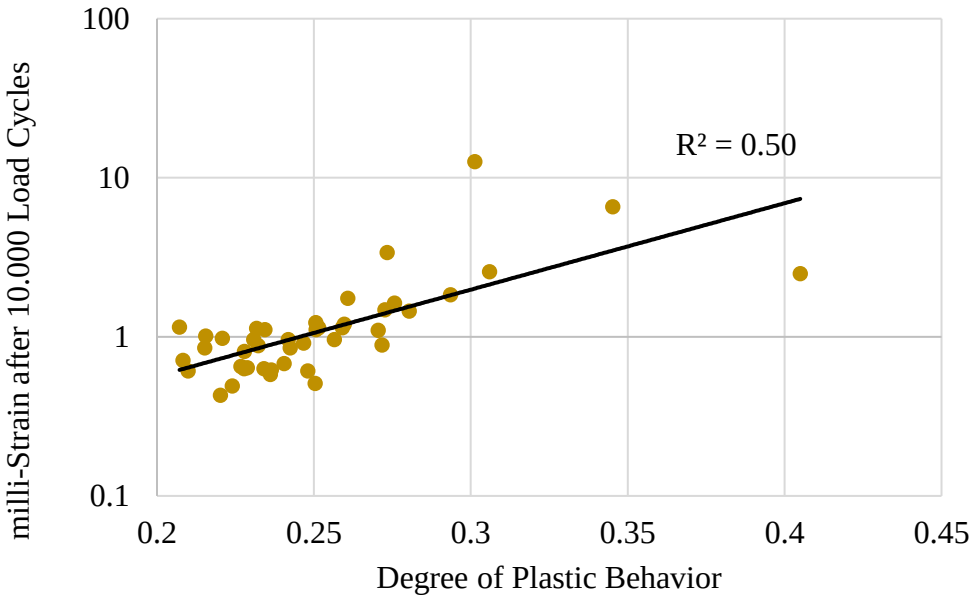

Figure 3.8: Correlation between the permanent deformation after the 10,000th load cycle and the degree of plastic behavior.

From the plot, a fair correlation (R^2 = .50) can be seen between the increase of the permanent deformation and the increase in the degree of plasticity. This behavior can be attributed to the material's high plastic behavior allowing for more storage of strain in the material. Similarly Figure 3.9 demonstrates the correlation between a material's modulus of elasticity and the total deformation at the 10,000th load cycle.

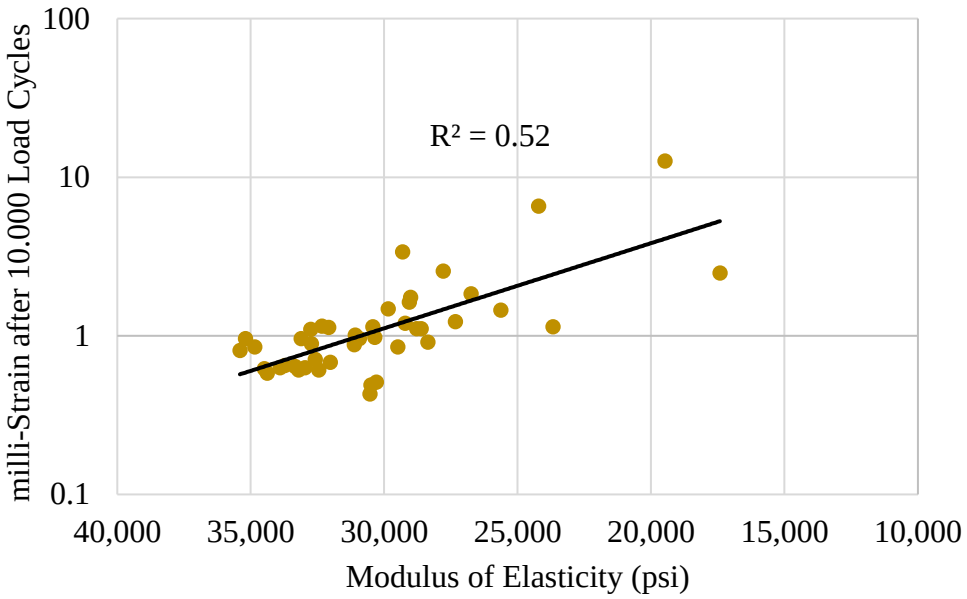

Figure 3.9: Correlation between the permanent deformation after the 10,000th load cycle and the modulus of elasticity.

Similar to Figure 3.8, the inverse relationship between the modulus and the degree of plastic behavior demonstrates that the specimens with lower moduli had higher degrees of plastic behavior resulting in higher permanent deformations.

PERMANENT DEFORMATION MODELING

A multi-dimensional aggregate feature database was developed in this study to identify the parameters that have the highest influence of the deformation behavior of geomaterials. The laboratory data were analyzed using statistical techniques to estimate the parameters of the permanent deformation model presented in Equation 1.16. The parameters of the regression model were in turn correlated to the most physically relevant features such as deviation from the degree of saturation, fines content, and the characteristics of the stress path length. The regression models and the goodness of the fit are reported in Table 3.1.

Table 3.1: Permanent Deformation Model Consisting of Degree of Saturation, Fine Content, and Length of Stress Path

Permanent deformation equation	Variables
$\varepsilon_p = \varepsilon_0 e^{-(\frac{\rho}{N})^{\beta}}$	$f\%$ - Fine content L - Stress path length $S\%$ - Degree of saturation $A_i, B_i, C_i, \varepsilon_0, \beta, \rho$ - Model parameters ε_p - Permanent strain N - Number of load applications
Regression Model Parameters	
$\varepsilon_0 = A_\varepsilon + B_\varepsilon S\% + C_\varepsilon f\%$, $R^2 = 0.88$ $A_\varepsilon = 3.99 - 1.98\ln(L)$ $B_\varepsilon = -0.047 + 0.034\ln(L)$ $C_\varepsilon = -0.533 + 0.206\ln(L)$	
$\rho = A_\rho + B_\rho S\% + C_\rho f\%$, $R^2 = 0.90$ $A_\rho = 1237 - 119.5L + 2.76L^2$ $B_\rho = -21.1 + 2.75L - 0.057L^2$ $C_\rho = -70.42 + 8.24L - 0.175L^2$	
$\beta = A_\beta + B_\beta S\% + C_\beta f\%$, $R^2 = 0.84$ $A_\beta = -0.693 + 0.059L - 0.001L^2$ $B_\beta = 0.009 - 0.0004L + 7X10^{-6}L^2$ $C_\beta = 0.025 - 0.002L + 7X10^{-5}L^2$	

The greatest difficulty found in the modeling of permanent deformation with variations in the moisture, fines content, and stresses was that the registered strains increased rapidly when the material exited the plastic shakedown behavior. For this reason, specimens tested at the highest stress states and highest moisture states were not included in the model. Figure 3.10 shows the relationship between the laboratory strain measurements at the 10,000th load cycle and the predicted values using the proposed model.

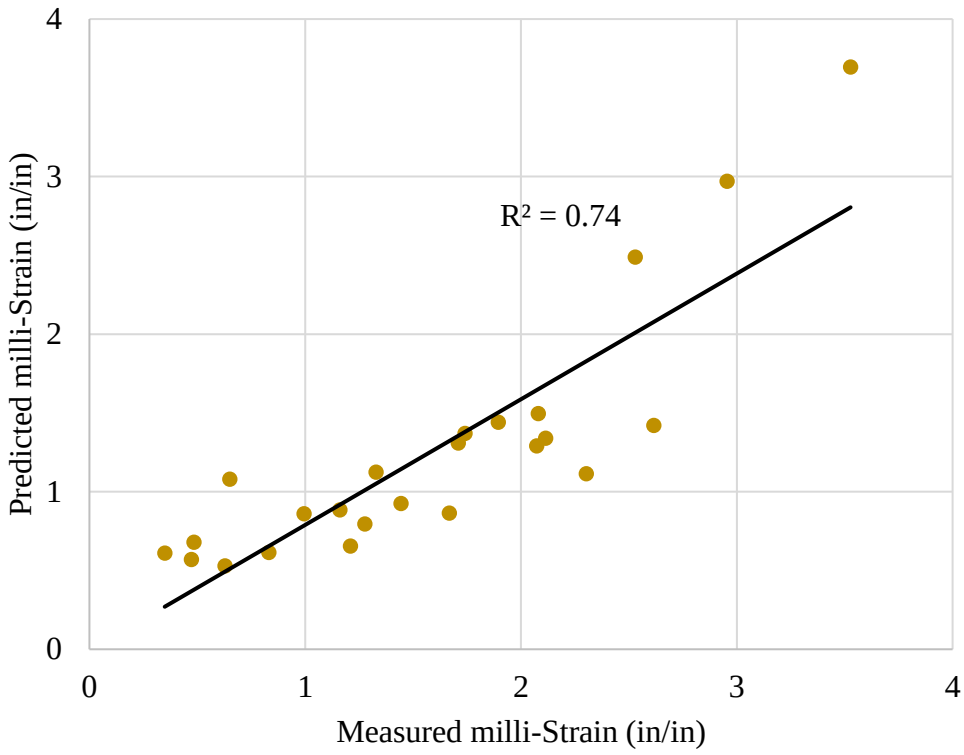

Figure 3.10: Measured strain versus predicted strain.

As seen in the plot a reasonable agreement exists between the measured and predicted data in this research. It is important to note that the presented model is more suitable for plastic shakedown behavior; specimens with the highest levels of moisture, fines content, and stress experienced a deviation from the equality line. Figure 3.11 shows the pairwise comparisons of measured strain versus predicted strain at the 10,000th load cycle.

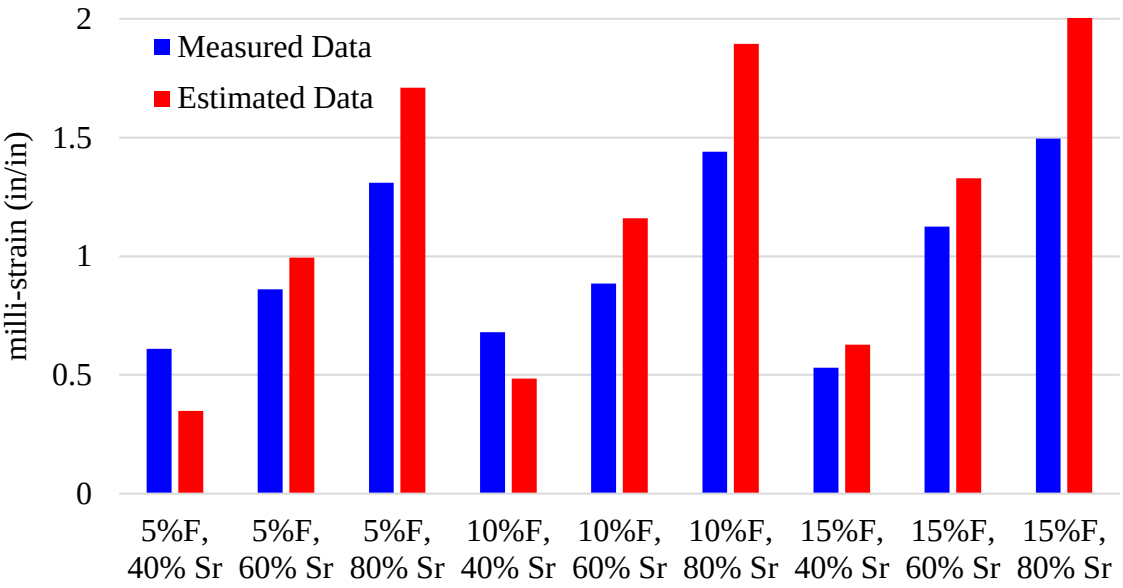
Measured Data
Estimated Data
milli-strain (in/in)
2
1.5
1
0.5
0
5%F, 40% Sr
5%F, 60% Sr
5%F, 80% Sr
10%F, 40% Sr
10%F, 60% Sr
10%F, 80% Sr
15%F, 40% Sr
15%F, 60% Sr
15%F, 80% Sr

(a)

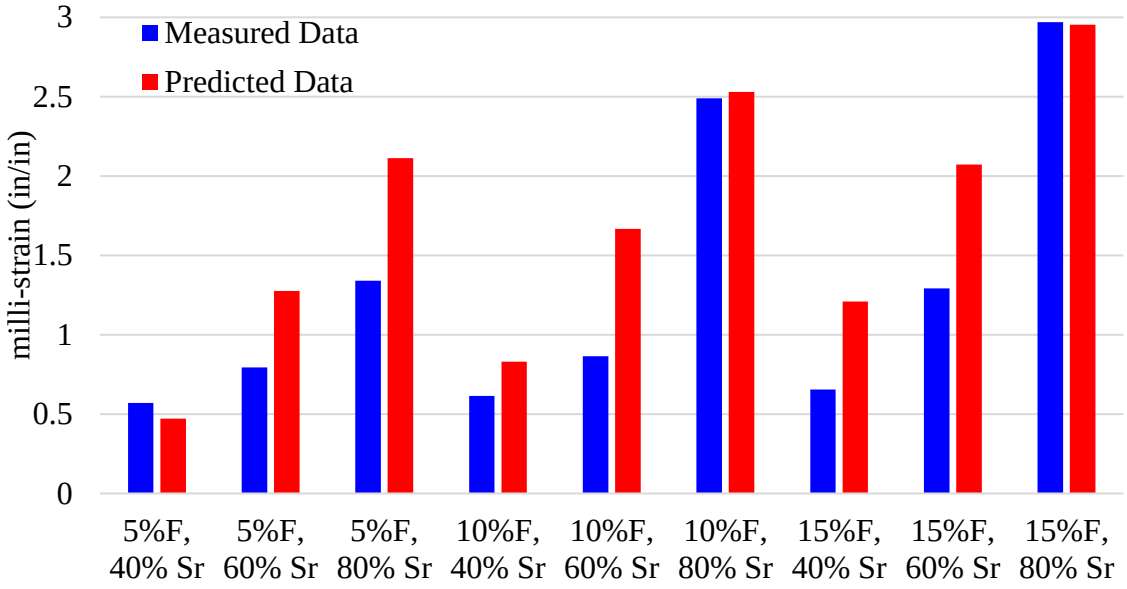
Measured Data
Predicted Data
milli-strain (in/in)
3
2.5
2
1.5
1
0.5
0
5%F, 40% Sr
5%F, 60% Sr
5%F, 80% Sr
10%F, 40% Sr
10%F, 60% Sr
10%F, 80% Sr
15%F, 40% Sr
15%F, 60% Sr
15%F, 80% Sr

(b)

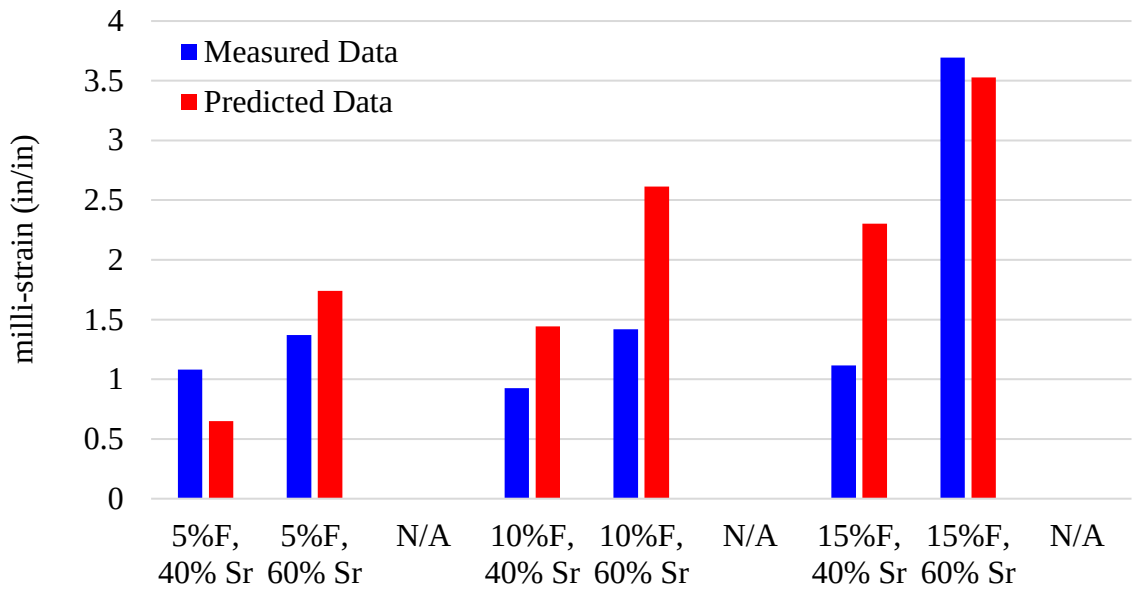

(c)

Figure 3.11: Estimated vs. predicted strain at the 10,000th loading cycle for (a) stress path 1, (b) stress path 2, and (c) stress path 3.

As shown in this plot, the agreement between laboratory measurements and predicted strains is highest for the primary stress path. However, as the stress states increase, the deviations between deformation gradients will also increase. This was confirmed by the analysis of the third stress path, which revealed the highest prediction discrepancies for the high fine, high moisture, and high stress states aggregate systems. Further, the permanent deformation model allows for a sensitivity analysis of the permanent deformation variations with changes in the permanent deformation factors. For the sensitivity analysis, the degree of saturation was maintained constant at 80%, the fines content was held constant at 5%, and the stress path length was kept constant with a value of 21.1 psi. A benefit that comes from considering the length of stress path in modeling purposes is that the length of the stress path is made of differences in the vertical stress and confinement.

Therefore, a sensitivity analysis can be made from both changes in the vertical stresses and changes in the confinement. Figure 3.12 shows the change in permanent deformation with an increase in the vertical stresses, ultimately demonstrating that higher vertical stresses generate higher strains.

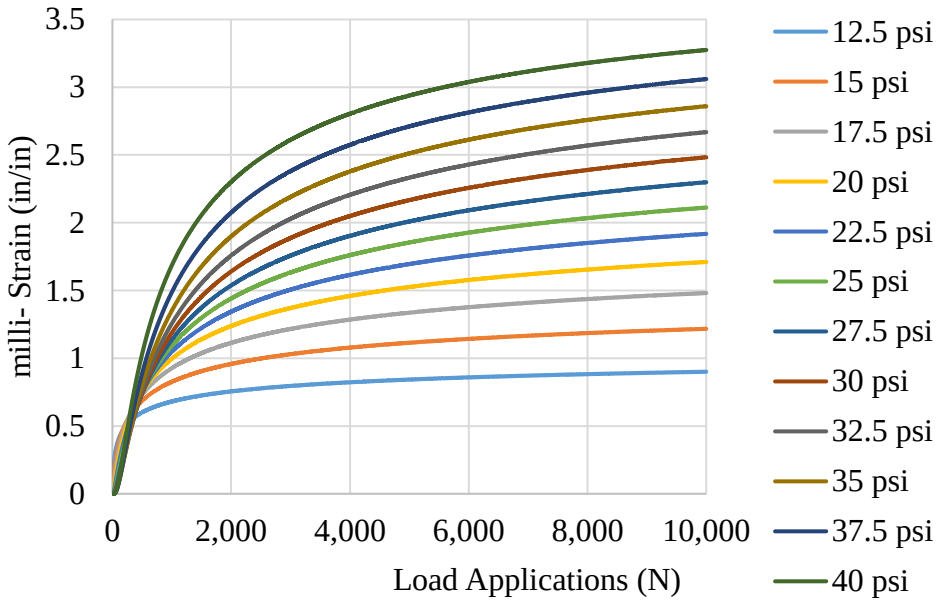

Figure 3.12: Sensitivity analysis performed with changes in the vertical stress.

When analyzing the effect of the all-around isotropic confinement as seen in Figure 3.13, the increase in the confinement generates a decrease in the permanent deformation. This behavior demonstrates that a higher confining stress in the UGLs results in greater particle to particle interactions that prevent volumetric displacement.

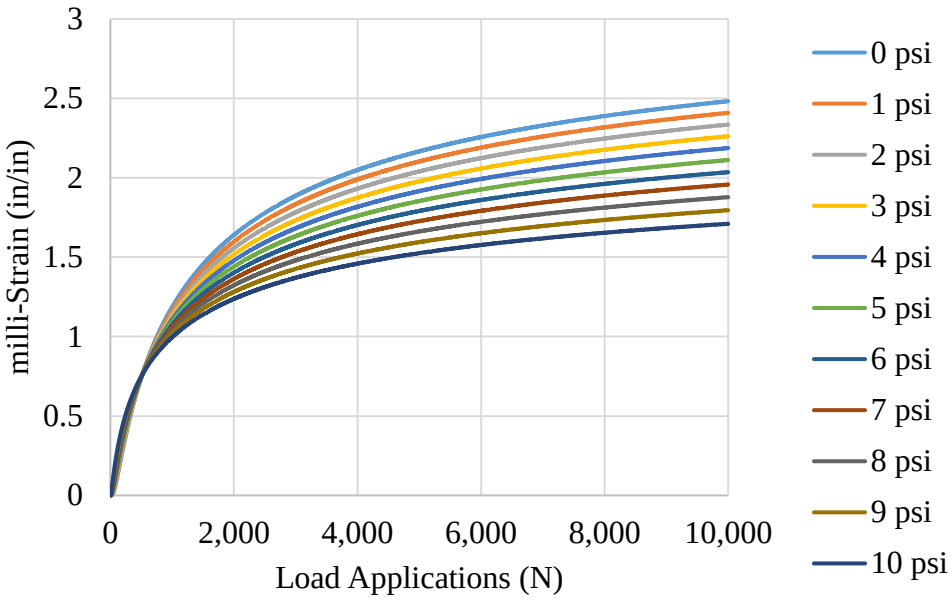

Figure 3.13: Sensitivity analysis performed with changes in the confinement.

Figure 3.14, demonstrates the influence of the fines in the permanent deformation potential. It can be noticed that the strain progressively increases as the amount of fines content increase.

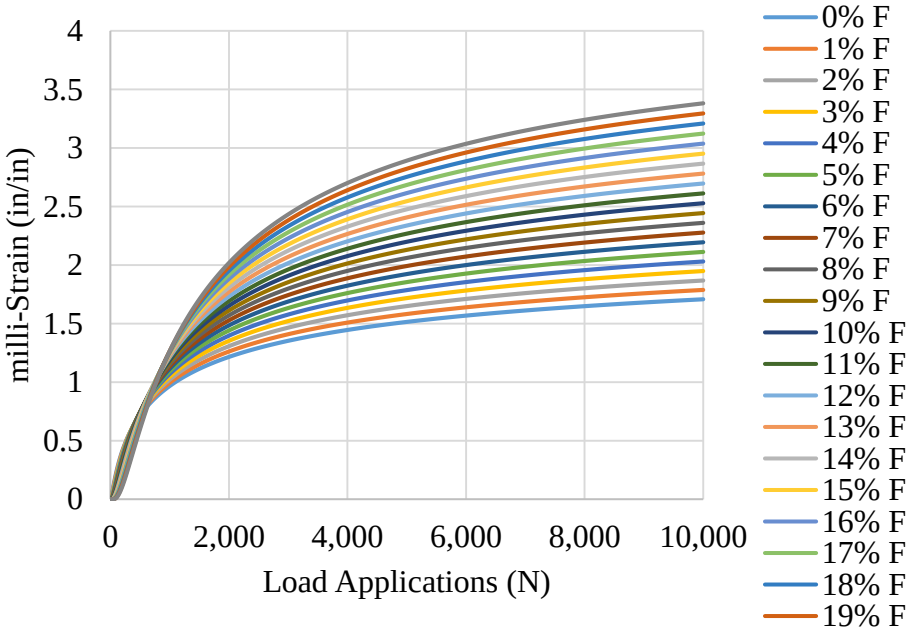

Figure 3.14: Sensitivity analysis performed with changes in the fines content.

Analysis of the effect of moisture in the permanent deformation potential demonstrated that the moisture greatly impacts the rate of deformation. Figure 3.15, shows the increase in permanent deformation with increase of the degree of saturation.

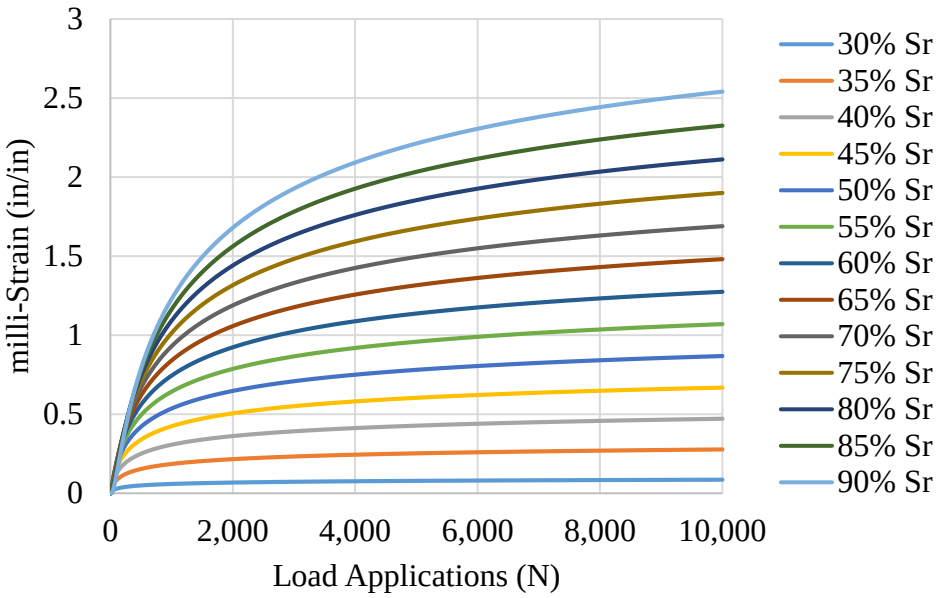

Figure 3.15: Sensitivity analysis with changes in the degree of saturation.

Chapter 4: Conclusions

The objective of this study was to investigate the impact of moisture state, fines content, and the parameters of the stress path on permanent deformation behavior of geomaterials. To achieve this objective, 54 El Paso limestone aggregate specimens with variable fines content and degrees of saturation were subjected to several constant confining pressure stress path tests. The [ε_p-N] curves showed significantly different deformation potential of the granular specimens due to synergistic interactions of fines, degree of saturation, and the stresses in the repeated cyclic load tests. The hardening and softening of stiffness properties were in turn cross-validated with the analysis of the dissipated energy in cyclic loading. This information provided valuable insights regarding the stored energy, modulus, and degree of plastic behavior of the specimen. Additionally, analysis of the hysteresis loops at pre-determined load cycles underscored the capability of energy methods to identify the onset of incremental collapse behavior in geomaterials. This novel approach can provide valuable information for practitioners and the pavement design industry to develop criteria to limit the distresses associated with field rutting.

In another effort, a series of prediction models were developed to estimate the degree of plastic behavior as a function of the moisture state of the specimen. This demonstrated that materials with lower moduli are more prone to experience higher degrees of plasticity in the repeated load permanent deformation tests. Similarly, the cumulative permanent deformation after 10,000 loading cycles was used to characterize the deformation potential of each variant of the experiment design. The results showed that the high fines systems shaped at elevated saturation levels underperformed their counterparts in terms of developing higher plastic strains upon application of 10,000 load cycles. In a separate effort, the general form-function for the rutting model at the MEPDG was selected, and the parameters of the model were estimated based on the

moisture state, fines content, and the parameters of the stress path test. Further a sensitivity analysis was performed on the parameters of the model to validate the physical sense of the developed models. The results clearly showed how the influence of the length of the stress path, which is a measure of the magnitude of the imparted loads on the pavement, affected the strain development in the tested specimen. Additionally, the numerical analysis proved the capability of the models to capture the role of the intermediate principal stress and confining pressure, on the hardening behavior of geomaterials. When implementing increments of the confining pressure, the results clearly showed the reduction of the magnitude and slope of the progression of plastic deformation. Similar behavior was observed with additions of the fines content in the mixes. Based on the sensitivity analysis of the parameters of the model, the degree of saturation was found to have the highest impact on the accumulated plastic strains after 10,000 load cycles.

FUTURE WORK

In order to enhance the generalization of the permanent deformation models developed in this study, future research should incorporate a broader range of granular materials. The integration of a wider selection of materials would in turn account for the role of mineralogy and particle geometry on the rutting potential of granular layers in the field. This would allow for better understanding of the role of particle surface properties and their interaction with moisture to improve or degrade the rutting resistance of granular layers. Additionally, future research should focus on the successful incorporation of the dynamic confinement stress path to more realistically simulate the nature of the moving vehicle loads. This would allow for the incorporation of the slope of the stress path as a measure of the stress regimes imparted on the pavements. Finally, comparing and contrasting field permanent deformation to laboratory permanent deformation is necessary to validate the prediction models.

References

Adlinge, S. S. (2013) “Pavement Deterioration and its Causes*”. Journal of Mechanical & Civil Engineering*, ISSN: 2278-1684, pp. 09-15.

Ahmad, N. Y. (2014) “Evaluation the Factors Affecting Permanent Deformation Using Cyclic Loading Test for Stabilized Subgrade Soil”. *Journal of Babylon University*. Volume: 22. Issue: 2. pp: 362-374.

Arnold, G. K. (2004) “Rutting of Granular Pavements*”*. University of Nottingham.

Ashtiani R., D. N. Little and E. Masad, (2007) “Evaluation of Impact of Fines on the Performance of Lightly Cement Stabilized Aggregate Systems”. *Presented at 86th Annual Meeting of Transportation Research Board*, Washington D.C.

Ashtiani R., D. N. Little and E. Masad, (2008) “Material Factors that Influence Anisotropic Behavior of Aggregate Systems”. *Presented at 87th Annual Meeting of Transportation Research Board*, Washington D.C.

Ashtiani, *R.* (2009) *“*Anisotropic Characterization and Performance Prediction of Chemically And Hydraulic Bound Pavement Foundation”. Texas A&M University.

Atkinson, J. (2000). "Nonlinear Soil Stiffness in Routine Design." *Geotechnique*, 50(5), 487-588.

Barksdale, R. D. (1972) “Laboratory evaluation of rutting in base course materials”. *Proc., 3rd Int. Conf. on Struct. Des. Of Asphalt pavements*, 1972. pp. 161-174

Benedetto, H. Di, T. Nishi, and F. Tatsuoka. (2003) "A Framework for Modelling of the Time Effects on the Stress–strain Behaviour of Geomaterials." *Deformation Characteristics of Geomaterials / Comportement Des Sols Et Des Roches Tendres*.

Bittelli, Marco, Gaylon S. Campbell, and Markus Flury. (1999) "Characterization of Particle Size Distribution in Soils with a Fragmentation Model." *Soil Science Society of America Journal* 63.4 pp: 782.

Deb, Kousik, V. Sawant, and A. Kiran. (2010) "Effects of Fines on Compaction Characteristics of Poorly Graded Sands." *International Journal of Geotechnical Engineering* 4.2 pp 299-304.

Elliot, R. P. (2007) “Permanent Deformation of Subgrade Soils*”*. University of Arkansas. Fayetteville 72701.

Enright, B and Obrien, E. J, (2012) “Monte Carlo Simulation of Extreme Traffic Loading on Short and Medium Span Bridges*”. Structure and Infrastructure Engineering*, 9 (12), pp. 1267-1282.

Fakhri, Mansour, Kaveh Hassani, and Ali Reza Ghanizadeh. (2013) "Impact of Loading Frequency on the Fatigue Behavior of SBS Modified Asphalt Mixtures." *Procedia Social and Behavioral Sciences* 104: pp 69-78.

Ghanizadeh, Ali Reza, and Mansour Fakhri. (2013) "Effect of Waveform, Duration and Rest Period on the Resilient Modulus of Asphalt Mixes." *Procedia - Social and Behavioral Sciences* 104: 79-88. Web.

Holtz, R. D., and William D. Kovacs. (1981) *An Introduction to Geotechnical Engineering*. Englewood Cliffs, NJ: Prentice-Hall. Print

Karan, P., Wilson, D. J., Larkin, T. J. (1990) "Axial Deformation Measurement in Repeated Load Triaxial Testing. Technical Note." *International Journal of Rock Mechanics and Mining Sciences & Geomechanics Abstracts* 27.5: pp 260.

Kim, I. T. (2005a) "Permanent Deformation Behavior of Airport Flexible Pavements Base and Subbase Courses". University of Illinois.

Kim, I. T. (2005b) "Unbound Aggregate Rutting Models for Stress Rotations and Effect of Moving Wheel Loads". *Journal of the Transportation Research Board*, No. 1913, pp. 41 – 49.

Li, Yanrong. (2013) "Effects of Particle Shape and Size Distribution on the Shear Strength Behavior of Composite Soils." *Bulletin of Engineering Geology and the Environment* 72.3-4: pp 371-81.

Monismisth, C. L., Ogawa, N., Freeme, C. R. (1975). "A permanent deformation characteristic of subgrade soils due to repeated loading". *Transportation research record 537*, Washington D.C., TRB, pp 1-17.

National Cooperative Highway Research Program (NCHRP) (2004). "Calibration of permanent deformation models for flexible pavements". *Transpiration research board ARA*, Inc., ERES Division. 505 West University Avenue. Champaign, Illinois 61820.

Ohiduzzaman, M., S. C. R. Lo, and O. Craciun. (2012) "Influence of Fines Content on Unbound Granular Base Materials (UGB) under Cyclic Axial and Radial Stress." *GeoCongress*.

Pan, Tongyan, Erol Tutumluer, and Joseph Anochie-Boateng. (2006) "Aggregate Morphology Affecting Resilient Behavior of Unbound Granular Materials." *Transportation Research Record: Journal of the Transportation Research Board* 1952: pp 12-20.

Parry, R. H. G. (2004) *Mohr circles, stress paths and geotechnics* (2nd ed.). London: Spons Architecture Price Book. Print

Pasten, Cesar, and J. Carlos Santamarina. (2011) "Energy Geo-storage — Analysis and Geomechanical Implications." *KSCE Journal of Civil Engineering* 15.4: pp 655-67.

Petersen, Dr, Re Link, and C-Y Kuo. (2002) "Correlating Permanent Deformation Characteristics of Hot Mix Asphalt with Aggregate Geometric Irregularities." *Journal of Testing and Evaluation* 30.2: pp 136.

Qian, Yu, Erol Tutumluer, Youssef M. A. Hashash, and Jamshid Ghaboussi. (2014) "Effects of Ballast Degradation on Permanent Deformation Behavior from Large-Scale Triaxial Tests." *2014 Joint Rail Conference.*

Rahman, M. M., S. R. Lo, and C. T. Gnanendran. (2008) "On Equivalent Granular Void Ratio and Steady State Behaviour of Loose Sand with Fines." *Canadian Geotechnical Journal* 45.10: pp 1439-456.

Santamarina, J. C., K. A. Klein, Y. H. Wang, and E. Prencke. (2002) "Specific Surface: Determination and Relevance." *Canadian Geotechnical Journal* 39.1: pp 233-41.

Seyhan, U. (2002) "Characterization of anisotropic granular behavior in flexible pavement", PhD dissertation, University of Illinois, Urbana, U.S.

Seyhan, Umit, Erol Tutumluer, and Hamza Yesilyurt. (2005) "Anisotropic Aggregate Base Inputs for Mechanistic Pavement Analysis Considering Effects of Moving Wheel Loads." *Journal of Materials in Civil Engineering* 17.5: pp 505-12.

Soliman, H, and Ahmed Shalaby. (2015) "Permanent Deformation Behavior of Unbound Granular Base Materials with Varying Moisture and Fines Content." *Transportation Geotechnics* 4: pp 1-12.

Sweere, G. T. H. (1990) "Unbound Granular Bases for Roads". Civil Engineering and Geosciences.

Texas Department of Transportation. (Tex-113-E) (2011) Designation. Laboratory compaction characteristics and moisture density relationship of Base Materials. June 2011, http://ftp.dot.state.tx.us/pub/txdot-info/cst/TMS/100-E_series/pdfs/soi113.pdf , Accessed October 2016.

Texas Department of Transportation. (Tex-114-E) (2011) Designation. Laboratory compaction characteristics and moisture density relationship of subgrade, embankment soils, and backfill material. February 2011, https://ftp.dot.state.tx.us/pub/txdot-info/cst/TMS/100E_series/archives/113-0111.pdf, Accessed July 2016.

Texas Department of Transportation. (Tex-241-F) (2015) Designation. Compacting Bituminous Specimens Using The Suerpave Gyratory Compactor (SGC), December 2015 http://ftp.dot.state.tx.us/pub/txdot-info/cst/TMS/200-F_series/pdfs/bit241.pdf Accessed October 2016.

Texas Department of Transportation. (Tex-410-A) (1999) Designation. Abrasion of Coarse Aggregate Using the Los Angeles Machine, August 1999

http://ftp.dot.state.tx.us/pub/txdot-info/cst/TMS/400-A_series/pdfs/cnn410.pdf Accessed October 2016.

Theyse, H., Maina, J., and Kannemeyer, L. (2007) "Revision of the South African Flexible Pavement Design Method; Mechanistic-Empirical Components." *Proceedings of the 9th Conference on Asphalt Pavements for Southern Africa (CAPSA)*, Gaborone, Botswana, pp 256-292.

Tutumluer, E., and U. Seyhan. (1999) "Laboratory Determination of Anisotropic Aggregate Resilient Moduli Using an Innovative Test Device". In Transportation Research Record: *Journal of the Transportation Research Board, No. 1687*, TRB, National Research Council, Washington, D.C., pp. 13–21.

Tutumluer, Erol, and Tongyan Pan. (2008) "Aggregate Morphology Affecting Strength and Permanent Deformation Behavior of Unbound Aggregate Materials." *Journal of Materials in Civil Engineering* 20.9: pp 617-27.

Tseng K. H, Lytton R. L. (1989) "Prediction of permanent deformation in flexible pavement materials". Implications of aggregates in design, construction, and performance of flexible pavements. In: Schreuders HG, Marek CR, editors ASTM STP1016. Philadelphia: American society of testing and materials. P. 154-172.

Uzan, Jacob. (2004) "Permanent Deformation in Flexible Pavements." *Journal of Transportation Engineering* 130.1: pp 6-13.

Veverka, V. (1979). "Raming van de spoordiepte bij wegen met een bitumineuze verharding." De Wegentechniek, 24(3), 25–45 (in Dutch).

Wang, H. and Imad, A. (2009) "Combined Effect of Moving Wheel Loading and Three Dimensional Contact Stresses on Perpetual Pavement Responses". *Transportation Research Record: Journal of the Transportation Research Board* 2095. pp: 53-61.

Wang, H. (2011) "Analysis of Tire-Pavement Interaction and Pavement Response Using A Decoupling Modeling Approach". University of Illinois. Urbana-Champaign.

Appendix A Permanent Deformation Graphs

Figures A-1 through A-3 demonstrate the recorded permanent deformations for the first stress path.

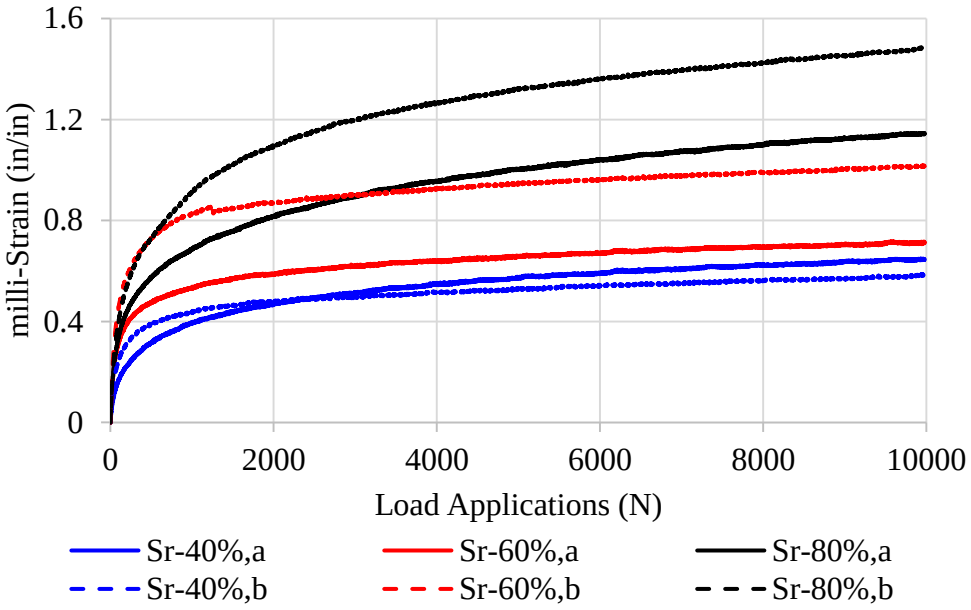

Figure A-1: Permanent deformation of coarse gradation under the first stress path.

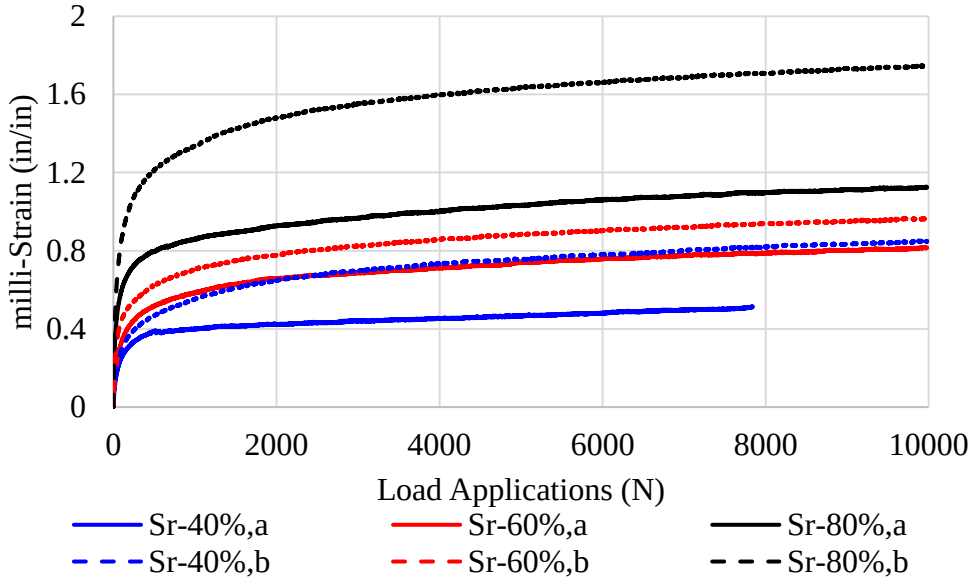

Figure A-2: Permanent deformation of intermediate gradation under the first stress path.

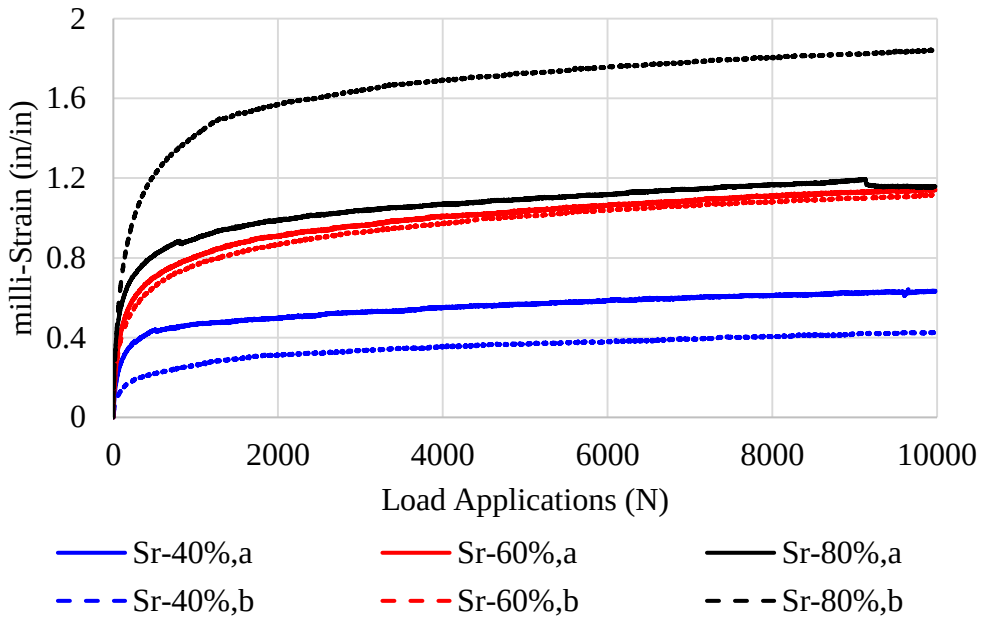

Figure A-3: Permanent deformation of fines gradation under the first stress path.

Figures A-4 through A-6 demonstrate the recorded permanent deformations for the second stress path.

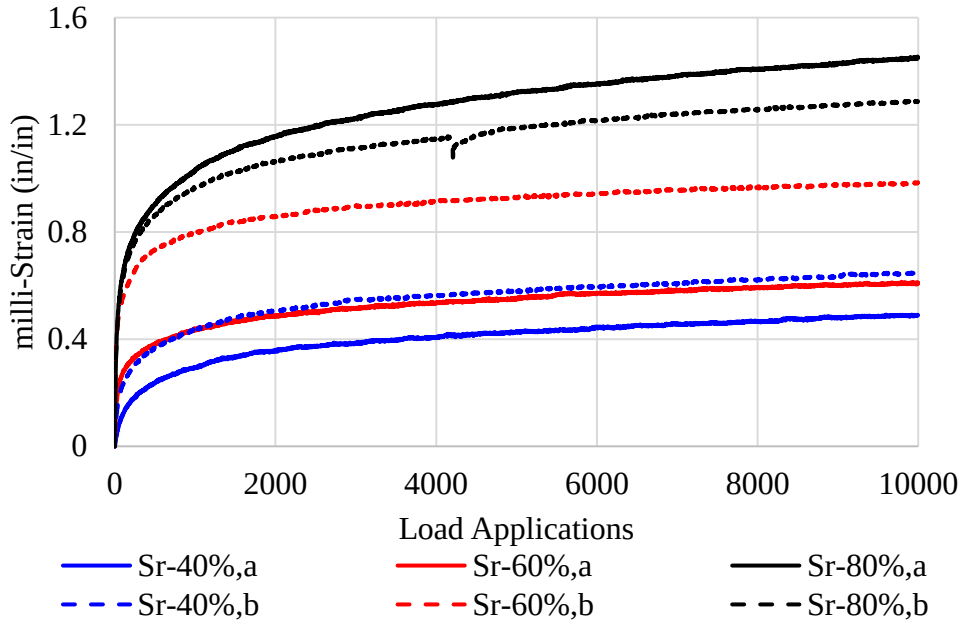

Figure A-4: Permanent deformation of coarse gradation under the second stress path.

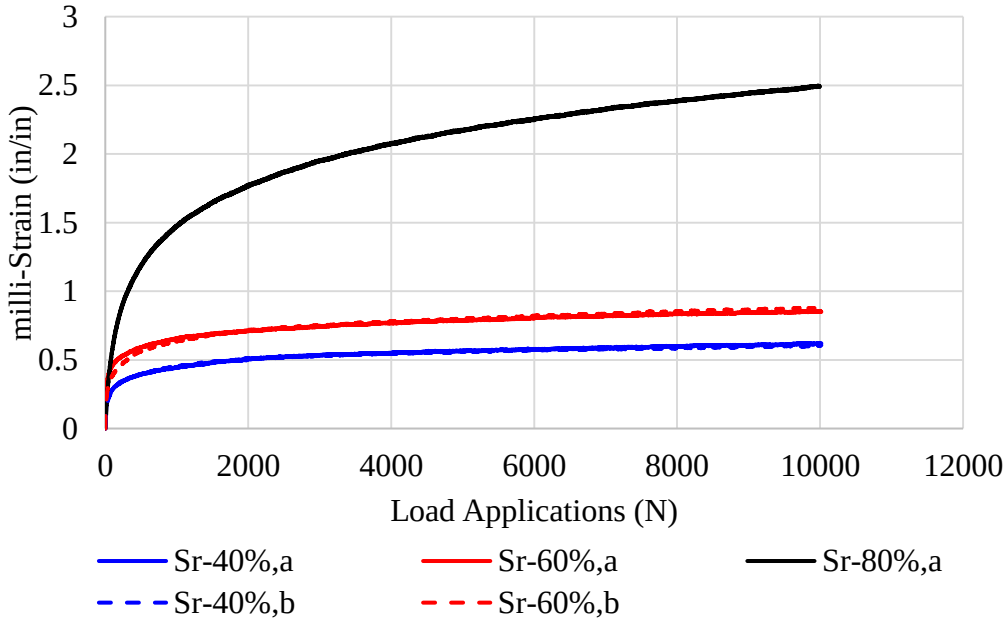

Figure A-5: Permanent deformation of intermediate gradation under the second stress path.

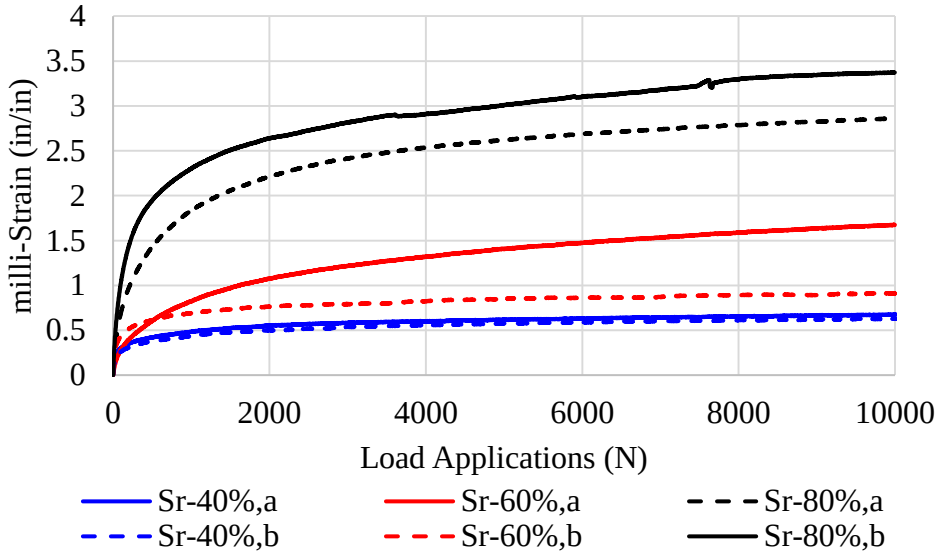

Figure A-6: Permanent deformation of fines gradation under the second stress path.

Figures A-7 through A-9 demonstrate the recorded permanent deformations for the third stress path.

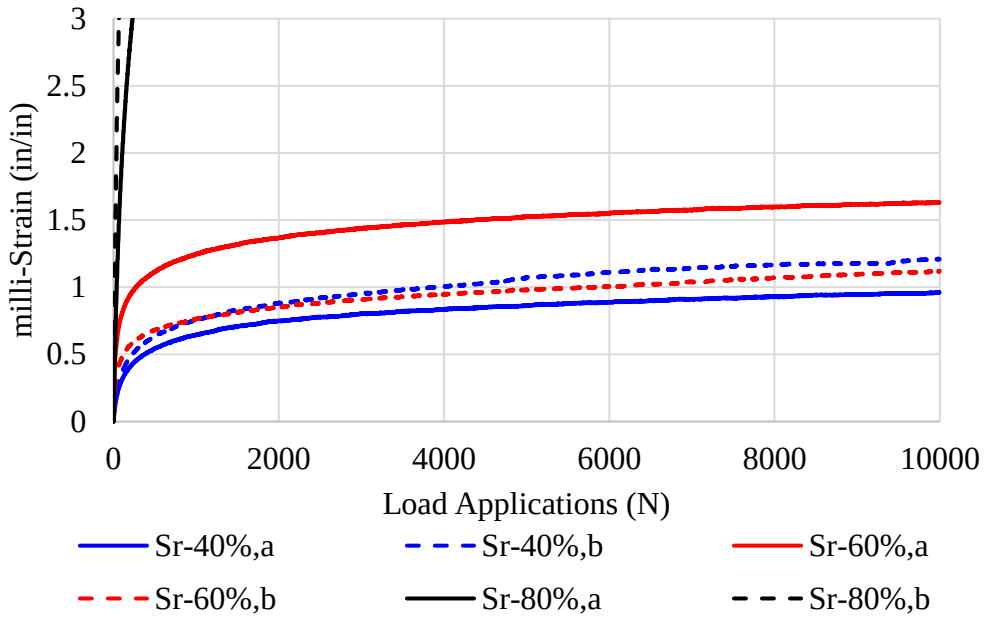

Figure A-7: Permanent deformation of coarse gradation under the third stress path.

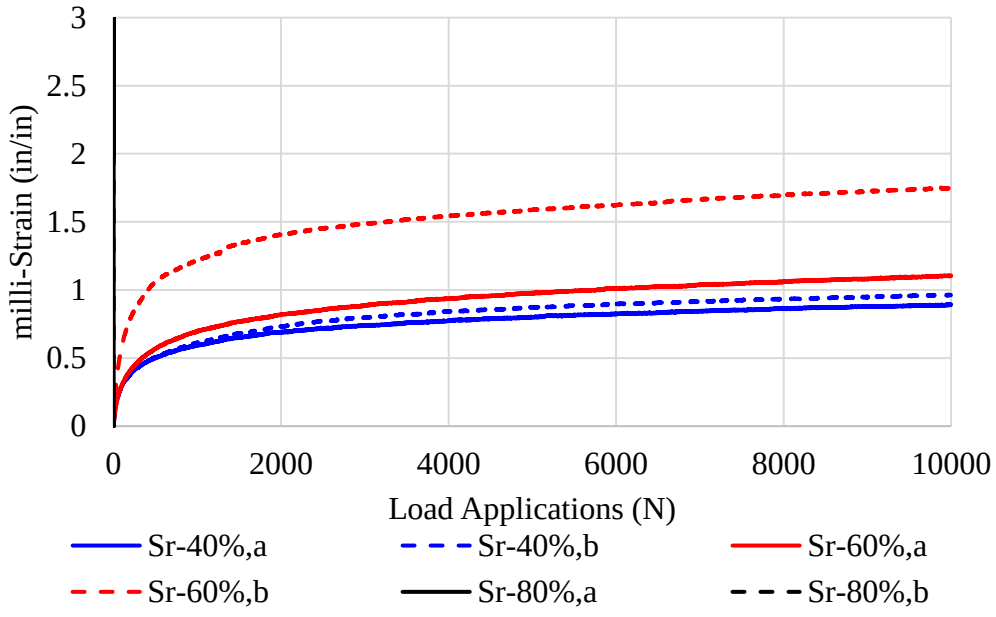

Figure A-8: Permanent deformation of intermediate gradation under the third stress path.

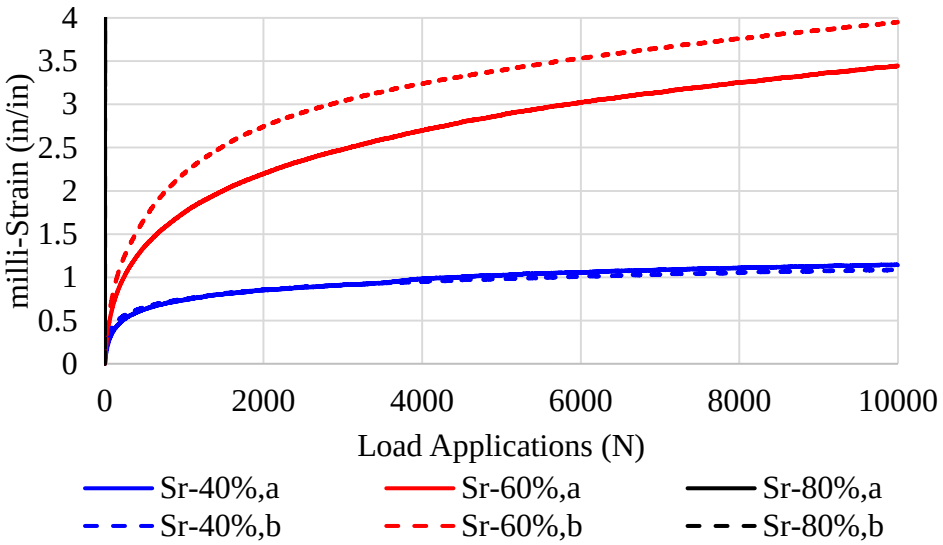

Figure A-9: Permanent deformation of fines gradation under the third stress path.

Appendix B Hysteresis Loops

Figures B-1 through B-18 demonstrate the recorded hysteresis loops for the first stress path.

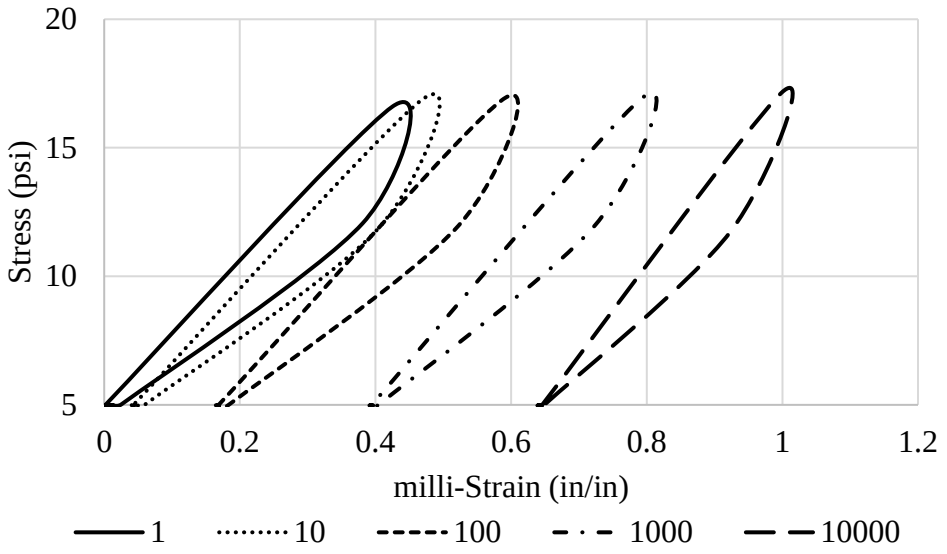

Figure B-1: Hysteresis Loops of the 1st, 10th, 100th, 1000th and 10,000th load application for the first stress path, coarse gradation, and 40% degree of saturation specimen.

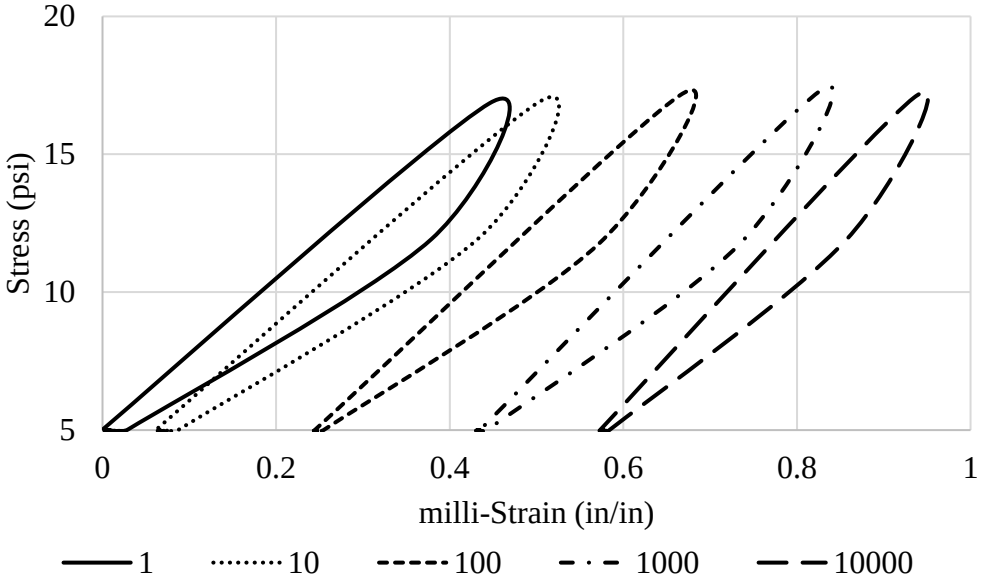

Figure B-2: Hysteresis Loops of the 1st, 10th, 100th, 1000th and 10,000th load application for the first stress path, coarse gradation, and 40% degree of saturation duplicate specimen.

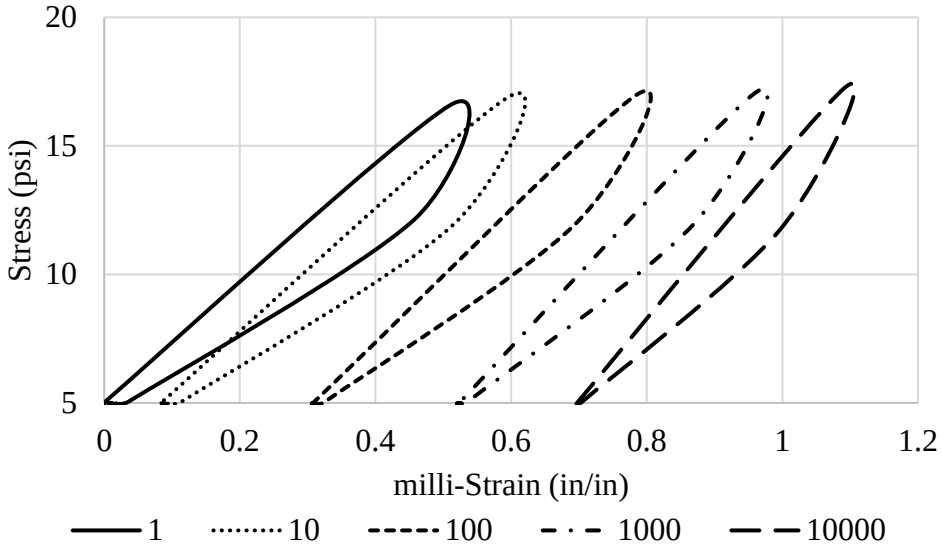

Figure B-3: Hysteresis Loops of the 1st, 10th, 100th, 1000th and 10,000th load application for the first stress path, coarse gradation, and 60% degree of saturation specimen.

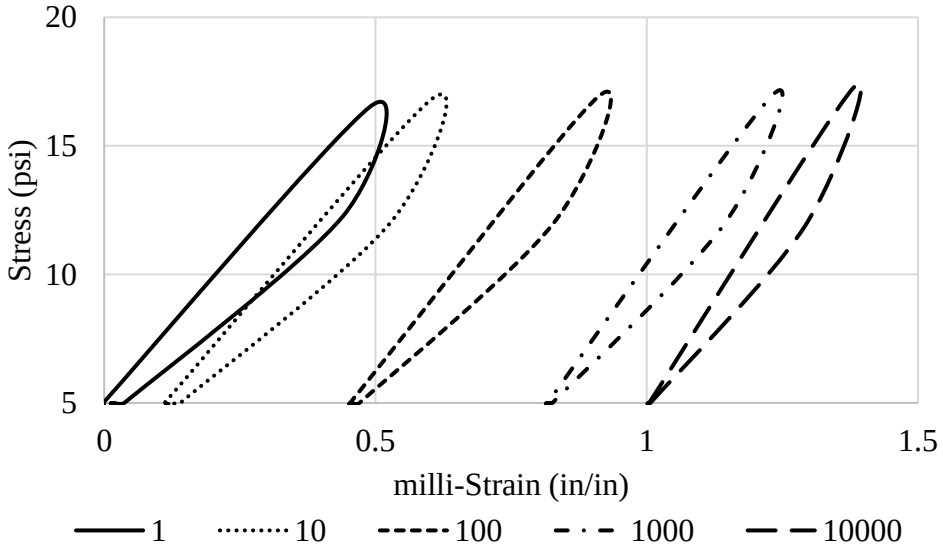

Figure B-4: Hysteresis Loops of the 1st, 10th, 100th, 1000th and 10,000th load application for the first stress path, coarse gradation, and 60% degree of saturation duplicate specimen.

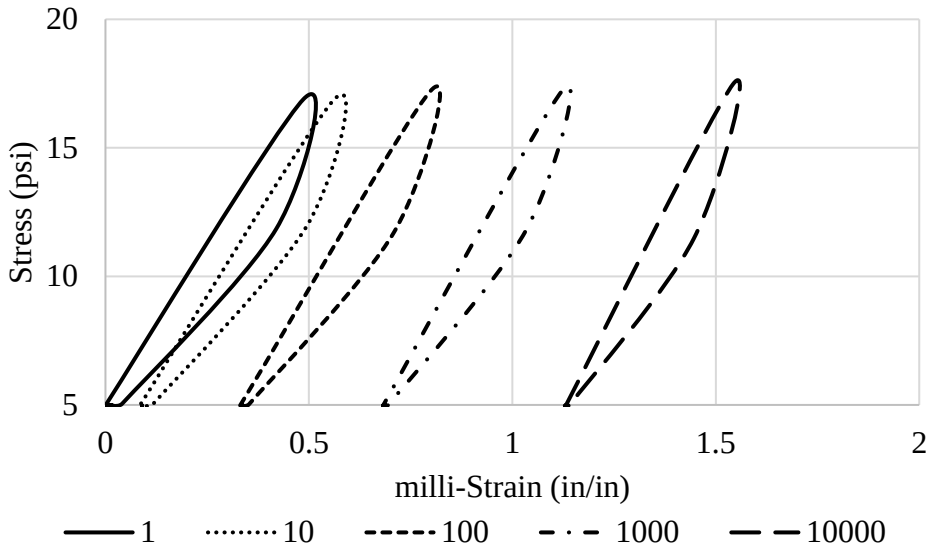

Figure B-5: Hysteresis Loops of the 1st, 10th, 100th, 1000th and 10,000th load application for the first stress path, coarse gradation, and 80% degree of saturation specimen.

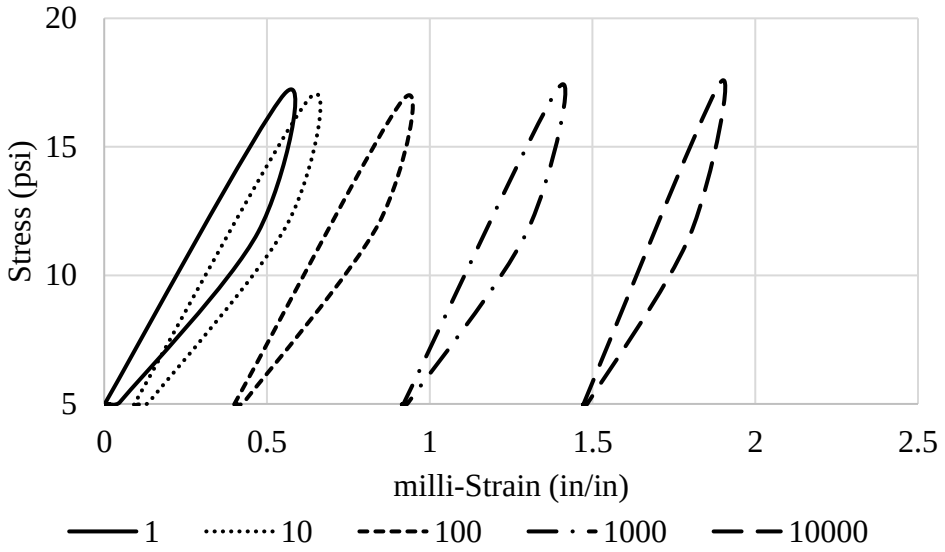

Figure B-6: Hysteresis Loops of the 1st, 10th, 100th, 1000th and 10,000th load application for the first stress path, coarse gradation, and 80% degree of saturation duplicate specimen.

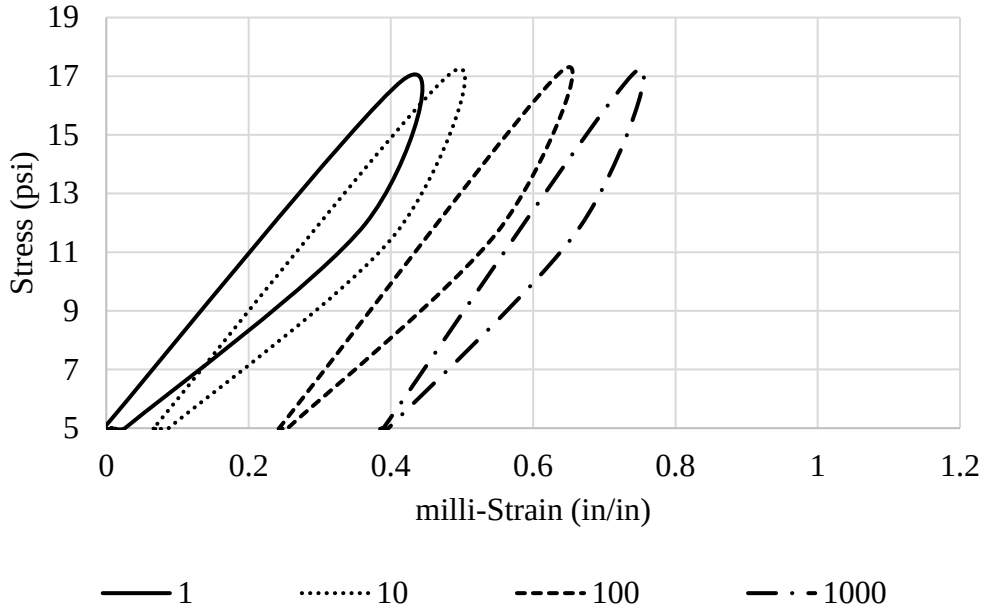

Figure B-7: Hysteresis Loops of the 1st, 10th, 100th, and 1000th load application for the first stress path, intermediate gradation, and 40% degree of saturation specimen.

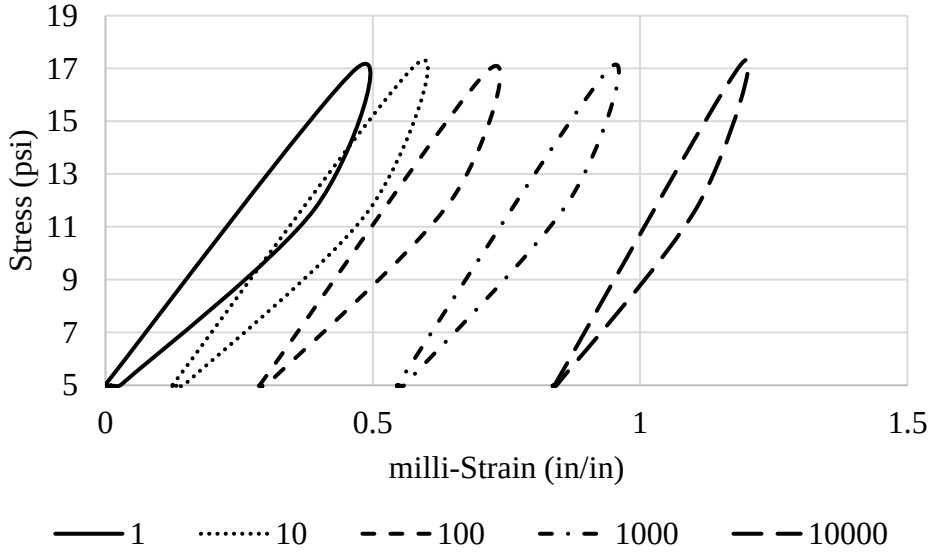

Figure B-8: Hysteresis Loops of the 1st, 10th, 100th, 1000th and 10,000th load application for the first stress path, intermediate gradation, and 40% degree of saturation duplicate specimen.

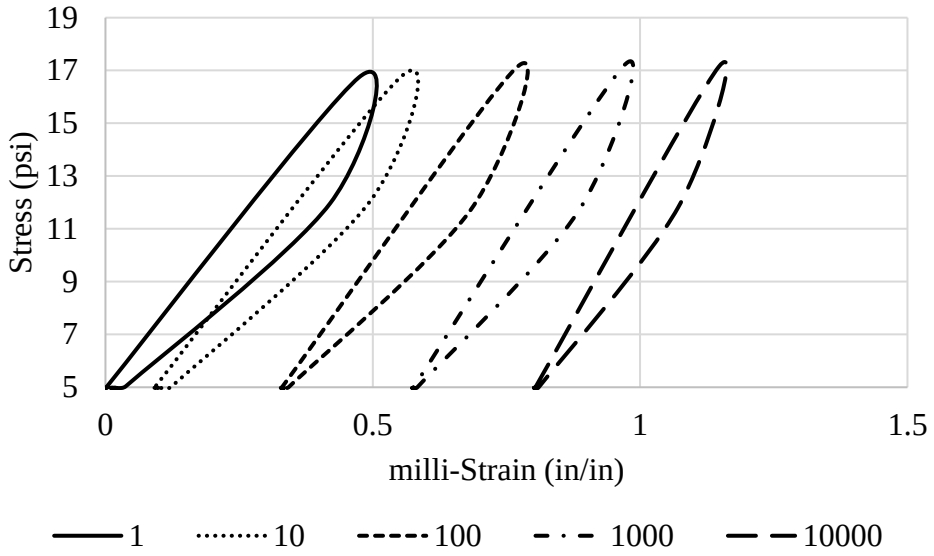

Figure B-9: Hysteresis Loops of the 1st, 10th, 100th, 1000th and 10,000th load application for the first stress path, intermediate gradation, and 60% degree of saturation specimen.

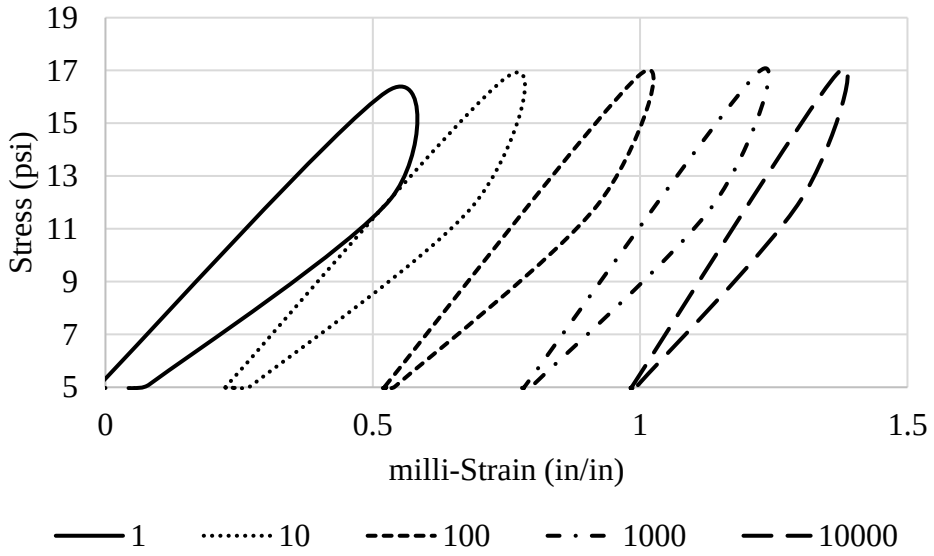

Figure B-10: Hysteresis Loops of the 1st, 10th, 100th, 1000th and 10,000th load application for the first stress path, intermediate gradation, and 60% degree of saturation duplicate specimen.

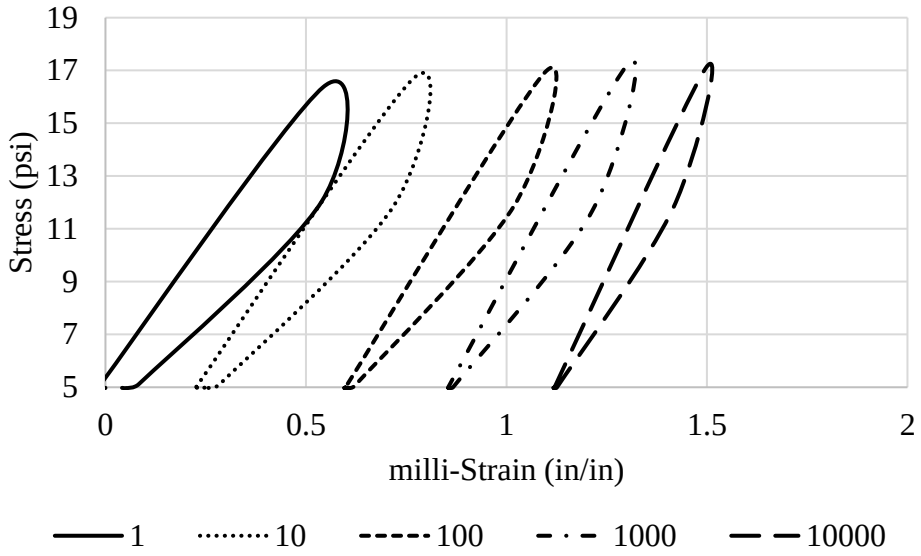

Figure B-11: Hysteresis Loops of the 1st, 10th, 100th, 1000th and 10,000th load application for the first stress path, intermediate gradation, and 80% degree of saturation specimen.

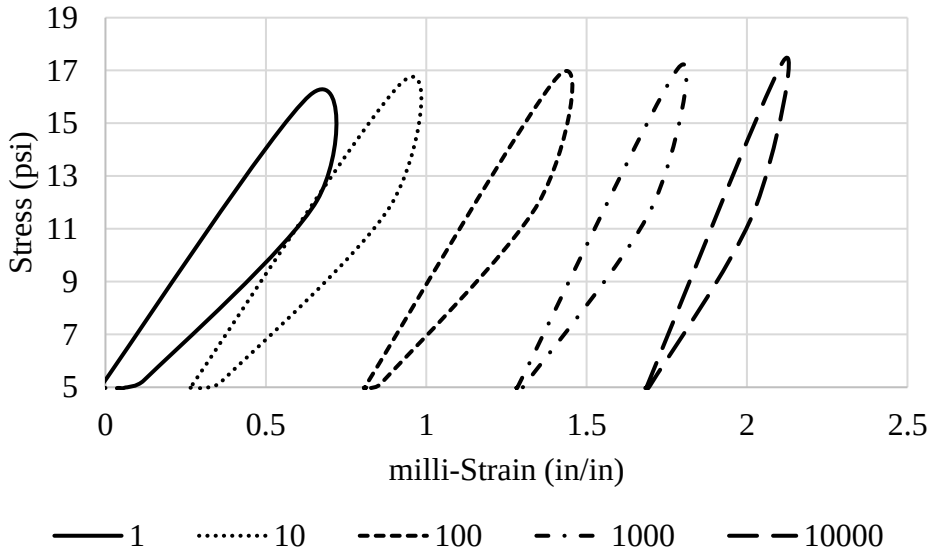

Figure B-12: Hysteresis Loops of the 1st, 10th, 100th, 1000th and 10,000th load application for the first stress path, intermediate gradation, and 80% degree of saturation duplicate specimen.

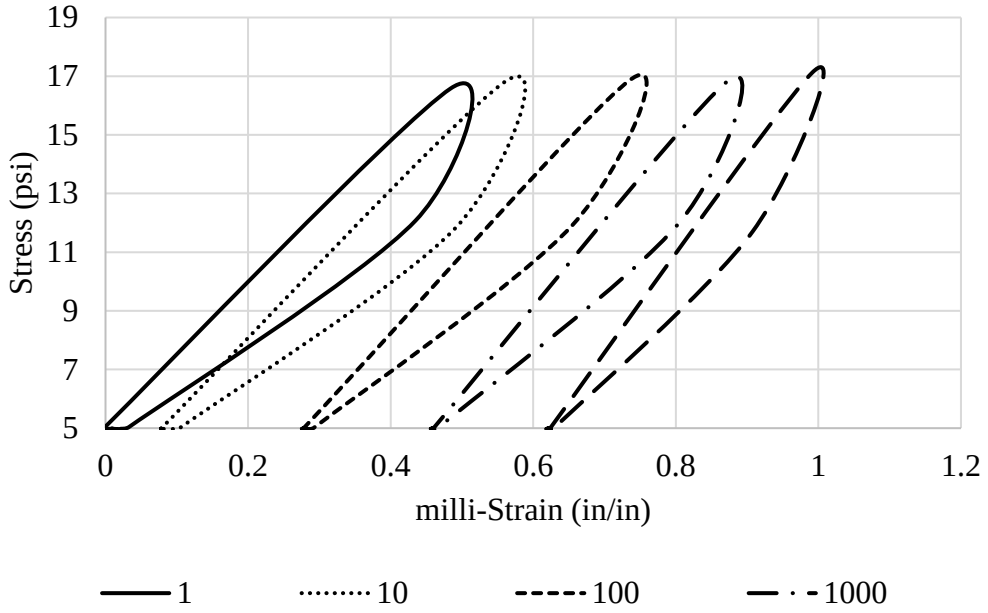

Figure B-13: Hysteresis Loops of the 1st, 10th, 100th, 1000th, and 10,000th load application for the first stress path, fines gradation, and 40% degree of saturation specimen.

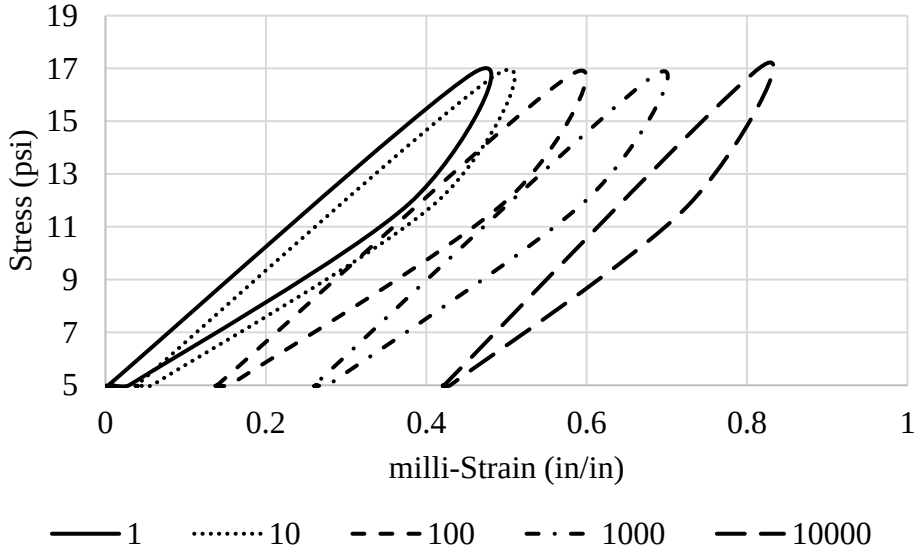

Figure B-14: Hysteresis Loops of the 1st, 10th, 100th, 1000th and 10,000th load application for the first stress path, fines gradation, and 40% degree of saturation duplicate specimen.

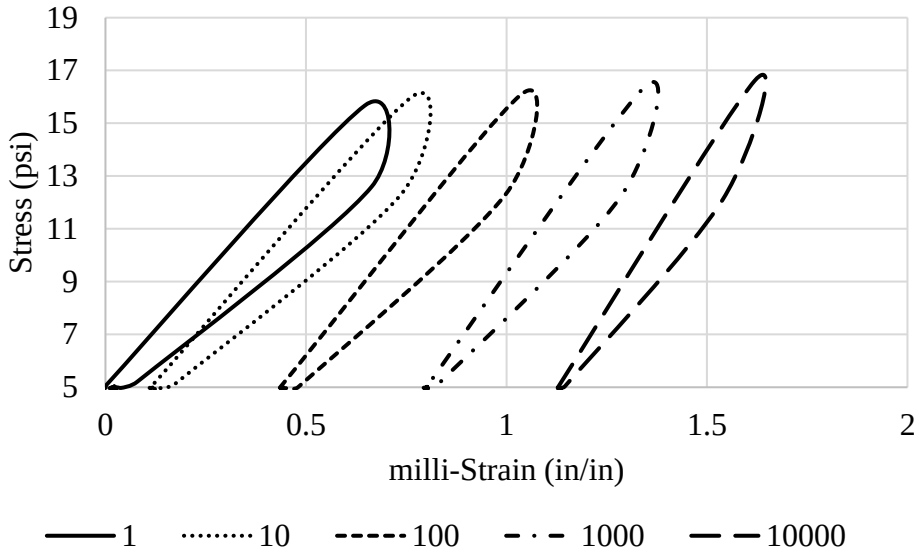

Figure B-15: Hysteresis Loops of the 1st, 10th, 100th, 1000th and 10,000th load application for the first stress path, fines gradation, and 60% degree of saturation specimen.

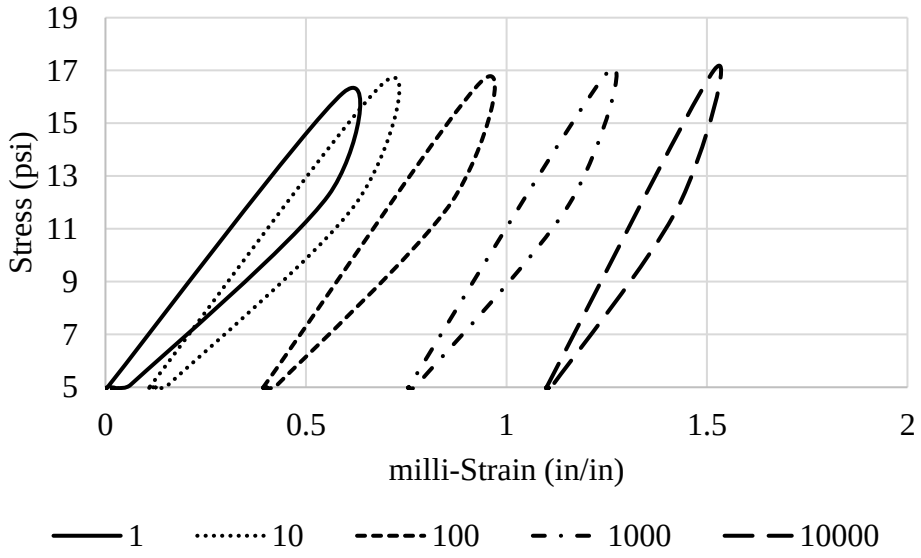

Figure B-16: Hysteresis Loops of the 1st, 10th, 100th, 1000th and 10,000th load application for the first stress path, fines gradation, and 60% degree of saturation duplicate specimen.

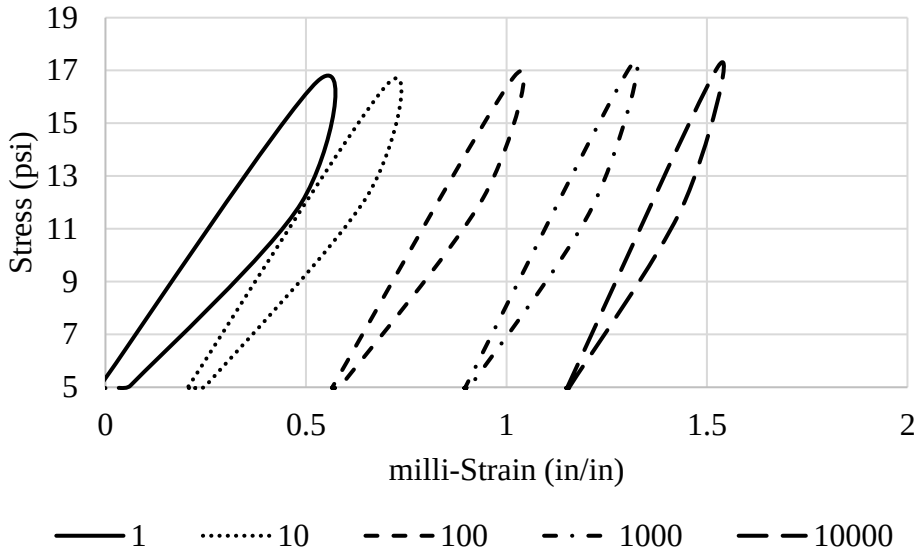

Figure B-17: Hysteresis Loops of the 1st, 10th, 100th, 1000th and 10,000th load application for the first stress path, fines gradation, and 80% degree of saturation specimen.

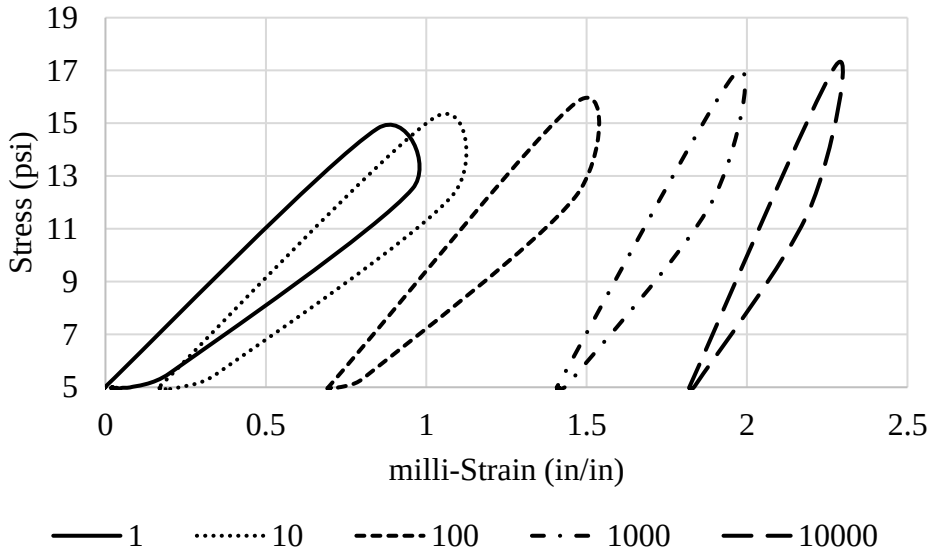

Figure B-18: Hysteresis Loops of the 1st, 10th, 100th, 1000th and 10,000th load application for the first stress path, fines gradation, and 80% degree of saturation duplicate specimen.

Figures B-19 through B-34 demonstrate the recorded hysteresis loops for the second stress path.

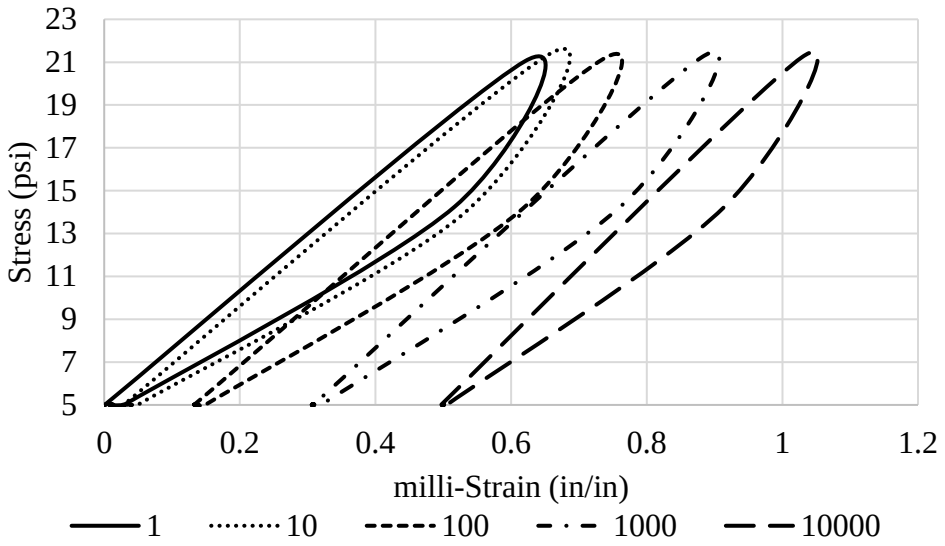

Figure B-19: Hysteresis Loops of the 1st, 10th, 100th, 1000th and 10,000th load application for the second stress path, coarse gradation, and 40% degree of saturation specimen.

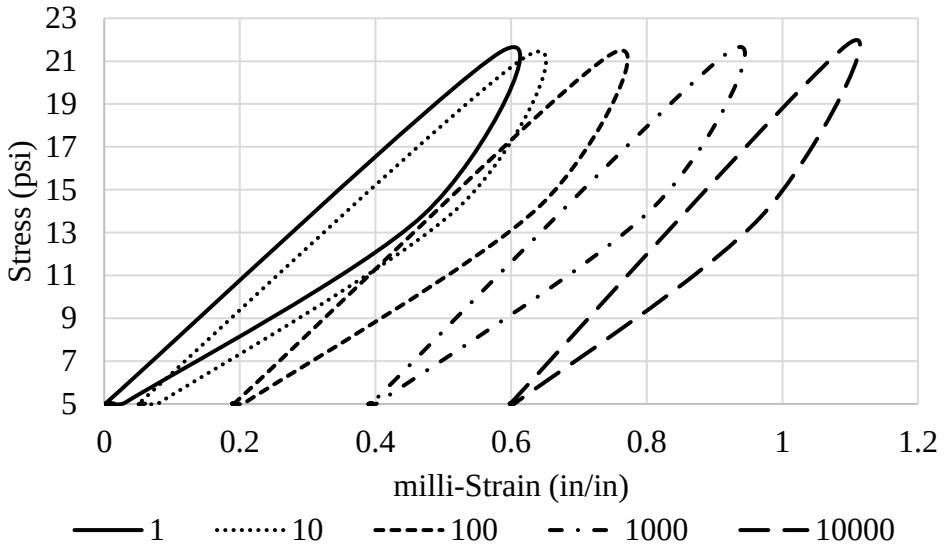

Figure B-20: Hysteresis Loops of the 1st, 10th, 100th, 1000th and 10,000th load application for the second stress path, coarse gradation, and 40% degree of saturation duplicate specimen.

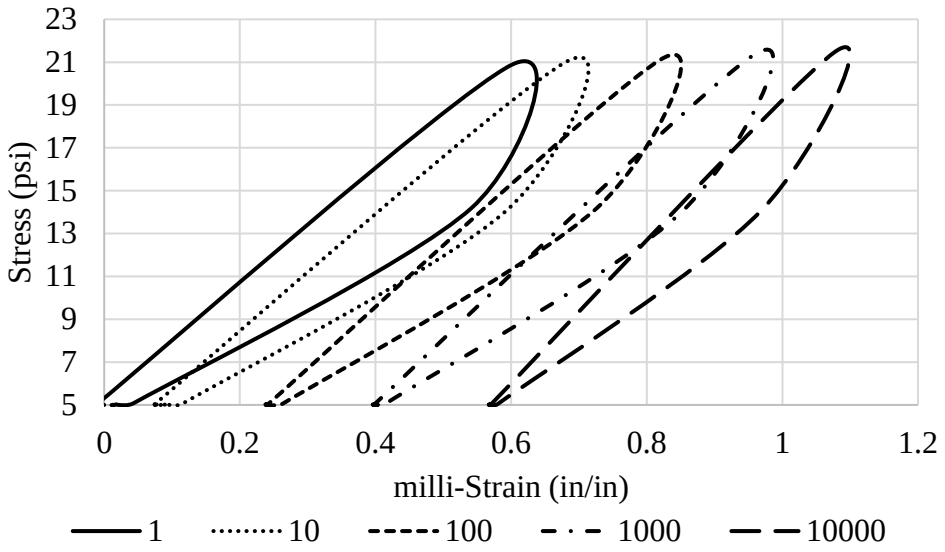

Figure B-21: Hysteresis Loops of the 1st, 10th, 100th, 1000th and 10,000th load application for the second stress path, coarse gradation, and 60% degree of saturation specimen.

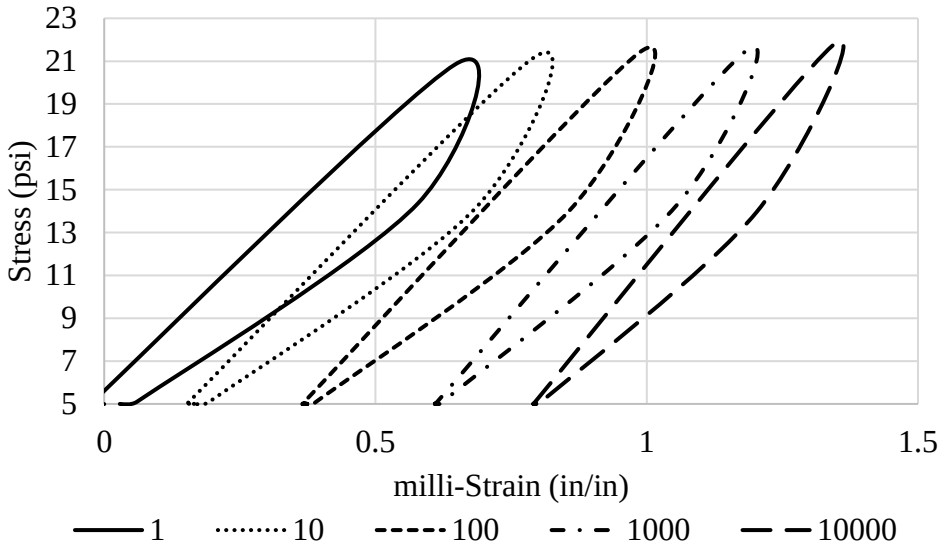

Figure B-22: Hysteresis Loops of the 1st, 10th, 100th, 1000th and 10,000th load application for the second stress path, coarse gradation, and 60% degree of saturation duplicate specimen.

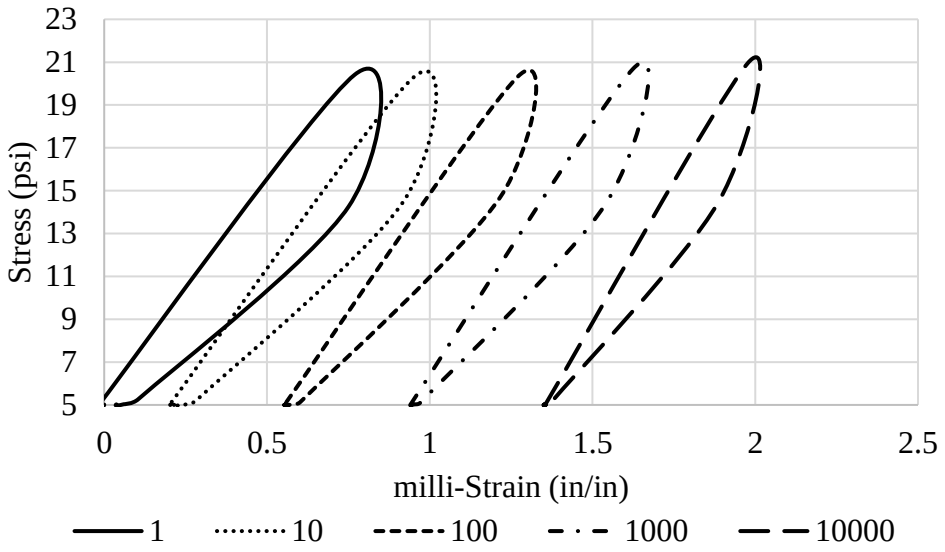

Figure B-23: Hysteresis Loops of the 1st, 10th, 100th, 1000th and 10,000th load application for the second stress path, coarse gradation, and 80% degree of saturation specimen.

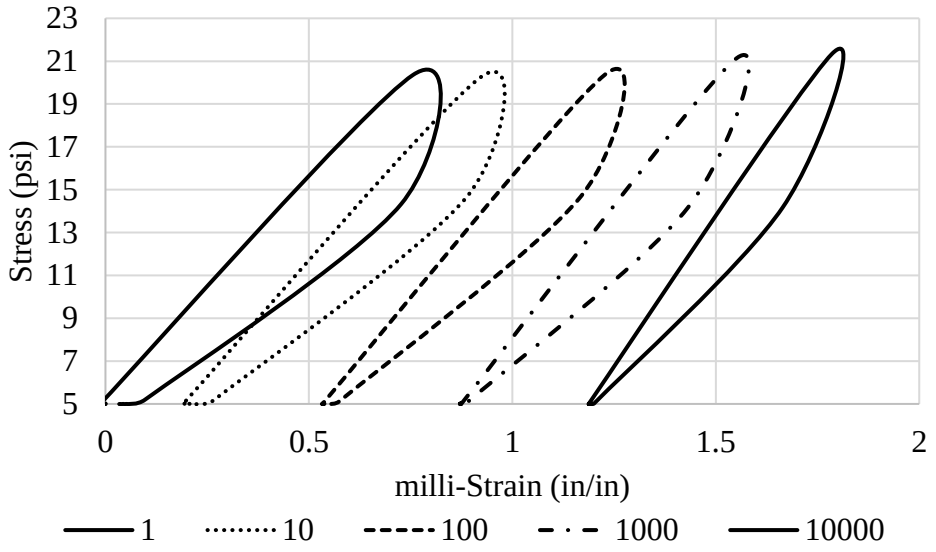

Figure B-24: Hysteresis Loops of the 1st, 10th, 100th, 1000th and 10,000th load application for the second stress path, coarse gradation, and 80% degree of saturation duplicate specimen.

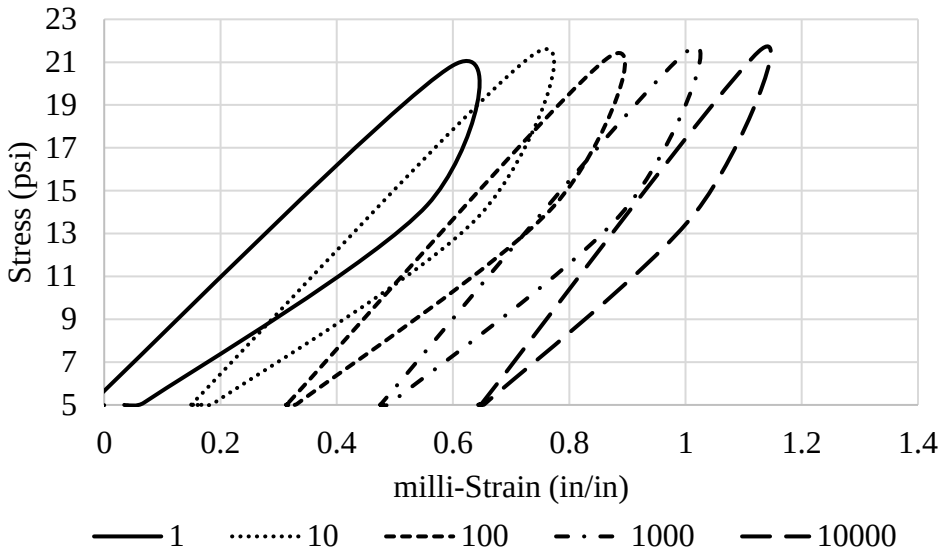

Figure B-25: Hysteresis Loops of the 1st, 10th, 100th, 1000th and 10,000th load application for the second stress path, intermediate gradation, and 40% degree of saturation specimen.

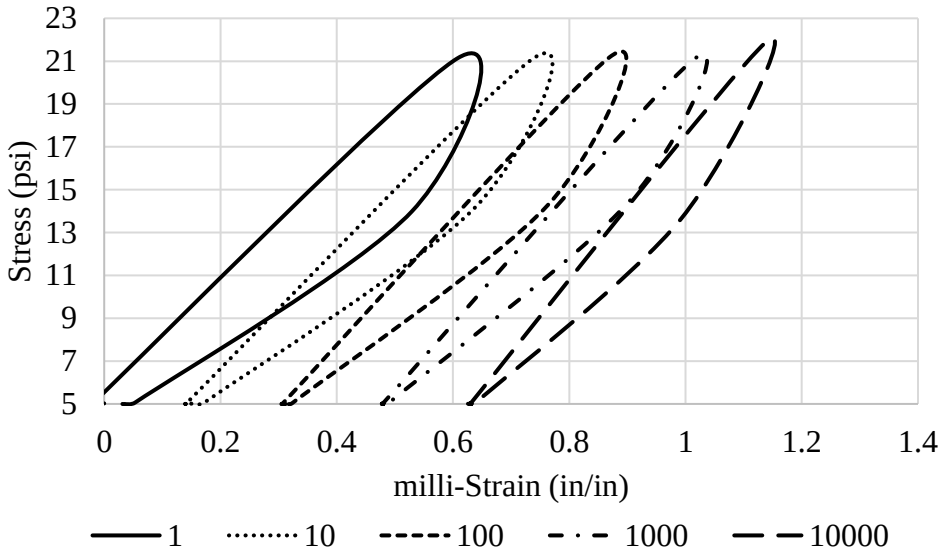

Figure B-26: Hysteresis Loops of the 1st, 10th, 100th, 1000th and 10,000th load application for the second stress path, intermediate gradation, and 40% degree of saturation duplicate specimen.

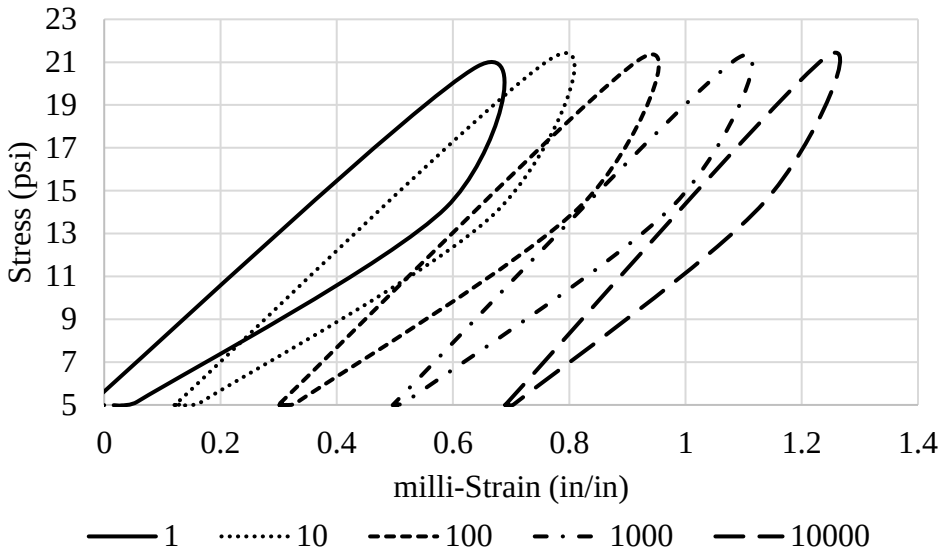

Figure B-27: Hysteresis Loops of the 1st, 10th, 100th, 1000th and 10,000th load application for the second stress path, intermediate gradation, and 60% degree of saturation specimen.

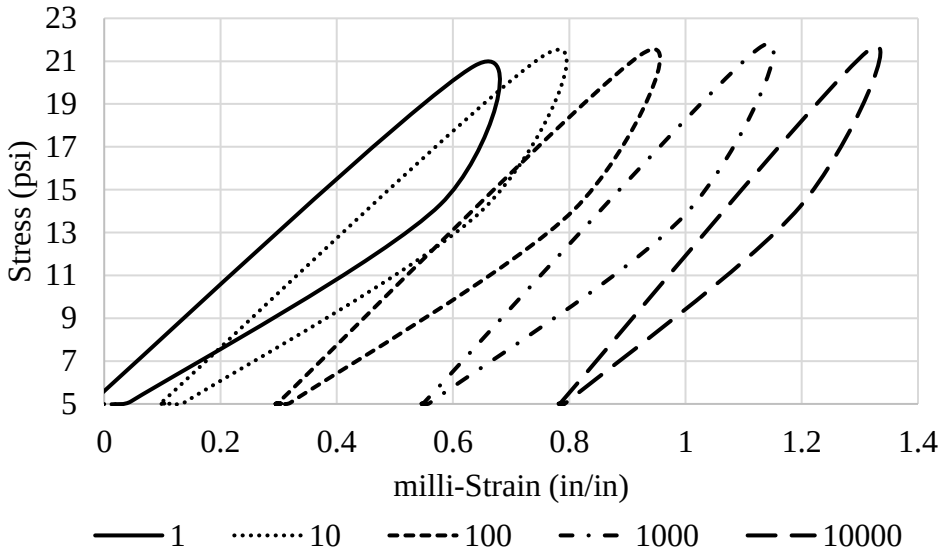

Figure B-28: Hysteresis Loops of the 1st, 10th, 100th, 1000th and 10,000th load application for the second stress path, intermediate gradation, and 60% degree of saturation duplicate specimen.

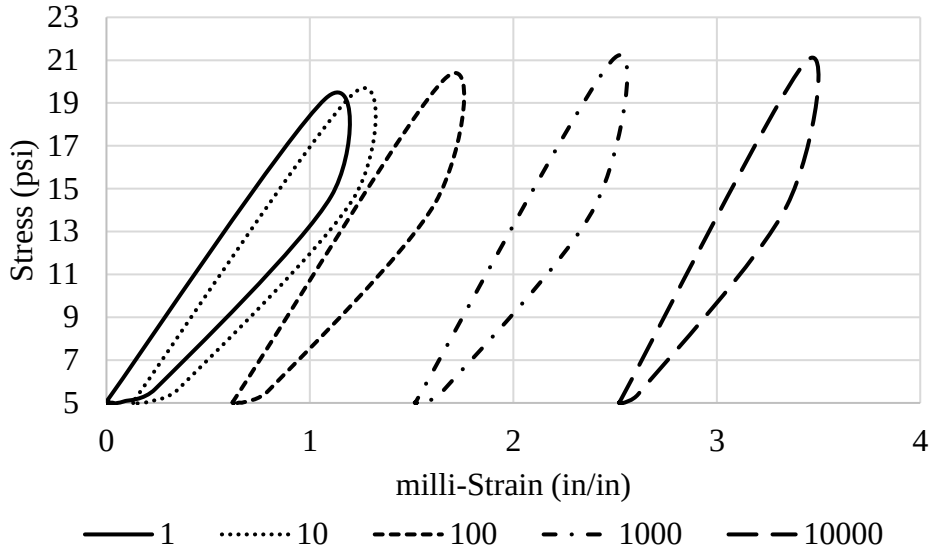

Figure B-29: Hysteresis Loops of the 1st, 10th, 100th, 1000th and 10,000th load application for the second stress path, intermediate gradation, and 80% degree of saturation specimen.

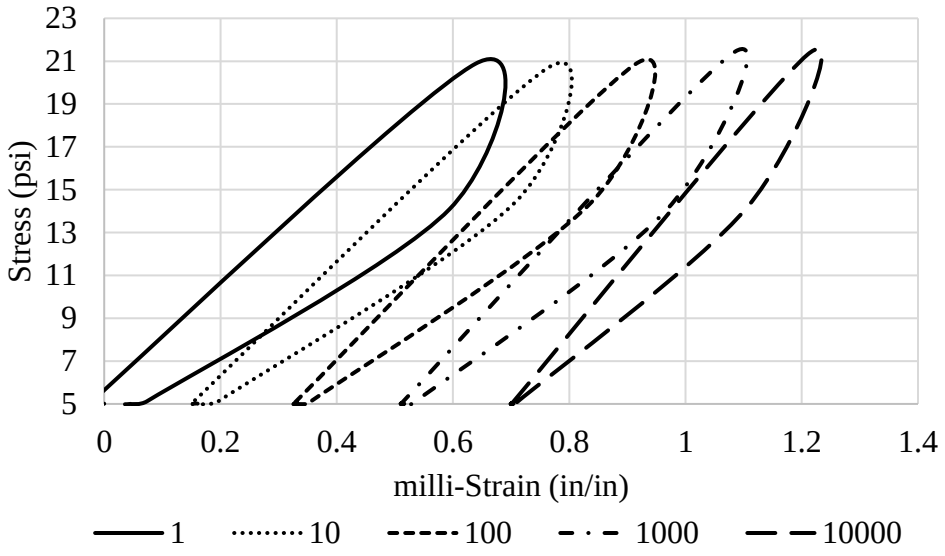

Figure B-30: Hysteresis Loops of the 1st, 10th, 100th, 1000th and 10,000th load application for the second stress path, fines gradation, and 40% degree of saturation specimen.

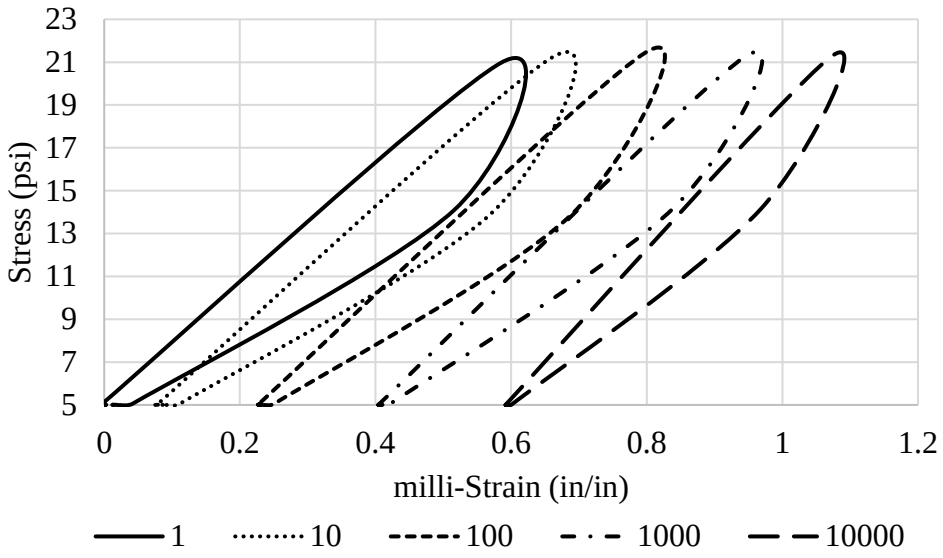

Figure B-31: Hysteresis Loops of the 1st, 10th, 100th, 1000th and 10,000th load application for the second stress path, fines gradation, and 40% degree of saturation duplicate specimen.

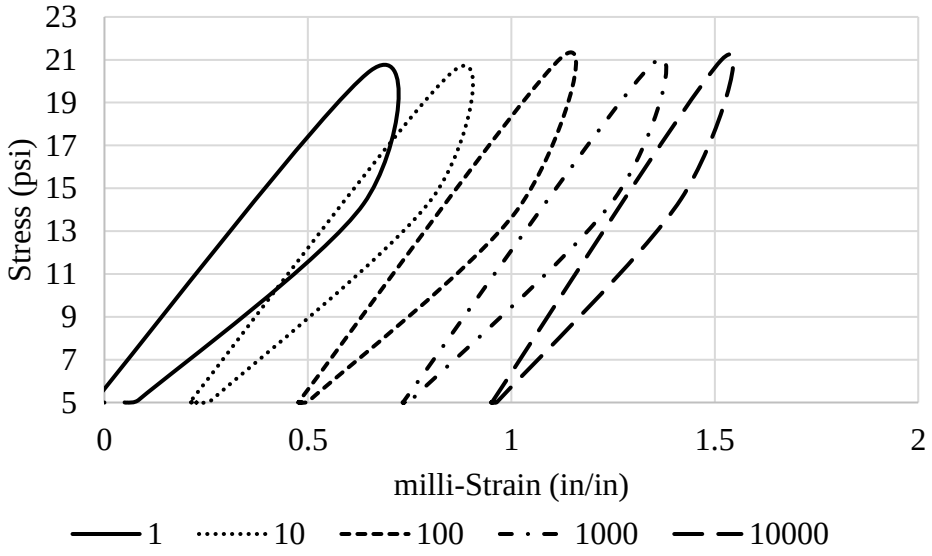

Figure B-32: Hysteresis Loops of the 1st, 10th, 100th, 1000th and 10,000th load application for the second stress path, fines gradation, and 60% degree of saturation duplicate specimen.

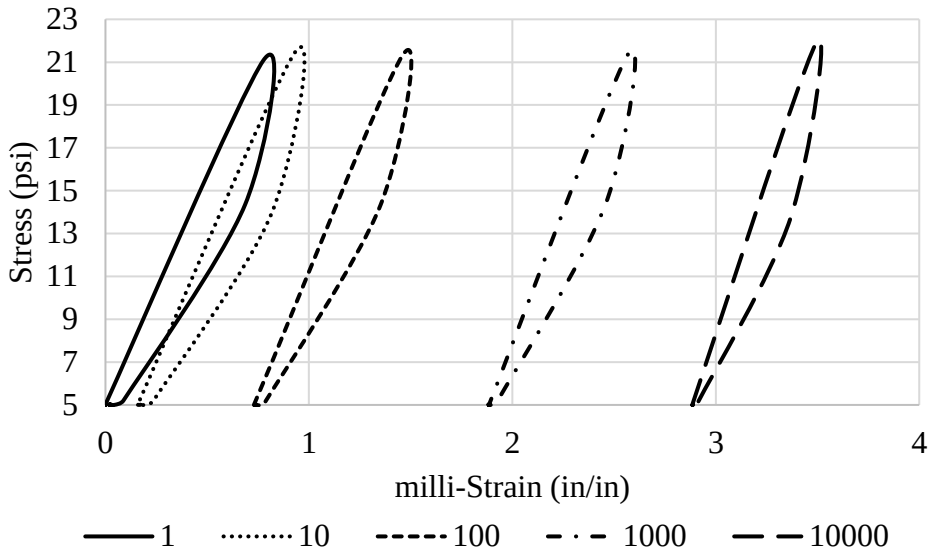

Figure B-33: Hysteresis Loops of the 1st, 10th, 100th, 1000th and 10,000th load application for the second stress path, fines gradation, and 80% degree of saturation specimen.

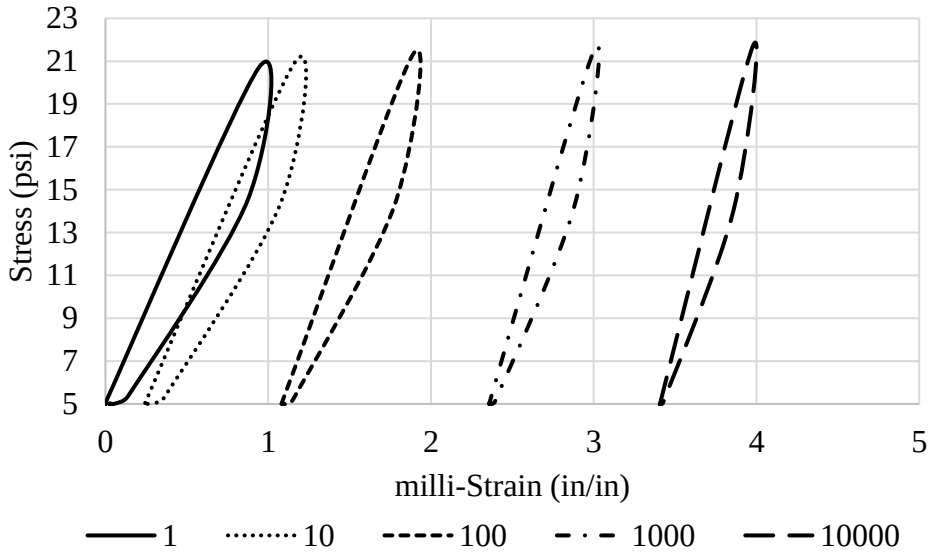

Figure B-34: Hysteresis Loops of the 1st, 10th, 100th, 1000th and 10,000th load application for the second stress path, fines gradation, and 80% degree of saturation duplicate specimen.

Figures B-35 through B-52 demonstrate the recorded hysteresis loops for the third stress path.

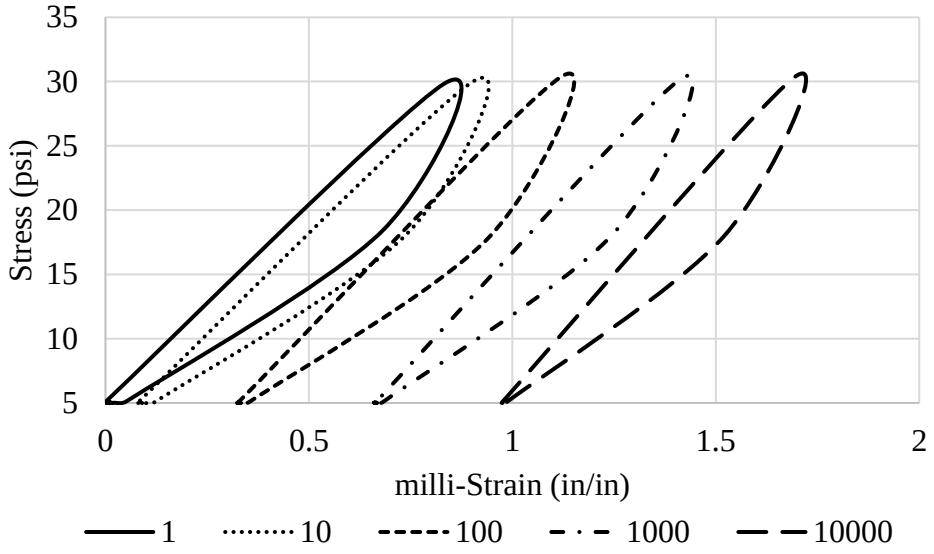

Figure B-35: Hysteresis Loops of the 1st, 10th, 100th, 1000th and 10,000th load application for the third stress path, coarse gradation, and 40% degree of saturation specimen.

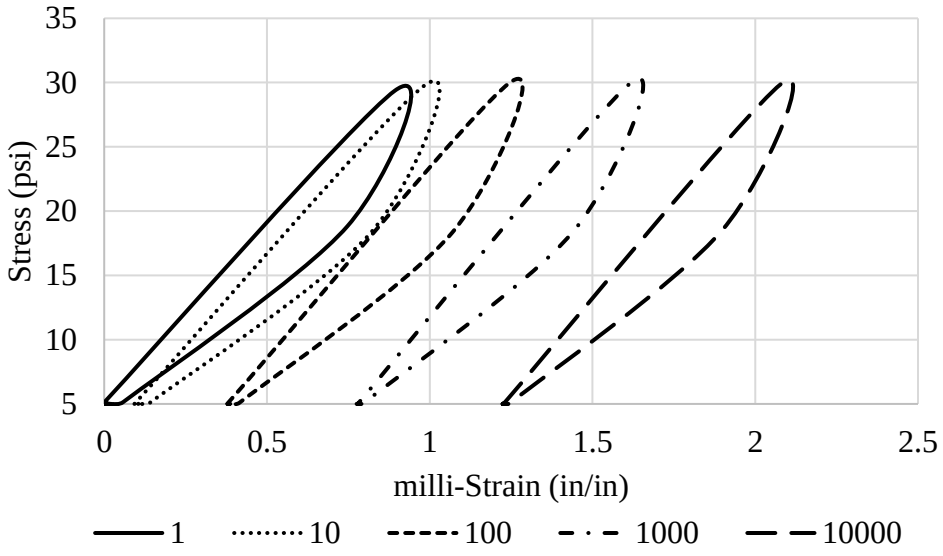

Figure B-36: Hysteresis Loops of the 1st, 10th, 100th, 1000th and 10,000th load application for the third stress path, coarse gradation, and 40% degree of saturation duplicate specimen.

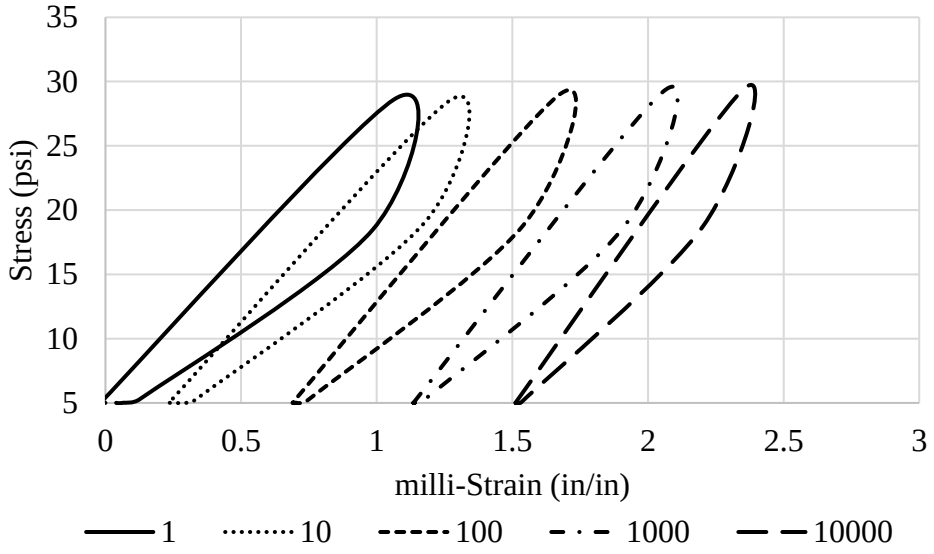

Figure B-37: Hysteresis Loops of the 1st, 10th, 100th, 1000th and 10,000th load application for the third stress path, coarse gradation, and 60% degree of saturation specimen.

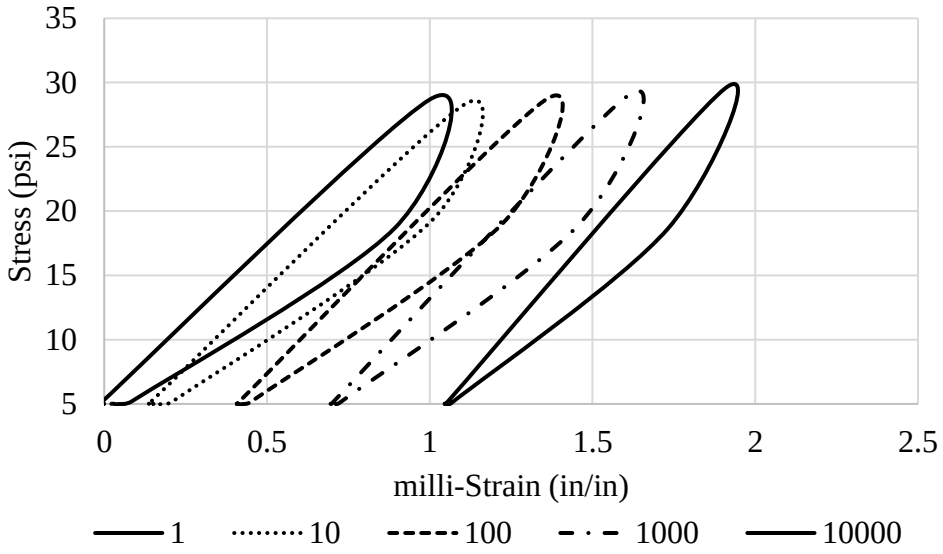

Figure B-38: Hysteresis Loops of the 1st, 10th, 100th, 1000th and 10,000th load application for the third stress path, coarse gradation, and 60% degree of saturation duplicate specimen.

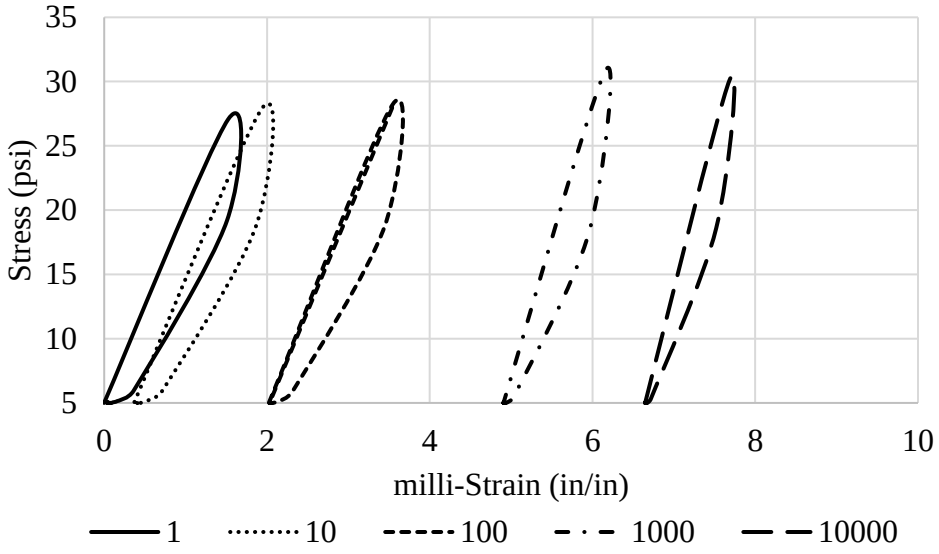

Figure B-39: Hysteresis Loops of the 1st, 10th, 100th, 1000th and 10,000th load application for the third stress path, coarse gradation, and 80% degree of saturation specimen.

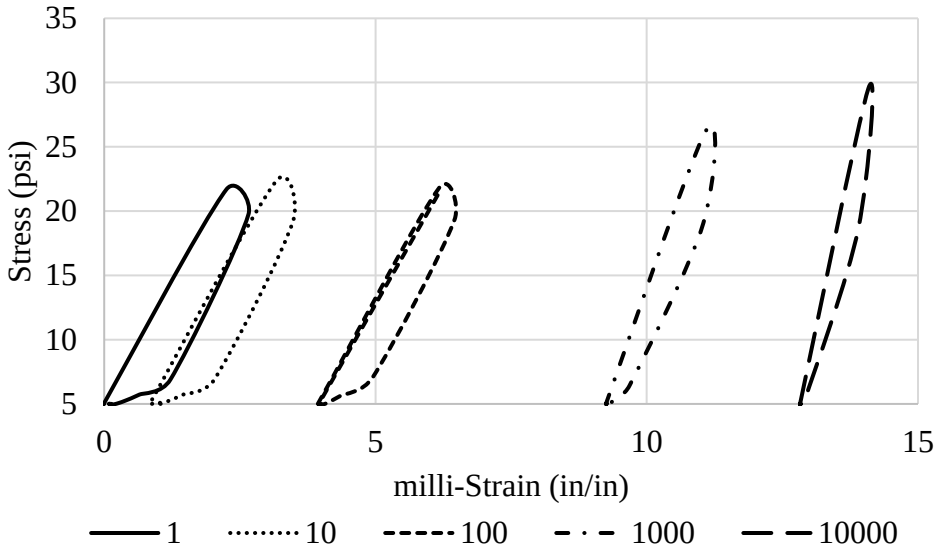

Figure B-40: Hysteresis Loops of the 1st, 10th, 100th, 1000th and 10,000th load application for the third stress path, coarse gradation, and 80% degree of saturation duplicate specimen.

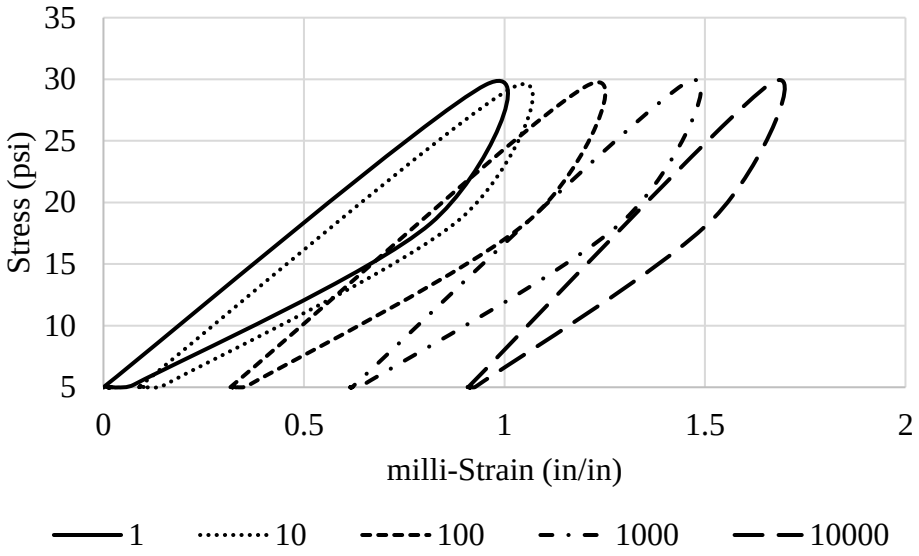

Figure B-41: Hysteresis Loops of the 1st, 10th, 100th, 1000th and 10,000th load application for the third stress path, intermediate gradation, and 40% degree of saturation specimen.

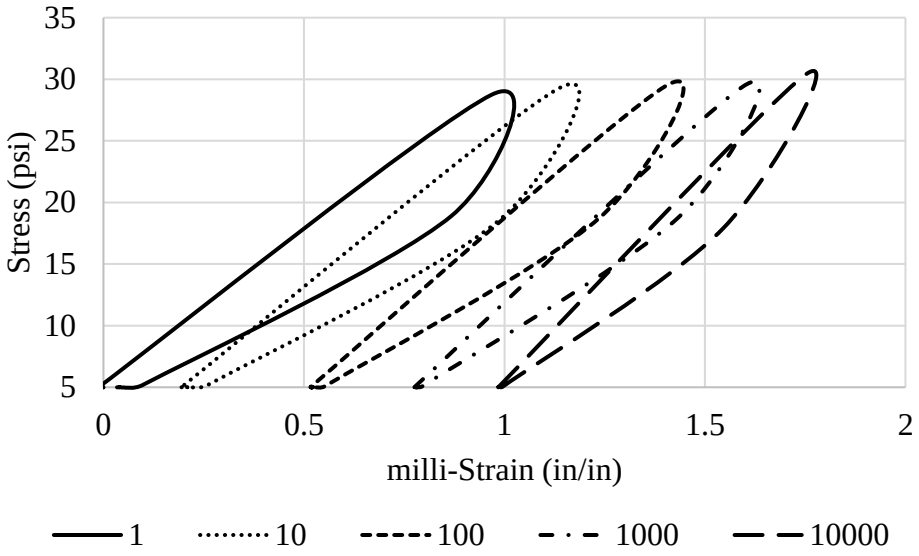

Figure B-42: Hysteresis Loops of the 1st, 10th, 100th, 1000th and 10,000th load application for the third stress path, intermediate gradation, and 40% degree of saturation duplicate specimen.

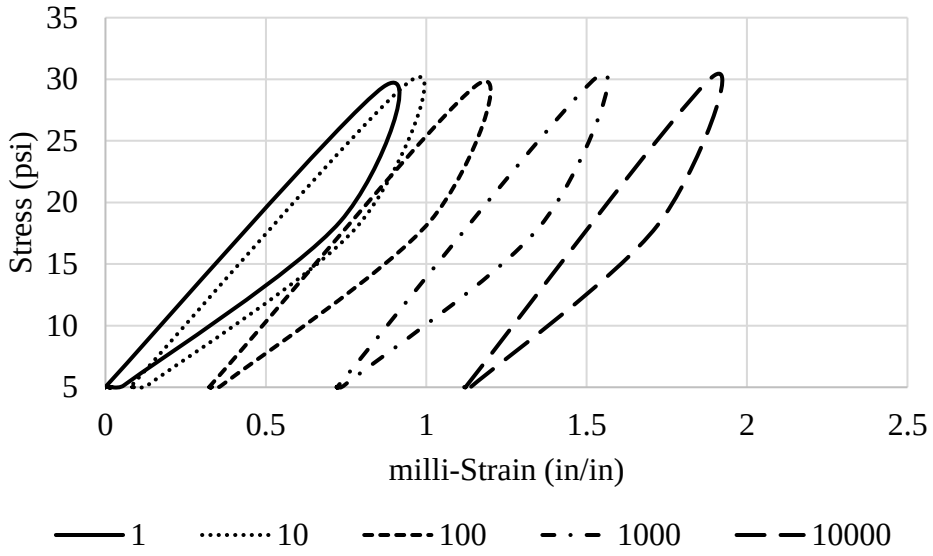

Figure B-43: Hysteresis Loops of the 1st, 10th, 100th, 1000th and 10,000th load application for the third stress path, intermediate gradation, and 60% degree of saturation specimen.

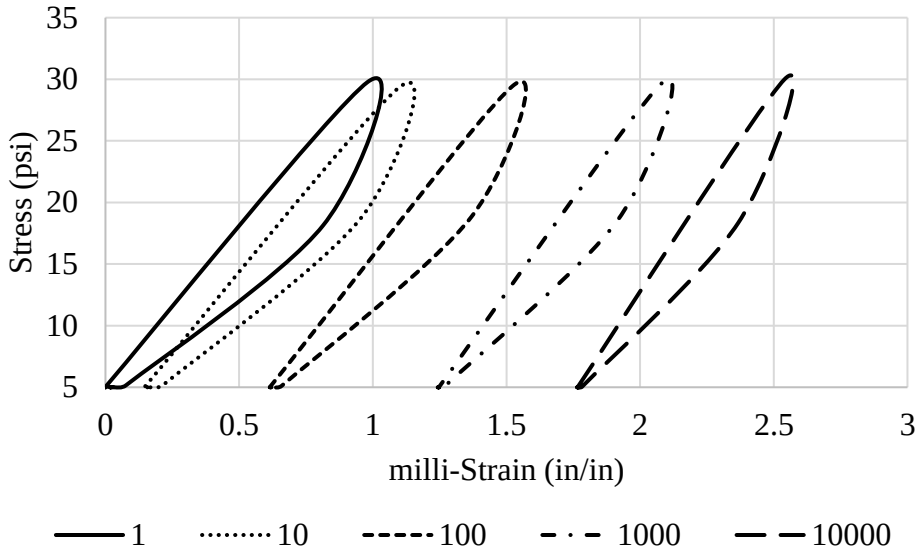

Figure B-44: Hysteresis Loops of the 1st, 10th, 100th, 1000th and 10,000th load application for the third stress path, intermediate gradation, and 60% degree of saturation duplicate specimen.

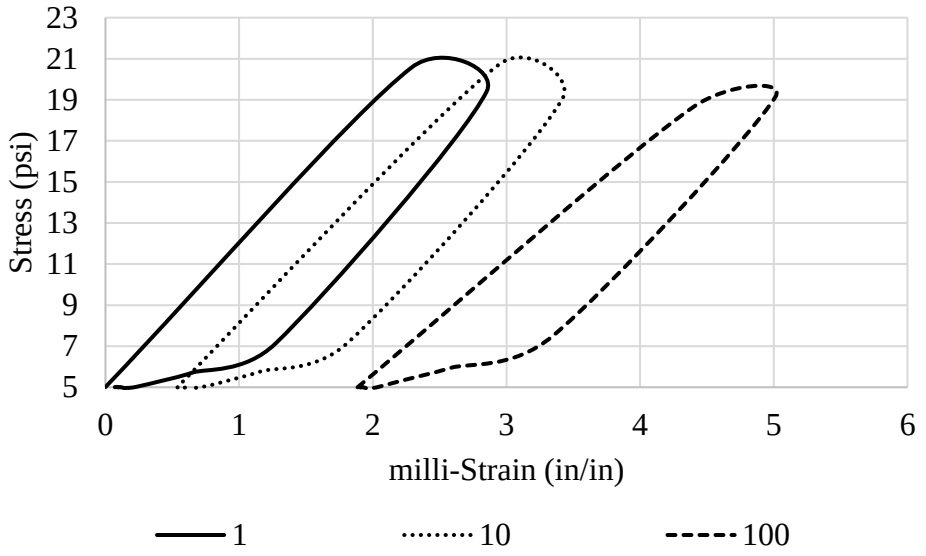

Figure B-45: Hysteresis Loops of the 1st, 10th, and 100th load application for the third stress path, intermediate gradation, and 80% degree of saturation specimen.

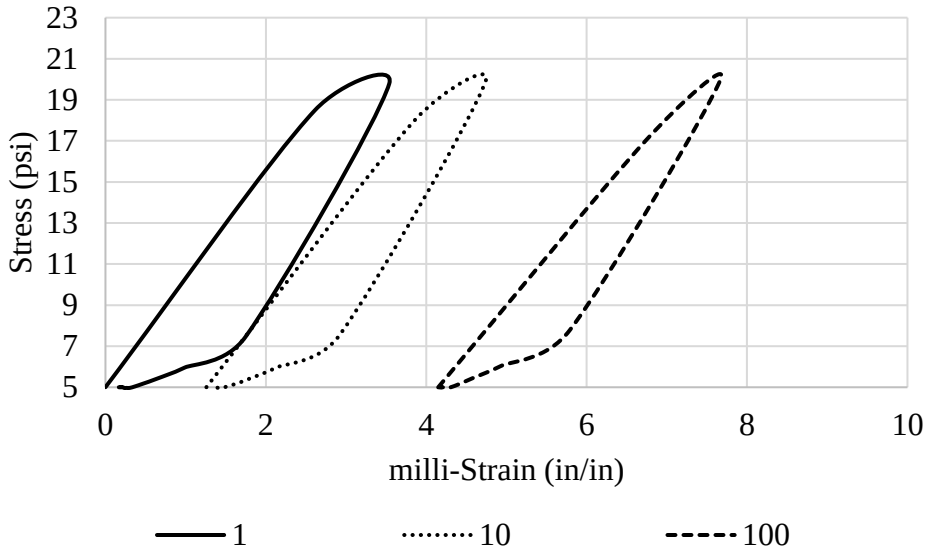

Figure B-46: Hysteresis Loops of the 1st, 10th, and 100th load application for the third stress path, intermediate gradation, and 80% degree of saturation duplicate specimen.

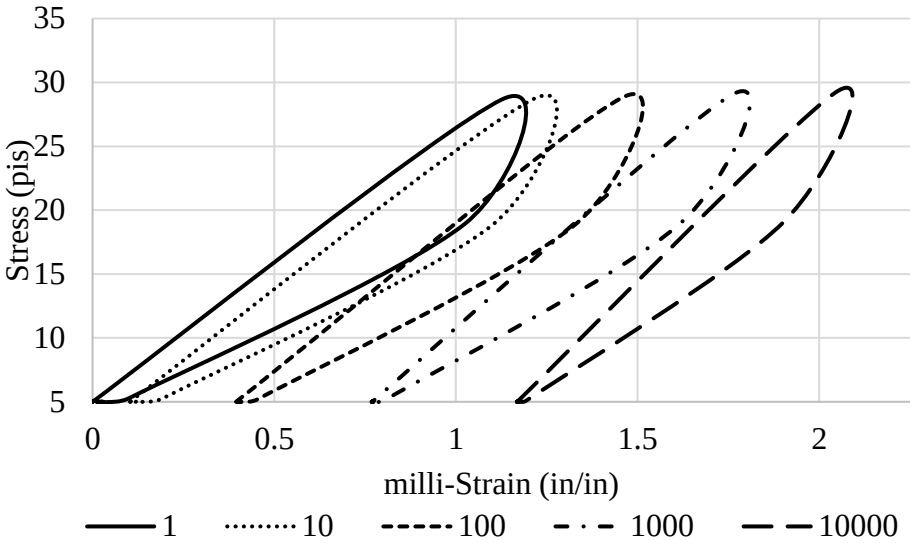

Figure B-47: Hysteresis Loops of the 1st, 10th, 100th, 1000th and 10,000th load application for the third stress path, fines gradation, and 40% degree of saturation specimen.

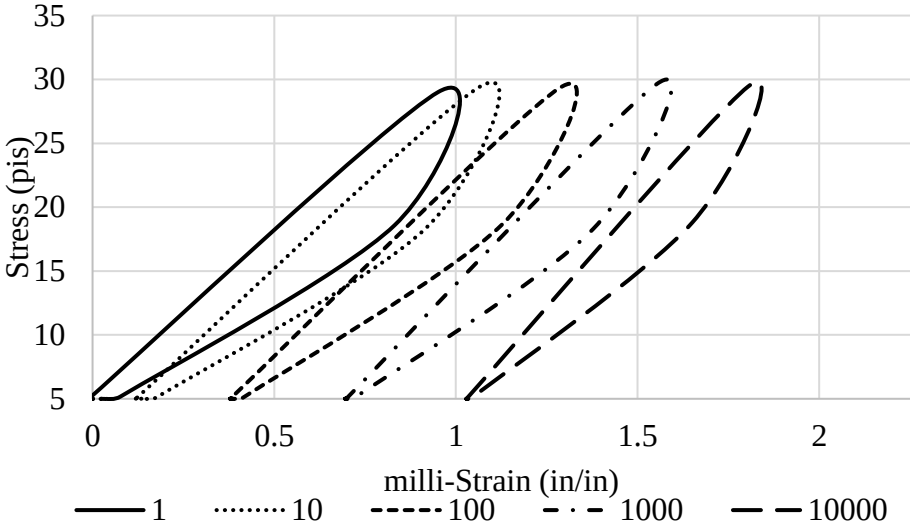

Figure B-48: Hysteresis Loops of the 1st, 10th, 100th, 1000th and 10,000th load application for the third stress path, fines gradation, and 40% degree of saturation duplicate specimen.

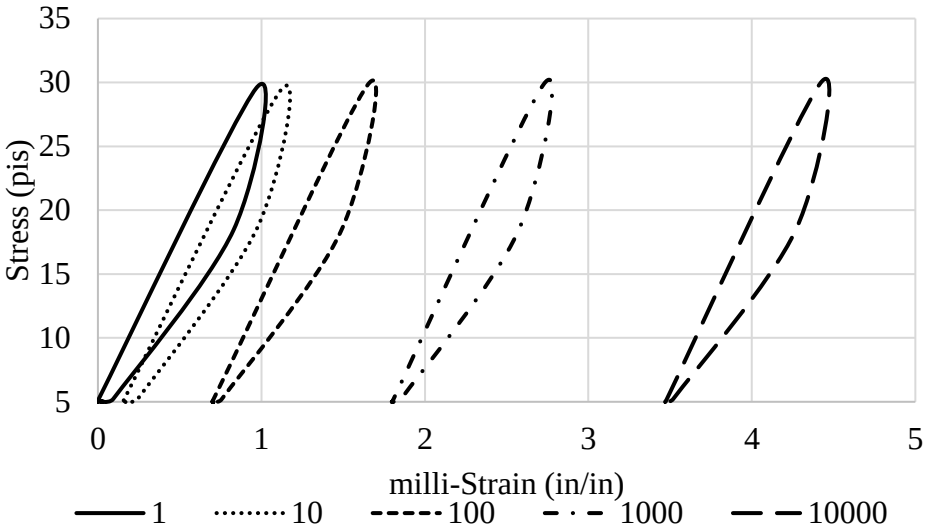

Figure B-49: Hysteresis Loops of the 1st, 10th, 100th, 1000th and 10,000th load application for the third stress path, fines gradation, and 60% degree of saturation specimen.

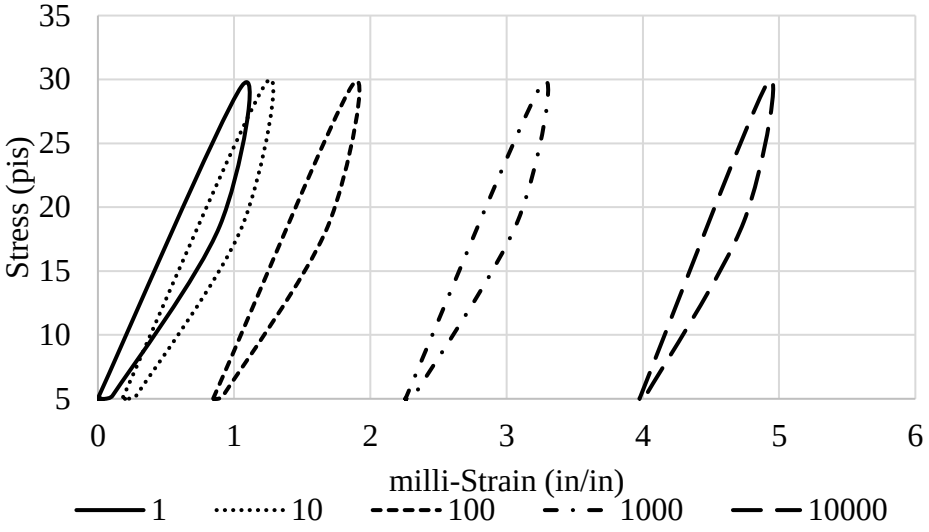

Figure B-50: Hysteresis Loops of the 1st, 10th, 100th, 1000th and 10,000th load application for the third stress path, fines gradation, and 60% degree of saturation duplicate specimen.

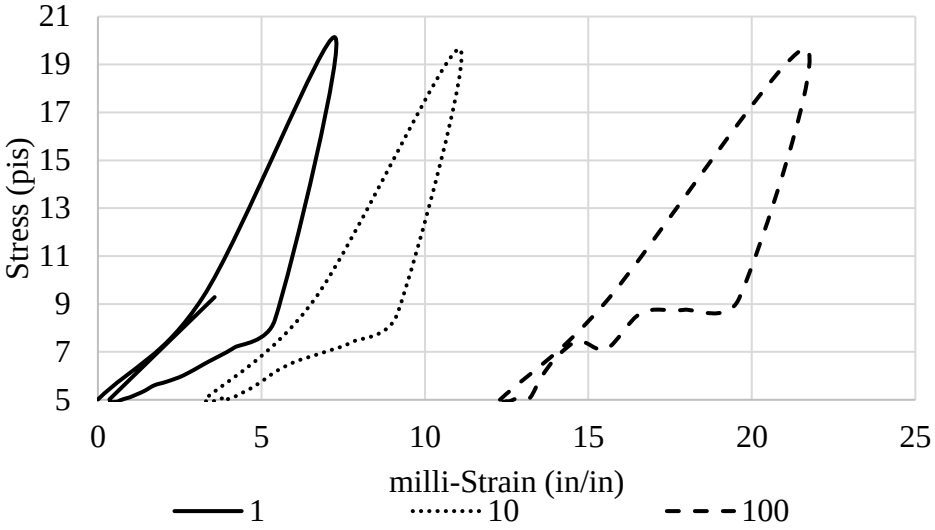

Figure B-51: Hysteresis Loops of the 1st, 10th, and 100th load application for the third stress path, fines gradation, and 80% degree of saturation specimen.

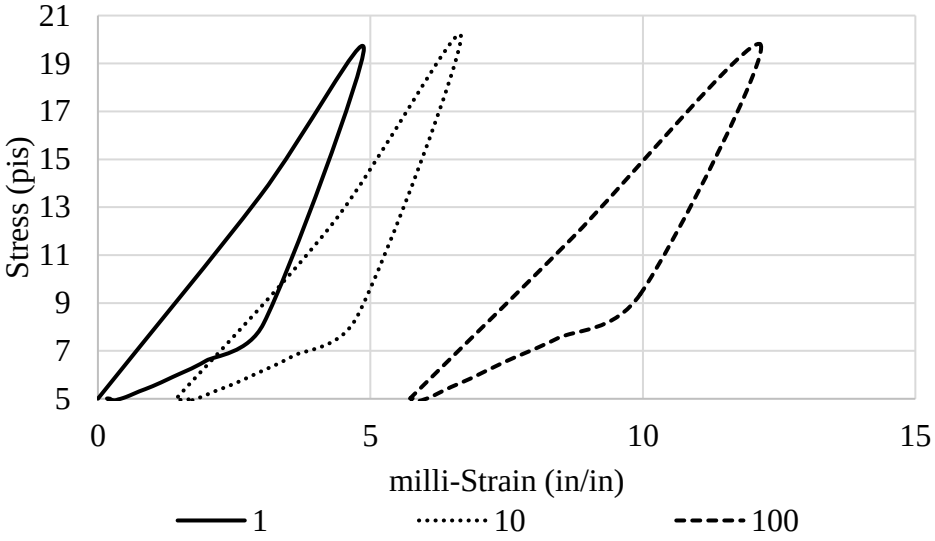

Figure B-52 Hysteresis Loops of the 1st, 10th, and 100th load application for the third stress path, fines gradation, and 80% degree of saturation duplicate specimen.

Data for the duplicate specimen of the second stress path under the intermediate gradation with 80% degree of saturation, and data for the specimen of the second stress path under the fine gradation with 60% degree of saturation, are not available due to systematic errors that occurred during the testing.

Curriculum Vita

Arteaga, Uriel B
El Paso, Texas | 915-503-4483 | uarte01@gmail.com

As a Hispanic individual, I grew up in the El Paso and Juarez region, where I developed great bilingual skills in the Spanish and English languages. I contributed to the community by volunteering in the Socorro Independent School District as a soccer coach and as a soccer referee. In 2015, I obtained a Bachelor's of Science degree in Civil Engineering at The University of Texas at El Paso. I graduated with a summa cum laude award for my hard work and dedication. During the course of my undergraduate and graduate studies, I worked at the Center for Transportation and Infrastructure Systems as a research assistant. There I was assigned to the soils laboratory where I focused in research to characterize the factors that influence permanent deformation. During the course of writing papers related to my findings, I was recommended for a presentation at the Transportation Research Board at Washington for the submission of the "Permanent Deformation Prediction of Unbound Granular Layers with Varying Moisture and Fines Content using Constant Confining Pressure Stress Paths" paper. Currently I have submitted another paper called "Analysis of Cyclic Behavior of Geomaterials using Dissipated Energy Concept", to the American Society of Civil Engineering journal. Both paper focus in the characterization of the rutting performance of geomaterials.

This thesis was typed by Uriel Brian Arteaga.